Neuronal Structural Plasticity in the Medial Prefrontal Cortex: Regulation by Dopamine and PSA-NCAM

DOCTORAL THESIS

Esther Castillo Gómez

2011

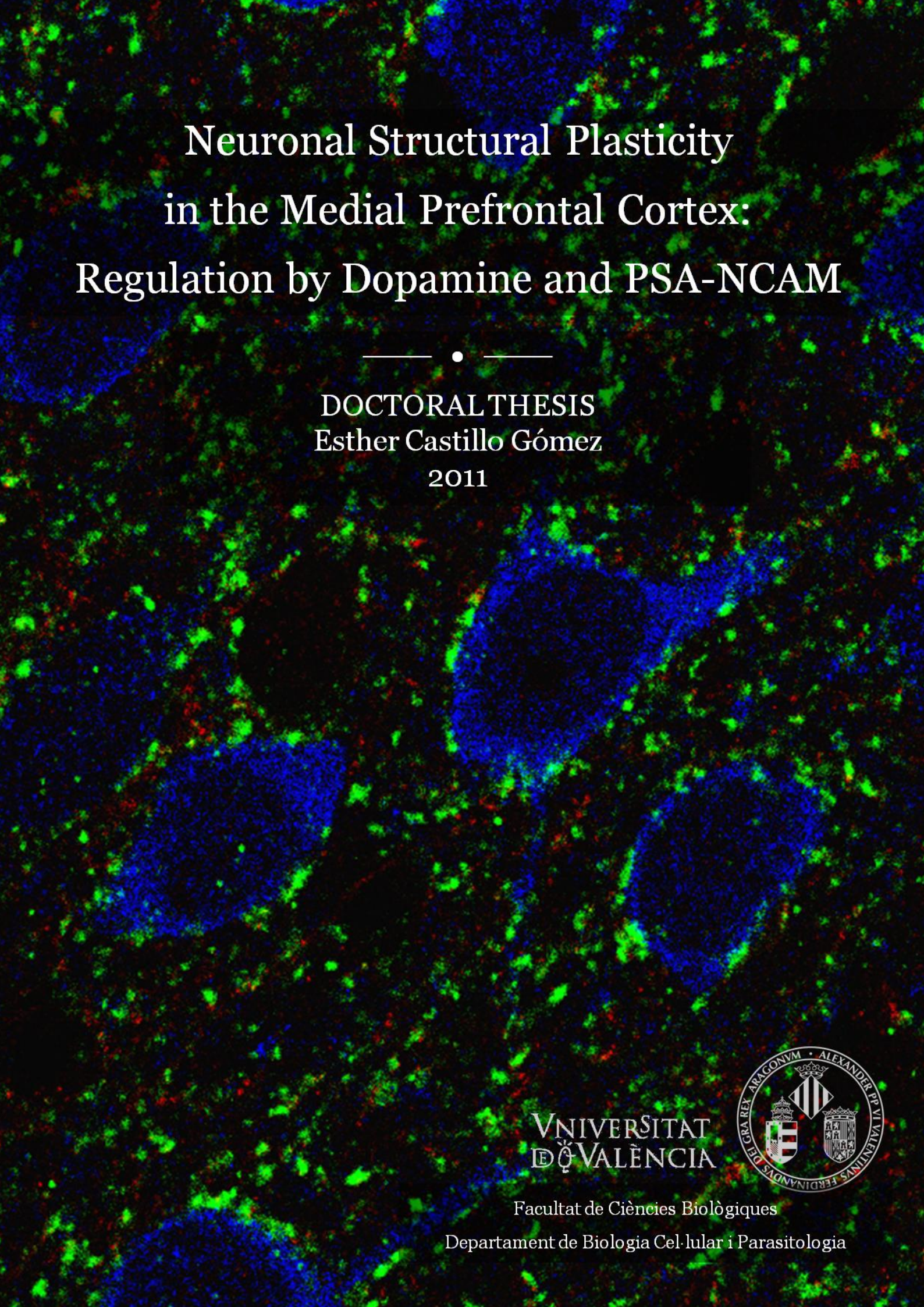

VNIVERSITAT DE VALÈNCIA

Facultat de Ciències Biològiques

Departament de Biologia Cel·lular i Parasitologia

VNIVERSITAT DE VALÈNCIA

Facultat de Ciències Biològiques

Departament de Biologia Cel·lular

Dr. Juan S. Nacher
Neurobiology
Cell Biology Dpt.
Universitat de València
Dr. Moliner, 50
Burjassot, 46100
Spain
Tel: 34 96 3544378
Fax: 34 96 3544781

D. **Juan Salvador Nácher Roselló**, Doctor en Biología y Profesor Titular del Departamento de Biología Celular y Parasitología de la Facultad de Ciencias Biológicas de la Universidad de Valencia,

CERTIFICA QUE

Dña. **Esther Castillo Gómez**, licenciada en Biología por la Universidad de Valencia, ha realizado bajo su dirección el presente trabajo titulado: ***"Neuronal Structural Plasticity in the Medial Prefrontal Cortex: Regulation by Dopamine and PSA-NCAM"***, y que hallándose concluido, autoriza su presentación a fin de que pueda ser juzgado por el tribunal correspondiente y optar así a la obtención del grado de Doctor por la Universidad de Valencia, con la Mención de "Doctor Europeus", dentro del Programa de Doctorado en Neurociencias Básicas y Aplicadas.

Y para que así conste, en cumplimiento de la legislación, firmo el presente certificado en:

Valencia, 14 de Marzo de 2011

Dr. Juan Salvador Nácher Roselló

Para la realización de esta tesis, la autora ha sido beneficiaria de una beca pre-doctoral del Programa Nacional de Profesorado Universitario concedida por el Ministerio de Educación y Ciencia (MEC-FPU, AP2006-01953) según la resolución del 2 de abril de 2007, de la Secretaría de Estado de Universidades e Investigación y de una beca pre-doctoral de investigación del Programa “V Segles” concedida por la Universitat de València según la resolución del 23 de junio de 2006, del Vicerrectorado de Investigación.

A Miguel Ángel

A mis padres y mi hermana

“Los hombres deberían saber que del cerebro, y nada más que del cerebro, vienen el placer y la alegría, la diversión y las risas, y también las penas, tristezas y llantos. Y gracias al cerebro, de manera especial, adquirimos sabiduría y conocimientos, y vemos, oímos y sabemos lo que es repugnante y lo que es bello, lo que es dulce y lo que es insípido. Y gracias a este órgano nos volvemos locos y deliramos y los miedos y terrores nos asaltan. Todas estas cosas debemos soportarlas de nuestro cerebro cuando no está sano. Y en este sentido, soy de la opinión de que esta víscera ejerce en el ser humano el mayor poder”.

Hipócrates, “Sobre las enfermedades sagradas” (460-470 a.C.)

ACKNOWLEDGEMENTS/ AGRADECIMIENTOS

Después de ver por fin plasmado en papel el resultado de todos estos años de trabajo, me gustaría dar las gracias a todas aquellas personas que han hecho posible que hoy pueda estar aquí, escribiendo estas líneas.

En primer lugar, mi más sincero agradecimiento al Dr. Juan Nácher, mi director de tesis, por haberme brindado la oportunidad de descubrir este apasionante mundo de la investigación. Gracias Juan, por tu confianza en mi trabajo, por lo que me has enseñado y por todas las horas que has invertido en dirigir esta tesis.

Especial agradecimiento también, al resto de personas que forman o formaron parte del laboratorio de Neurobiología. A los profesores: Emilio, Carlos, José Miguel y Paco Pepe, darles las gracias por todas las técnicas y conocimientos que he aprendido de ellos. A mis compañeros de “alegrías y penurias”, ¡¡qué decirles que ellos ya no sepan después de tantas “meriendas de máquina” compartidas!! A Mª Ángeles y Ramón, que empezamos juntos esta aventura, gracias por los miles de recuerdos que me llevo de estos años y me es imposible resumir aquí; por los buenos ratos vividos y por vuestro apoyo en algunos que no fueron tan buenos. A Javi, porque todo lo que sé de qRT-PCR es gracias a él; por los buenos ratos de “speak in English” y por el “tostón” que me da con la estadística y los logaritmos. A Sandra y Clara, que llegaron cuando yo ya estaba apuntito de “enclaustrarme” para escribir, muchísimas gracias por su ayuda en mis últimos experimentos y por lo que me aguantaron en esos momentos de mayor agobio. A Samuel, por las veces que se ha quedado hasta tarde por ayudarme a montar. A Laura, por ese agosto que nos pasamos mano a mano en el lab. A Teresa, por las “charlitas” durante las inmunos. A los que estuvieron poco tiempo (Amparo, Pepo, Gregori) o ya se fueron (Anabel, María, Javi), por la huella que dejaron. Y a todos los que empezáis ahora vuestro camino o lo empezaréis en breve (David, Marta, María, Ulisses, Héctor), os deseo lo mejor y os animo a que continuéis siempre adelante por muchas dificultades que os vayan surgiendo, porque este trabajo, aunque a veces es duro, acaba siendo recompensante.

Gracias a todas las personas del Departamento que durante estos años me han ayudado de alguna u otra manera; bien con cuestiones de “papeleo” (Pilar, Xavi,

Mª Carmen), enseñándome a dar sus clases (Carlos López, Chonchi, Isabel, Quique) o enseñándome los “truquitos” de algún aparato (Sabina).

Thanks very much to Dr. Zimmer and all the people in his lab that made possible my stay in Denmark and taught me everything I know about organotypic cultures. Especial agradecimiento a Sara y María, por pasarse largas horas conmigo en el lab hasta que por fin conseguimos poner a punto los cultivos. Pero sobretodo, a ellas dos, a Esther y también a Joost y la “peque, Joana”, por todos los buenos recuerdos que de allí me llevo gracias a ellos; por todas esas cenitas, por los paseos por el centro, por la “Spanish omelette” de Joost, por los buenos ratos en el café Biografen y los “Hyldeblomsts” (que nunca llegué a pronunciar bien). Gracias por estar ahí cuando os necesité y por seguir estándolo a pesar de la distancia.

A mis amigos, por todos esos ratos que han hecho que me olvidara de la ciencia y del trabajo y disfrutara simplemente de la vida.

Y, por supuesto, el agradecimiento más sentido y profundo va para mi familia más próxima, a los que perjudiqué con mis frecuentes ausencias para concentrarme en la tesis. A mis padres, por enseñarme desde pequeña que con esfuerzo y tesón todo es posible y que uno nunca sabe lo lejos que puede llegar, si no se arriesga a intentarlo. A Noelia, por sentirse tan orgullosa de su hermana mayor y tomarme siempre como ejemplo; gracias por hacerme sentir que soy tan importante para ti. A Miguel y Cristina, porque sin su apoyo y su cariño esta tesis tampoco hubiera sido posible. A mis abuelos, tías y primos, que engordan 10 kilos cada vez que hablan de mi, muchísimas gracias también por vuestro cariño. Finalmente, el mayor de mis agradecimientos va para Miguel Ángel, al que no tengo palabras suficientes para agradecerle todo lo que ha hecho por mí. Gracias por animarme a empezar este camino, a pesar de saber lo duro que iba a ser; por alegrarte más que yo cuando las cosas salían bien y animarme a continuar cuando ya no tenía fuerzas; por tu enorme paciencia, por todo el tiempo que esta tesis te ha robado y por tantos planes personales pospuestos hasta que “Esther acabe la tesis”. Sin tu apoyo, nunca lo hubiera conseguido.

TABLE OF CONTENTS

ABBREVIATIONS

6-OHDA	6-hydroxydopamine hydrobromide
ABC	Avidin-biotin-peroxidase
ACC	Anterior cingulate cortex
ACd	Anterior cingulate cortex dorsal
ACv	Anterior cingulate cortex ventral
AId	Dorsal agranular insular cortex
AIv	Ventral agranular insular cortex
CaMKII-α	α subunit of the Ca^{2+} /calmodulin dependent protein kinase II
CAMs	Cell adhesion molecules
CB	Calbindin
cc	Corpus callosum
CCK	Cholecystokinin
Cg 2	Ventral cingulate cortex
Cg1	Dorsal cingulate cortex
c.m.	Culture medium
CR	Calretinin
C_T	Cycle threshold
D1R	Dopamine D1 receptor
D2R	Dopamine D2 receptor
D3R	Dopamine D3 receptor
D4R	Dopamine D4 receptor
D5R	Dopamine D5 receptor
DA	Dopamine
DAB	3,3'- diaminobenzidine tetrahydrochloride
DAT	Dopamine transporter
DDC	DOPA-decarboxylase
DIV	Days *in vitro*
ECL	Enhanced chemiluminescence system
Endo-N	Endo-N-acetylneuraminidase
EN	Endopiriform nucleus

GABA	γ-aminobutyric acid
GAD67	67 kDa isoform of the glutamate decarboxilase enzime
GAD65/67	65 and 67 kDa isoform of the glutamate decarboxilase enzime
GFP	Green fluorescent protein
GL	Grey Levels
GPI	Glycosylphosphatidylinositol
IHC	Immunohistochemistry
i.p.	Intraperitoneal
Ig	Immunoglobulin
IL	Infralimbic cortex
lPFC	Lateral prefrontal cortex
LTD	Long-term depression
LTP	Long-term potentiation
M2	Secondary motor cortex
MAO	Monoamine oxidase
MAP2	Microtubule associated protein 2
mPFC	Medial prefrontal cortex
NCAM	Neural cell adhesion molecule
NDS	Normal donkey serum
NPY	Neuropeptide-Y
OB	Olfactory bulb
OD	Optic Density
OFC	Orbitofrontal cortex
PB	Phosphate buffer
PBS	Phosphate buffered saline
PFC	Prefrontal cortex
PrL	Prelimbic cortex
PPHT	2-(N-Phenethyl-N-propyl) amino-5-hydroxytetralin hydrochloride
PSA-NCAM	Polysialylated form of the Neural Cell Adhesion Molecule
PV	Parvalbumin
RT-PCR	Reverse transcription Polymerase Chain Reaction
RT qRT-PCR	Real time quantitative RT-PCR
S.E.M	Standard error of the mean
SN	Substantia nigra

SST	Somatostatin
ST8SiaII	Polysialyltransferase II
ST8SiaIV	Polysialyltransferase IV
SVZ	Subventicular zone
SYN	Synaptophysin
TH	Tyrosine hydroxylase
Tyr	Tyrosine
VGAT	Vesicular γ-aminobutyric acid (GABA) transporter
VGLUT1	Vesicular glutamate transporter 1
VIP	Vasoactive intestinal peptide
VLO	Ventrolateral orbital cortex;
VO	Ventral orbital cortex
VTA	Ventral tegmental area
VTN	Ventral thalamic nucleus
WM	White matter

LIST OF FIGURES

LIST OF TABLES

Chapter 1

INTRODUCTION

1. PREFRONTAL CORTEX

The **prefrontal cortex** (PFC) is the anterior part of the frontal lobe of the mammalian brain, located rostrally to the premotor and motor cortices (Fuster, 2008). It has been classically defined and delineated attending to different **anatomical criteria** such as cytoarchitectonic features (granular vs. agranular characteristics) (Brodmann, 1909), reciprocal connectivity with the mediodorsal nucleus of the thalamus (Rose and Woolsey, 1948) or with the main nuclei of origin of cholinergic and monoaminergic neurotransmitter systems (Uylings et al., 2003 for review). But the PFC as a whole shows enormous variation across species when it is defined by a single **anatomical** or **functional** (electrophysiology and behavior) criterion, so it is now generally agreed that several anatomical and functional features have to be taken into account when studying this region (Uylings, 2003; Seamans, 2008).

On the bases of these criteria, three main regions of PFC can be identified in the rat (**figure 1**). The first, the **medial prefrontal cortex** (**mPFC**), is a medial frontal division situated rostral to the genu of the corpus callosum. The second, the **orbitofrontal cortex** (**OFC**), is a ventral region located in the dorsal bank of the rostral end of the rhinal sulcus. Finally, the third region is the **lateral prefrontal cortex (lPFC)**, also called sulcal PFC or agranular insular cortex, which is located in the anterior part of the rhinal sulcus (Uylings et al. 2003; Fuster 2008 for review).

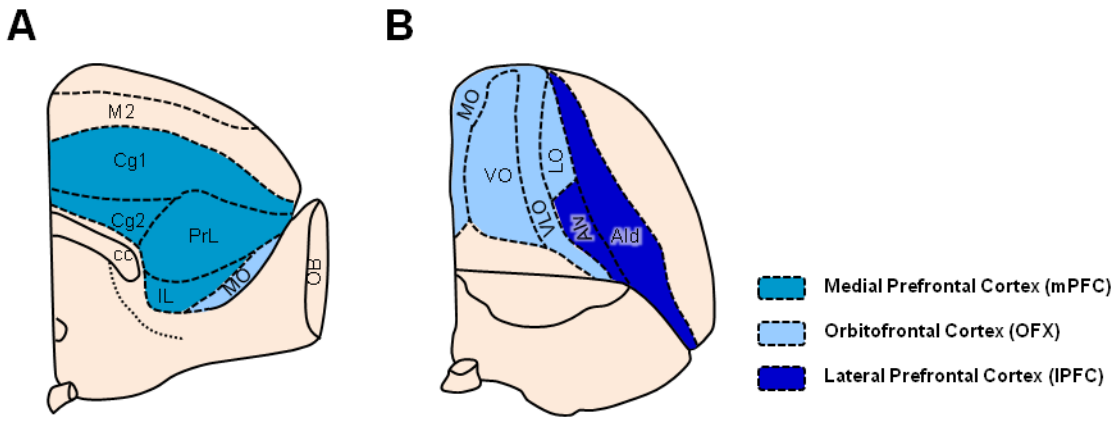

Figure 1. Schematic representation of the medial (A) and inferior view (B; tip of temporal lobe resected**) of the rat's prefrontal cortex, showing its extent and subdivisions.** Abbreviations: AId, dorsal agranular insular cortex; AIv, ventral agranular insular cortex, cc, corpus callosum; Cg1, dorsal cingulate cortex; Cg2, ventral cingulate cortex; IL, infralimbic cortex; LO, lateral orbital cortex; MO, medial orbital cortex; M2, secondary motor cortex; OB, olfactory bulb; PrL, prelimbic cortex; VLO, ventrolateral orbital cortex; VO, ventral orbital cortex. From Uylings et al. 2003 with some modifications according to Paxinos and Watson, 2007.

2. MEDIAL PREFRONTAL CORTEX

The medial prefrontal cortex (mPFC) will be the focus of this thesis. This region of the prefrontal cortex in rats can be further divided into three areas with distinct anatomical and functional features (**figure 2**): (1) the rostral portion of the **anterior cingulate cortex** (ACC), which in turn is divided into a **dorsal** (ACd or Cg1) and a **ventral** (ACv or Cg2) area; (2) the **infralimbic cortex** (IL) and, (3) the **prelimbic cortex** (PrL) (Uylings et al., 2003; Paxinos and Watson, 2007; Seamans et al., 2008).

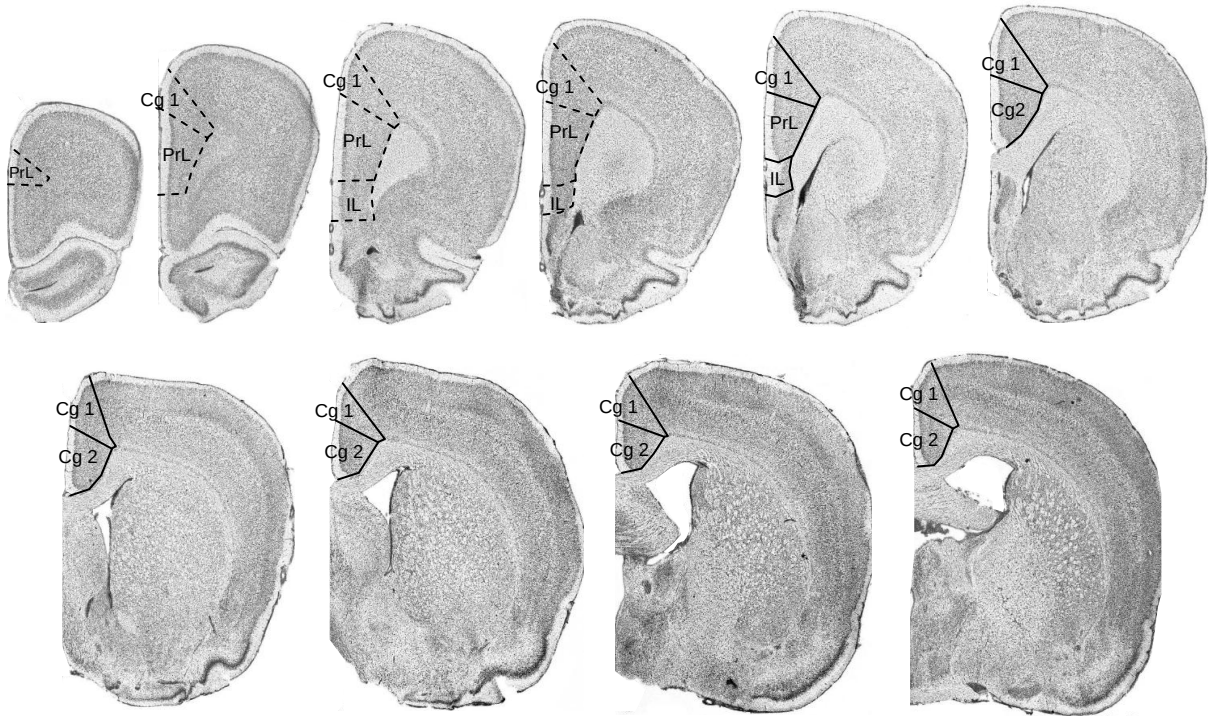

Figure 2. Nissl stained coronal sections of the rat brain, showing the subdivisions of the medial prefrontal cortex (mPFC). Please, note that sections are not equally spaced but cover the overall extent of the mPFC [from Bregma + 5.16 mm **(top left)** to Bregma - 1.56 mm **(bottom right)**, according to the atlas of Paxinos and Watson, 2007]. Abbreviations: Cg1, dorsal cingulate cortex; Cg2, ventral cingulate cortex; IL, infralimbic cortex; PrL, prelimbic cortex.

On cytoarchitectonic grounds, these regions are considered equivalent to the human/primate Brodmann's areas 24, 25 and 32 respectively. However, although the rat PFC is not as differentiated as it is in primates, and the appearance of new specializations later in the evolution is likely, dorsolateral-like features (Brodmann's areas 46 and 9), including both anatomical and functional ones, are also present in rats. In general, it appears that the rat PrL region is involved in attentional and response selection functions, as well as visual working memory, whereas the more dorsal regions (Cg) are involved in the generation of rules associated with temporal ordering and motor sequencing of behavior. The IL region plays a special role in

autonomic control, and especially in the modulation of fear-related behaviors (Uylings et al., 2003; Paxinos and Watson, 2007; Seamans et al., 2008).

2.1. Microscopic architecture of the rodent mPFC

The architectural order of cells and fibers in the rodent mPFC basically conforms to the structural plan prevailing throughout the neocortical regions in mammals, but lacking the *internal granule cell layer* (layer IV) (Gabbot et al. 1997; Fuster, 2008). Therefore, the rodent mPFC is organized in five layers (**figure 3**) that run parallel to the cortical surface and are numbered from the outer surface of the cortex (*pia mater*) to the white matter as follows (Kandel et al., 2000; Paxinos, 2004; Fuster, 2008):

- **Layer I** (*molecular or plexiform layer)* is an acellular layer occupied by the dendrites of the cells located deeper in the cortex and axons that travel through this layer or form connections in there.
- **Layer II** (*external granule cell layer)* is comprised mainly of small spherical cells called granule cells. Some small pyramidal cells are also present in this layer and connect with other cortical areas from the same hemisphere.
- **Layer III** (*external pyramidal cell layer)* contains a variety of cell types, many of which are pyramidally shaped and connect either with the contra-lateral hemisphere or with other cortical areas from the same hemisphere. In cortices organized in five layers, layer III receives most of the projections coming from the thalamus.
- **Layer V** *(internal pyramidal cell layer)* contains mainly pyramidal neurons that are typically larger and more densely packed than those in layer III. Many of these neurons have been shown to project to the basal ganglia, the thalamus, many nuclei of the brainstem and midbrain, and to the spinal cord (Lambe et al., 2000 for review).
- **Layer VI** *(polymorphic or multiform layer)* is a fairly heterogeneous layer of neurons. It blends into the white matter that forms the deep limit of the cortex and carries axons to the thalamus and to/from other areas of the cortex (DeFelipe and Fariñas, 1992; Groenwegen *et al.*, 1997).

Although each layer of the cerebral cortex is defined primarily by the presence or absence of neuronal cell bodies, each layer also contains additional elements. Thus, layers I-III contain the apical dendrites of neurons that have their cell bodies in layers V and VI, while layers V and VI contain the basal dendrites of neurons with cell bodies in layer II. The profile of inputs to a particular cortical neuron depends more on the distribution of its dendrites than on the location of its cell body (Kandel et al., 2000).

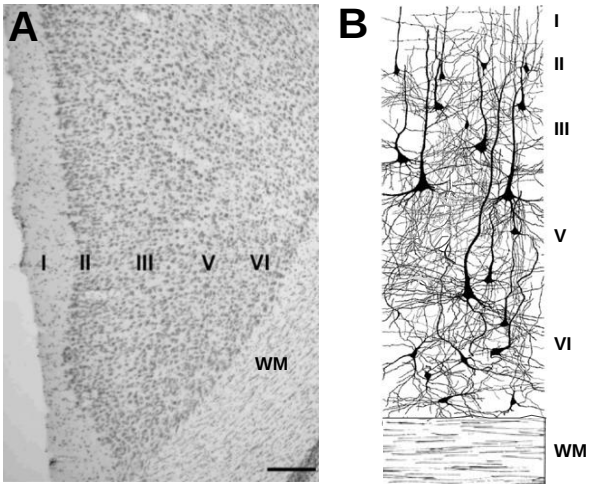

Figure 3. Microscopic architecture of the rat medial prefrontal cortex (mPFC). (A) Panoramic view of the rat cingulated cortex stained with cresyl violet, showing the five layers (I, II, III, V and VI) in which this area is organized. Scale bar: 250 µm. **(B)** Schematic drawing representing the five layers of the rat mPFC as they can be observed in a Golgi staining (modified from Fuster, 2008). Abbreviations: WM, white matter.

2.2. Neuronal cell types in the mPFC

There are two major neuronal cell types in the rat mPFC: (1) pyramidal cells, to which pertain most of mPFC neurons, and (2) interneurons, the 16% of neurons in this region (Gabbott et al., 1997).

Pyramidal cells are projection neurons located in layers II-VI of mPFC, which use the excitatory amino acid glutamate as their primary neurotransmitter (they establish asymmetric synapses). They typically have a triangular shaped soma with a single axon and two separate dendritic trees (apical and basal). Whereas only one dendrite leaves the apex of the soma and ascends vertically into more superficial layers (usually reaching layer I and forming an apical tuft), several dendrites emerge from the base of the soma and extend horizontally within the same layer (Dégenètais et al., 2002). Both apical and basal dendrites of mPFC pyramidal cells branch extensively and are studded with dendritic spines. These spines are usually contacted by a single glutamatergic terminal (excitatory asymmetric synapse), although they may also receive dual input from both a glutamatergic terminal and

either a GABAergic, dopaminergic, serotoninergic or cholinergic terminal or even may not receive any input (Kubota et al., 2007; Yao et al., 2008; Miner et al., 2003; Duffy et al., 2009; Arellano et al., 2007). Such configurations modulate the excitatory transmission at the level of the spine and have important consequences for the efficacy of synaptic transmission (Nimchinsky et al., 2002). The axon of mPFC pyramidal cells emerges from the base of the soma and projects to other areas of the cortex or to subcortical areas (**figure 4**) (Lambe et al., 2000).

Interneurons are local-circuit neurons distributed within all layers of the mPFC (I-VI), that are characterized by their use of the γ-aminobutyric acid (GABA) as primary neurotransmitter (they establish inhibitory symmetric synapses). Contrary to pyramidal cells, cortical interneurons are a heterogeneous population of neurons with diverse morphological, electrophysiological, neurochemical and synaptic characteristics. Thus, multiple subpopulations of interneurons can be defined attending to these features, individually or in combination (Ascoli et al. 2008). In the rat mPFC, nearly 90% of all interneurons can be classified into subpopulations attending to their expression of one of three calcium-binding proteins [35-40% express parvalbumin (PV); 20-25 % express calbindin (CB); 25-30% express calretinin (CR)] (**figure 4**) (Kubota et al. 1994; Gabbott et al., 1997).

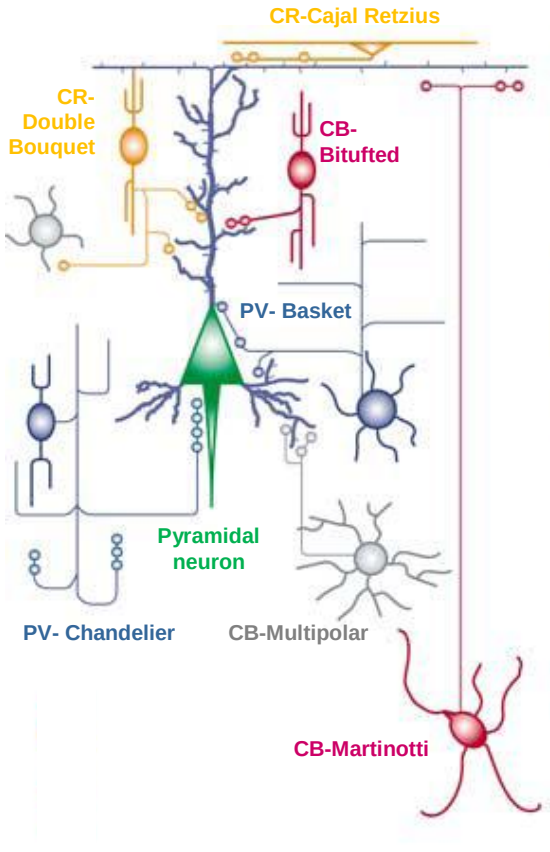

Figure 4. Schematic representation of pyramidal neurons and the major interneuronal subtypes in the rat medial prefrontal cortex (mPFC), attending their expression of calcium binding proteins. Abbreviations: CB, calbindin; CR, calretinin; PV, parvalbumin. From Lewis and González-Burgos, 2008, with some modifications.

PV-expressing interneurons in the rat mPFC are fast-spiking neurons with the morphology of basket cells (they innervate the soma and proximal dendrites of pyramidal cells) or chandelier cells (they innervate the initial segment of the axon of pyramidal cells). CR-expressing interneurons have variable morphology and include bipolar, double bouquet (both of them targeting the dendrites of pyramidal cells in different layers of the cortex) and Cajal-Retzius cells (Gabbott et al., 1997; Kawaguchi and Kubota, 1997; Somogyi et al. 1998; DeFelipe, 1997). CB-expressing interneurons are mainly multipolar, bitufted or Martinotti cells. The double bouquet morphotype, which is characteristic of this subpopulation of interneurons in primates and humans, has not been found in rat mPFC (Ballesteros-Yañez et al., 2005). Both CR- and CB-expressing interneurons in the rat mPFC are non-fast-spiking cells, but show different pre- and postsynaptic connections, with CB-expressing axons extending through cortical layers and accessing pyramidal cells of layer I, while CR-expressing axons stop short of this layer (Zaitsev et al., 2005). A subgroup of non-fast spiking cells that contain the calcium-binding protein calretinin (CR) also express vasoactive intestinal peptide (VIP) and make contacts onto other interneurons much more frequently than onto pyramidal cells and thus are called interneuron-selective interneurons (**figure 4**) (Gonzalez-Burgos and Lewis, 2008; Ascoli et al. 2008).

Although it has been classically considered that nearly all neocortical interneurons in the mature brain have aspiny dendrites (see Markram et al. 2004 for review), recent reports indicate that at least six different subtypes of interneurons in the adult mPFC form spines along their dendrites: non-fast spiking Martinotti cells, non-fast spiking small basket cells, non-fast spiking double bouquet cells, non-fast spiking large basket cells, late-spiking neurogliaform cells and fast-spiking basket cells (Kawaguchi et al., 2006; Kubota et al. 2011). Dendritic spine density varies within these subtypes. Non-fast spiking Martinotti cells have higher spine density than the other subtypes of interneurons, especially fast-spiking basket cells, but this density is clearly lower than that of cortical pyramidal neurons or excitatory spiny strellate cells (Kawaguchi et al., 2006). Contrary to pyramidal neurons, synaptic inputs to interneurons are made mainly onto the dendritic shaft, with fewer inputs generated on spines. The dendritic shaft is structurally stable, but spines are frequently coming out and disappearing (Trachtenberg et al. 2002). Synapses on the shaft may be made between dendrites and very nearby axons by axonal bouton formation (Wierenga et al. 2008). Thus synapse formation by spine protrusion is

considered to select specific axons among the many presynaptic axon candidates (Kubota et al. 2011).

2.3. Cholinergic and monoaminergic innervation to the mPFC

The mPFC of rats and primates plays a role in gating the inputs of the cholinergic and monoaminergic systems to the rest of the cerebral cortex (Ragozzino, 2000). Thus, although the entire neocortex receives inputs from cholinergic, dopaminergic, noradrenergic, and serotoninergic systems, only the mPFC sends reciprocal connections to the basal forebrain, locus coeruleus, and the dorsal and median raphe (e.g. Uylings and Van Eden, 1990; Arnsten, 1997; Everitt and Robbins, 1997). This feedback system is presumed to modulate these inputs and, consequently, drugs, such as antidepressants, that affect these systems have a significant impact upon frontal lobe functioning. The cholinergic and monoaminergic inputs are presumed to modulate whatever functions are ongoing in the prefrontal areas. In recent years, there has been an attempt to demonstrate how these inputs contribute to working memory and attention in particular (e.g. Sagawachi and Goldman-Rakic, 1994; Ragozzino, 2000). In addition, there are dynamic changes in monoamine release in the mPFC when there are changes in the environmental demands on animals, especially under conditions of stress, fear, or other affective stimuli (Rosenkranz and Grace, 2001; Pezze et al., 2003). Changes in monoaminergic neurotransmission have a particularly intense effect in the structure of prefrontocortical neurons and have been linked to the etiopathology of different psychiatric disorders and their treatments (Castren, 2005; Lewis and Gonzalez-Burgos, 2008). The research in our laboratory has been focused during recent years on how monoamines affect this structural plasticity (Varea et al., 2007a; Varea et al., 2007b; Guirado et al., 2009) and the main objective of this thesis is to particularly address how dopamine influences structural remodeling of the mPFC.

2.3.1. Dopaminergic neurotransmission

The DA-producing neurons in the mammalian brain are localized in nine cell groups (A8-A16), which are distributed from the mesencephalon to the olfactory bulb (Kandel et al., 2000; Paxinos, 2000) (**figure 5**).

The dopaminergic innervation of the rat forebrain is mainly constituted by the axons of neurons residing in the retrorubral area (A8), substantia nigra (SN, A9), ventral tegmental area (VTA, A10), arcuate nucleus of the hypothalamus (A12) and medial portion of the zona incerta (A13), which follow one of these pathways (**figure 5**):

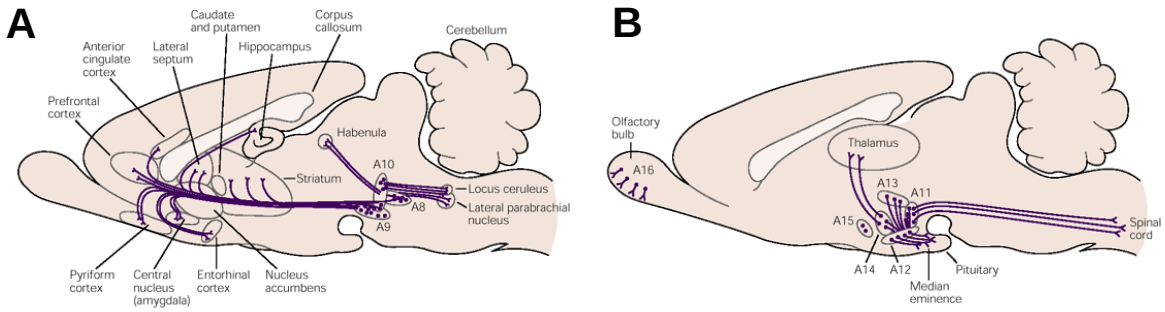

Figure 5. Dopaminergic neurons and pathways in the rat brain. (A) Pathways arising from A8, A9 and A10 dopaminergic neurons. **(B)** A11-A16 dopaminergic neurons and their projections. Modified from Kandel et al., 2000.

- **Nigrostriatal pathway**: it comes from neurons located in the SN and extends to the dorsal striatum (caudate and putamen). It plays a key role in the motor planning and execution of movement, but it is also involved in non-motor functions, such as cognition. The breakdown of neurons in this pathway is associated with the motor impairments that are characteristics of Parkinson's disease.
- **Mesolimbic pathway**: it arises from the VTA and projects to the ventral striatum, hippocampus, amygdala and septum. It is particularly important for motivation, the experience of pleasure, and reward.
- **Mesocortical pathway**: it also comes from the VTA, but projects to the entorhinal cortex and neocortex, mostly to its prefrontal areas. This pathway is believed to be important for concentration and executive functions such as working memory. Excessive dopaminergic transmission within these two later pathways is associated with the disordered thought and the inappropriate emotional behavior characteristic of schizophrenia.
- **Tuberoinfundibular pathway**: it comes from neurons in the arcuate nucleus of the hypothalamus and extends to the median eminence of the hypothalamus, where DA regulates the secretion of prolactin and growth hormone from the anterior pituitary.

- **Incertohypothalamic pathway**: it arises from the medial portion of the zona incerta and innervates amygdaloid and hypothalamic nuclei involved in sexual behavior (Dunlop, 2007; Iversen and Iversen, 2007).

2.3.1.1. Dopamine synthesis, release and receptors in the rat mPFC

The dopamine found in the mPFC is synthesized in the cytoplasm of neurons located in the VTA from the amino acid tyrosine (Tyr) by means of the enzymes tyrosine hydroxylase (TH) and DOPA-decarboxylase (DDC) (**figure 6**). Its release in the mPFC is modulated in association with a variety of events and behaviors. Appetitive events (food reward) and cognitive processing (several forms of learning or attention tasks) can increase DA release in the rat mPFC for tens of minutes, but aversive stimuli (stress, fear or pain) are particularly potent in this regard, being able to elevate DA levels by about 200% and for equally long lasting periods (Neve, 2009). A dense dopaminergic innervation can be found in all regions of the rat mPFC (IL, PrL, Cg1 and Cg2), being higher in layers V and VI than in layers II and III (Zhang et al., 2010). The major targets of these DA axon terminals are pyramidal cells and PV-expressing interneurons, although other interneurons may also receive dopaminergic innervation (Neve, 2009).

Once released from presynaptic axon terminals, DA interacts with five receptor subtypes, which are divided into 2 families, the D1-like receptors (comprising the D1 and D5 subtypes) and the D2-like receptors (comprising the D2, D3 and D4 subtypes), on the basis of amino-acid sequence homologies and pharmacological and functional profiles (**figure 6**). Each receptor subtype has a characteristic anatomical distribution, with D1 and D2 subtypes being present in significantly greater amounts than the others, and the D1 subtype being more abundant than the D2. D1-like receptors are located primarily on the dendritic spines and shafts of pyramidal neurons and on the dendrites and axon terminals of interneurons. Likewise, D2-like receptors are found in dendrites and spines, but they are also located outside the postsynaptic density at extra-synaptic and presynaptic sites where they act as auto-receptors to reduce DA release (Neve, 2009).

In this thesis we will focus our attention on the dopamine D2 subtype of receptors (D2R), since they have been largely implicated in the pathogenesis of

schizophrenia and major depression, as well as in the pharmacological action of antidepressants and antipsychotics (Seeman, 2010; Gershon et al., 2007).

In the rodent mPFC, D2R are expressed by restricted populations of pyramidal neurons and GABAergic interneurons (Zhang et al 2010; Santana et al. 2009). Regarding interneurons, D2R have been mainly found in PV expressing interneurons, but they are also present in a subpopulation of CB expressing cells (Le Moine and Gaspar, 1998).

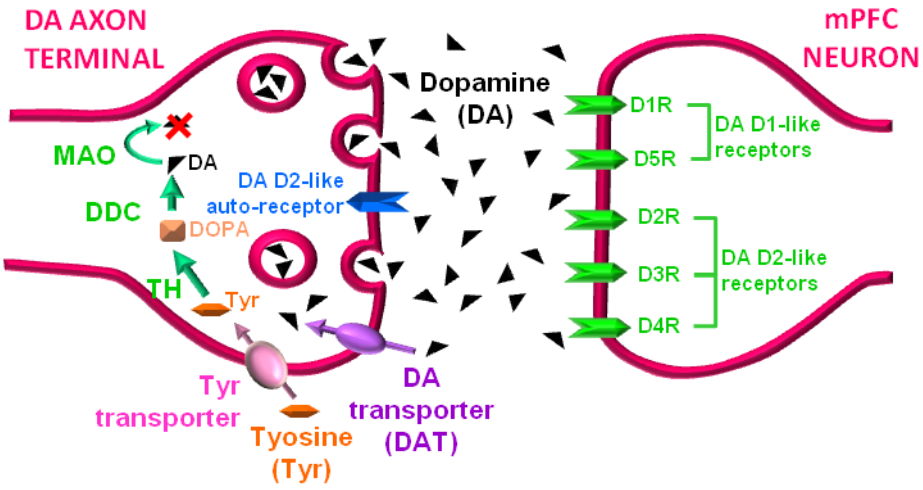

Figure 6. Schematic representation of dopamine synthesis, release and receptors in the medial prefrontal cortex (mPFC). Dopamine (DA) is produced in dopaminergic neurons located in the VTA from the aminoacid tyrosine (Tyr), which is transported into the neuron by an active transport pump (Tyr-transporter). Tyr, by means of the enzyme tyrosine hydoroxylase (TH), is converted into DOPA, which in turn, by means of the enzyme DOPA-decarboxylase (DDC), is converted into DA. DA is packaged after synthesis into vesicles, to be released in the mPFC. In the postsynaptic neuron, DA can interact with five receptor subtypes (D1R-D5R), which are grouped into two families (DA D1-like receptors and DA D2-like receptors). D2-like receptors can also be located in the presynaptic terminal, where they act as auto-receptors to regulate DA release. DA is destroyed by the enzyme monoamine oxidase (MAO) and re-uptaked into the presynaptic terminal by a re-uptake pump named DA transporter (DAT).

3. NEURONAL PLASTICITY

Neuronal plasticity can be defined as the ability of neurons to react with adaptive changes to intrinsic or extrinsic inputs, not only during early development, when the nervous system establishes precise patterns of functional connections by cell migration, axon guidance and synaptogenesis (see Hensch, 2004; de Graaf Peters and Hadders-Algra, 2006 for review), but also during adulthood. Although there is a decline in brain plasticity across the lifespan, the adult brain retains a substantial capacity for experience-dependent synaptic reorganization (de Magalhaes and Sandberg, 2005 for review). This plasticity is considered to be the

basis for learning and memory (Sutton and Schuman, 2006 for review) and it is crucial for adaptive responses to aversive experiences and recovery from brain damage and disease (see Krägeloh-Mann, 2004; Fox, 2008; Sabel, 2008 for review). This adaptive reorganization of neuronal connectivity involves a spectrum of modifications: from molecular to structural plasticity (Xerri, 2008 for review).

3.1. Neuronal molecular plasticity

There is evidence of a complexity of molecular mechanisms and signaling cascades involved in the modulation of neuronal plasticity. Many of these processes are largely dependent on protein dynamics in synapses, such as neurotransmitter receptor dynamics at excitatory and inhibitory synapses or the relationship between the exchange of these receptors and scaffold proteins (Renner et al., 2008 for review). Synaptic input onto neurons initiates membrane depolarization and calcium influx into the cytoplasm. This calcium signaling triggers multiple biochemical changes and activity-dependent transcriptional programs, which are required for long-term changes in neuronal function (Greer and Greenberg, 2008; Cohen and Greenberg, 2008). Some of these molecular changes underlie the structural remodeling of neurites and synapses and, consequently, they should involve regulation of the expression of neuronal cytoskeletal proteins and proteins implicated in cell to cell and cell to extracellular matrix adhesion.

The remodeling of protein filaments in the neuronal cytoskeleton is highly regulated by conserved signaling pathways, which are known to accompany different changes in the structure of synapses, axons, dendrites and spines. In the synapse, the cytoskeleton is likely to control dynamic synaptic functions and might induce morphological changes. In fact, microtubule-associated proteins have been implicated in synapse assembly and disassembly (Roos et al. 2000, Eaton et al. 2002). Different signaling pathways are also likely to regulate the actin cytoskeleton at the synapse (Meyer and Feldman; 2002). Actin remodeling in the postsynaptic compartment can also be initiated by a number of signaling molecules, such as the EphB2 receptor tyrosine kinase, via the small Rho GTPases, Rac1 and Cdc42. Other signaling molecules associated with the Rho GTPase pathway and with actin-binding proteins are also important for maintaining spine integrity (see Dillon and Goda; 2005 for review). In addition, adhesion molecules bind to a cytoplasmic network of scaffolding proteins, regulators of the actin cytoskeleton, and signal transduction

pathways that control the structural and functional organization of synapses (Yamada and Nelson; 2007). Moreover, cell adhesion molecules (CAMs), such as N-cadherin, influence synaptic structure via indirect interactions with the actin cytoskeleton (see Dillon and Goda; 2005 for review). The neural cell adhesion molecule (NCAM) also interacts with cytoskeletal proteins. The NCAM 140 and 180 isoforms, are normally associated with α- and β-tubulin, as well as α-actinin 1. In contrast, β-actin, tropomyosin, microtubule-associated protein MAP1A, and rhoA-binding kinase-α preferentially bind to NCAM 180 (Büttner et al., 2003).

Neural cell adhesion molecules can also activate “per se” transmembrane-signalling reactions and thereby contribute to the initiation of cellular responses directed to the regulation of synaptogenesis and synaptic plasticity. L1 and NCAM, activate intracellular signaling pathways in the growth cone, mediated by two different members of the src family of nonreceptor protein tyrosine kinases (PTKs), pp60 (c-src) and p59 (fyn5,6), and this activation induces neurite outgrowth (see Maness et al., 1996 for review). NCAM is also known to stimulate neurite outgrowth by the activation of both the Ras-MAP kinase pathway and the FGF receptor-PLCg-PKC pathway (Kolkova et al., 2000). NCAM also has marked influence on both the structure of spines and their post synaptic densities (Stewart et al., 2008).

3.2. Neuronal structural plasticity

The term neuronal structural plasticity refers to all types of changes, which modify the shape and structure of the central nervous system (CNS). These morphological changes can be organized in different levels: **(a) Synaptic plasticity** (synaptogenesis and synaptic removal); (**b) Neurite remodeling** (axonal and dendritic outgrowth/retraction) **and spine remodeling**; **(c) Neuron-glia plasticity**; **(d) Neurogenesis** (proliferation of neuronal precursors, neuronal migration and incorporation to functional neuronal circuits) (Xerri, 2008, for review).

The next paragraphs will deepen into the first two levels, focusing on the current information available on structural plasticity in the adult brain.

3.2.1. Synaptic plasticity

Synaptic plasticity is a term that describes changes in the efficacy of synaptic transmission, including also the structural reorganization of synapses.

Changes in synapse number and morphology are frequently associated with learning. Raising animals in an enriched environment or training them on a motor skill-learning task results in increases in the number of synapses in the visual cortex and in various hippocampal areas, including the dentate gyrus and CA3 (see Markham and Greenough; 2004 and Bruel-Jungerman et al., 2007 for review). Stereological electron microscopy studies of the hippocampal dentate gyrus have shown that training rats to find a hidden platform in a Morris water maze induces a significant but transient increase in axo-spinous synapse density and in the ratio of synapse per neuron (Eyre et al., 2003).

There is also strong evidence pointing at different hormones as major players in synaptic remodeling. Chronic stress and glucocorticoids strongly influence synaptic plasticity (McEwen; 2005). Other steroid hormones, such as the estrogens, also influence synaptic plasticity by increasing the density of axospinous synapses in the hippocampal stratum radiatum of CA1, both after estradiol treatment and during proestrus, when estradiol levels are naturally increased (Woolley and McEwen; 1992).

Aging also has a notorious influence in synaptic plasticity, especially in the hippocampus, where a decrease in the number of synaptic contacts in the mid-molecular layer of dentate gyrus has been found in aged animals (see Rosenzweig and Barnes; 2003 for review). Similarly, the numerical density of excitatory and inhibitory synapses is reduced in the neuropil of the primate prefrontal cortex during aging (Peters et al., 2008).

3.2.2. Axonal, dendritic and spine remodeling

Plasticity associated with cognitive functions, with aversive experiences or with brain repair involves dynamic remodeling of dendritic and axonal arbors, including branch formation/elimination, as well as collateral branching and spine remodeling (Wong et al., 2000; Diana et al., 2007; Cline and Haas, 2008; William et al., 2008 for review). As it occurs with synaptic plasticity, neurite remodeling is also influenced by environmental enrichment: animals raised in this condition have an increase in dendritic branching in the visual cortex (see Markham and Greenough; 2004 for

review). Different learning paradigms also influence neurite remodeling: Passive avoidance response increases spine number in the mid-molecular layer of the dorsal dentate gyrus at different post-training times (O'Connell and Regan, 1998; O'Malley et al., 1998) and trace eye blink conditioning, an associative learning task, also increases the density of dendritic spines on the pyramidal cells in hippocampal CA1 region (Leuner et al., 2003). Fear conditioning, another learning paradigm, increases dendritic spine density in the lateral amygdala (Radley et al., 2006). Moreover, there is a strong correlation between long-term potentiation (LTP) and morphological changes in dendritic spines. Several studies have shown the possible association between this structural remodeling with LTP (see Muller et al., 2000 a; Yuste and Bonhoeffer, 2001 for review).

Abundant experiments have demonstrated that chronic stress affects dendritic branching: it induces dendritic atrophy in various hippocampal regions, like retraction and simplification of dendrites of pyramidal neurons in the CA3 region (see McEwen; 1999 and 2000 for review). Dendritic atrophy was also observed in dentate granule and CA1 pyramidal neurons (Sousa et al., 2000). Chronic stress also causes retraction of the thorny excrescences (giant spines) upon which the mossy fiber terminals form their synapses (Stewart et al., 2005). Dendritic spines also show remodeling after chronic stress: for instance in the apical dendrites of CA3 neurons, which show increased spine density (Sunanda et al., 1995). This stress-induced neurite remodeling is not restricted to the hippocampus; chronic stress also induces dendritic atrophy in the mPFC (Radley et al., 2004; Cook and Wellman, 2004). Moreover, this aversive experience also induces a reduction in spine density on proximal basal dendrites of prefrontocortical pyramidal neurons (Perez-Cruz et al., 2009). On the contrary, chronic stress promotes dendritic growth and spinogenesis in some regions of the amygdala (Vyas et al., 2002; Mitra et al., 2005).

Antidepressants also influence neurite remodeling. For instance, chronic treatment with fluoxetine, an antidepressant of the selective serotonin reuptake inhibitor class, increases the density of spine synapses in pyramidal neurons of hippocampal CA1 and CA3 regions (Hajszan et al, 2005). In the same way, chronic administration of imipramine, a tricyclic antidepressant of the dibenzazepine group, also increases the density of asymmetric spine synapses in the hippocampal CA1 region (Chen et al., 2008).

Interestingly, the effects of chronic stress on neurite structure can be reverted or blocked by antidepressant treatment. Daily treatment with tianeptine, an atypical

antidepressant (a selective serotonin reuptake enhancer), prior to stress sessions, prevented the structural effects of chronic stress in hippocampal CA3 pyramidal dendrites (Watanabe et al., 1992). Treatment with this antidepressant also prevented the dendritic hypertrophy induced by chronic immobilization stress in certain amygdaloid nuclei (McEwen and Chattarji, 2004).

The effects of stress on structural plasticity seem to be mediated by the action of glucocorticoids and excitatory aminoacids. In fact, chronic corticosterone treatment also results in dendritic atrophy of CA3 pyramidal cells (see McEwen; 1999a and 2008 for review) and a recent report has also shown decreased branching, reduction in total dendritic length and diminished number of spines in CA1 pyramidal neurons (Morales-Medina et al., 2009). Significant redistribution of apical dendrites (Wellman; 2001) and spine density (Seib and Wellman; 2003) is also observed in the mPFC of animals chronically treated with corticosterone. Neurite remodeling is also induced by corticosteroids in the amygdala (Mitra and Sapolsky, 2007; Morales-Medina et al., 2009).

Estrogens play also an important role in dendritic and spine remodeling within the CNS. Ovariectomy decreases the density of dendritic spines in the CA1 region of the hippocampus, but not in CA3, and this effect can be reversed by estradiol replacement (Wallace et al., 2006). Furthermore, an increment of spine and synapse density occurs within the natural late proestrous (Moult and Harvey, 2008), when estrogen levels are high. In the rodent mPFC, ovariectomy decreases spine densities in pyramidal neurons (Wallace et al., 2006). Long-term cyclic treatment with estradiol in ovariectomized rhesus monkeys, does not affect total dendritic length and branching in the PFC, but increases apical and basal dendritic spine density (Hao et al., 2006). The structure of amygdaloid neurons is also a target for sexual steroids: In the posterodorsal medial amygdala, dendritic spine density increases following estradiol injections and this effect is potentiated by progesterone (de Castilhos et al., 2008).

Age also influences dendritic and spine structure. Aging induces a reduction in spine density and dendritic tree extension in both sexes, in the mPFC and hippocampal CA1 of rodents. However, significant decreases in spine density have been found only in the aged mPFC (Markham and Juraska; 2002, Markham et al., 2002; Markham et al., 2005). By contrast, although aged rodents display significantly more dendritic material in basolateral amygdala, aging does not appear to influence spine density in this region (Rubinow et al., 2009).

4. CELL ADHESION MOLECULES

Neuronal structural plasticity is largely dependent on cell adhesion molecules (CAMs). CAMs are proteins located on the cell surface, which are involved in stabilizing and modulating cellular interactions with other cells or with the extracellular matrix. They are critical for the assembly of CNS architecture during developmental stages and are critical for the proper function of the mature nervous system. There are four important families of adhesion proteins according to their functional and structural resemblance. These families of CAMs are: **(a) The immunoglobulin superfamily**, which includes the neural cell adhesion molecule (NCAM) and L1; **(b) Integrins**; **(c) Cadherins**; and **(d) Selectins** (see Walsh and Doherty, 1997; Murase and Schuman, 1999; and Chothia and Jones, 1997, for review).

4.1. Neural cell adhesion molecule (NCAM)

Among CAMs, NCAM is the most studied protein regarding cellular recognition processes and it is expressed on the surface of most neurons (Hoffman et al., 1982; Friedlander et al., 1986). NCAM is a surface glycoprotein (see Gascon et al., 2007; Maness and Schachner; 2007 and Katidou et al., 2008 for review), which presents three major isoforms, generated by alternative splicing, denominated **NCAM 180**, **NCAM 140** and **NCAM 120**, based on their molecular weights (Gegelashvili et al., 1993; Olsen et al., 1993; Kramer et al., 1997). All three isoforms share identical extracellular structures, consisting on five immunoglobulin-like domains and two fibronectin-type III repeats. The extracellular domain is a globular structure composed by around 70-110 amino acids. Both NCAM 140 and NCAM 180 isoforms contain a transmembrane and an intracellular domain, but the NCAM 120 isoform lacks those domains and it is anchored to the cell membrane via a glycosylphosphatidylinositol (GPI) linkage. Consequently, only NCAM 140 and NCAM 180 isoforms are detectable in synaptosomal membranes (Persohn et al., 1989; Rougon et al., 1990) (**figure 7**).

NCAM180 has a long cytoplasmic domain (**figure 7**), it is predominantly expressed on mature neurons and it is particularly enriched at sites of cell contact and postsynaptic densities (Barthels et al., 1988; Persohn et al., 1989); NCAM140 has a shorter cytoplasmic domain (**figure 7**) and it is particularly expressed on developing neurons, mediating growth cone guidance and neurite outgrowth responses, although it can also be found in mature neurons, both in pre- and

postsynaptic densities (Persohn et al., 1989; Doherty et al., 1992). While NCAM140 is expressed both by neurons and glia (Williams et al; 1985), NCAM120 is predominantly expressed by glial cells (Bhat and Silberberg, 1986; Walmod et al., 2004). NCAM molecules interact with like molecules (homophilic interaction) and non-like molecules (heterophilic interaction) on neighboring cells or on the extracellular matrix to regulate their position and dynamic interactions with other cells by diverse signal transduction pathways (see Walmod et al., 2004 for review). The functional properties of NCAM are strongly influenced by the addition of long chains of a complex sugar, the polysialic acid (PSA) (**figure 7, figure 8**) (Rutishauser et al., 1996; Bonfanti, 2006; and Gascon et al., 2007, for review).

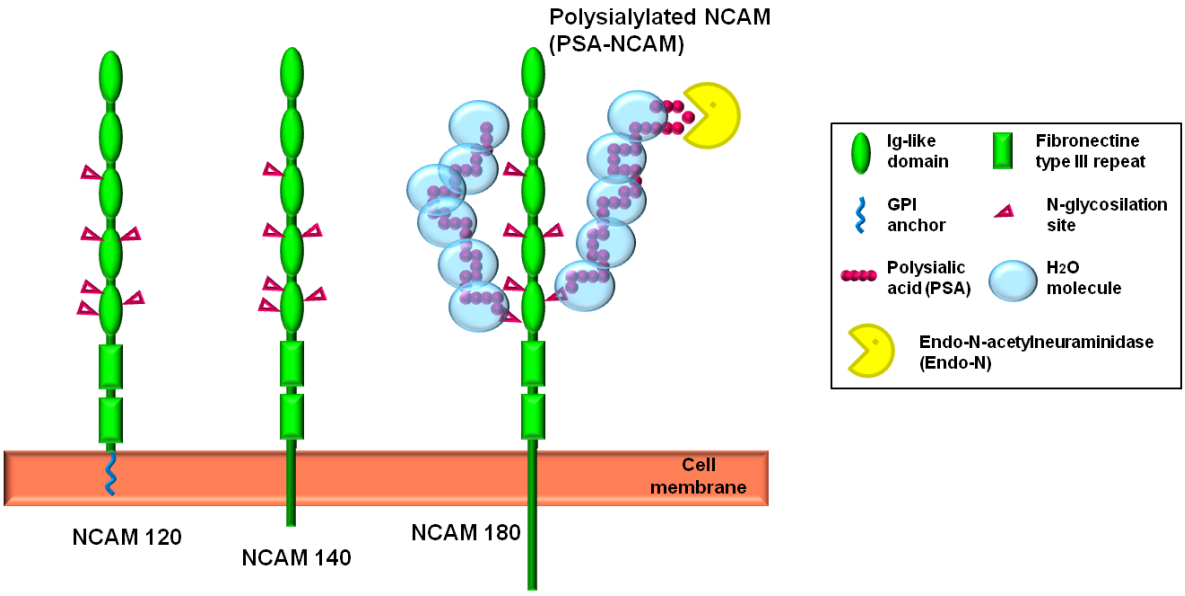

Figure 7. Scheme of the NCAM isoforms and the polysialylated form of the NCAM molecule (PSA-NCAM). The three major isoforms of the NCAM molecule (NCAM 120, NCAM 140 and NCAM 180) have identical extra-cellular structures (five immunoglobulin(Ig)-like domains and two fibronectine type III repeats), but differ in their molecular weight (120, 140 and 180 kDa, respectively) and the way in which they are anchored to the cell membrane. Whereas the NCAM 140 and the NCAM 180 isoforms contain a transmembrane and an intracellular domain, the NCAM 120 isoform lacks those domains and it is anchored to the cell membrane via a glycosylphosphatidylinositol (GPI) linkage. All isoforms can be modified by the addition of polysialic acid (PSA) on two N-glycosylation sites located in the fifth Ig-like domain. PSA is negatively charged and attracts H_2O molecules. PSA can be removed from mammals' brain by a phage enzyme, the Endo-N-acetylneuraminidase (Endo-N), that specifically cleaves α-2,8-linked N-acetylneuraminic acid polymers with a minimum chain length of 8 (see materials and methods, section 2.5, for more information).

4.2. The polysialylated form of the NCAM molecule (PSA-NCAM)

The NCAM protein core is submitted to several post-translational modifications, such as phosphorylations, addition of the carbohydrate epitopes L2 or HNK-1, sulfation, glypiation and glycosylation (see Rougon et al., 1990; Walmod et al., 2004 for review).

One of the most important glycosilation events is the addition of PSA. This unique and highly regulated post-translational modification of NCAM is critical during brain development, neural regeneration and plastic processes, including learning and memory (see Bork et al., 2007 and Hildebrandt et al., 2007 for review). In mammals, this molecule is a linear homopolymer of α-2,8-linked N-acetylneuraminic acid, which chains can extend to lengths ranging from 50 to 150 units (Kiss and Rougon, 1997; Livingston et al., 1988). PSA is attached exclusively to NCAM at the fifth immunoglobulin-like domain (**figure 7**) (Hoffman et al., 1982; Acheson et al., 1991). The degree of NCAM polysialylation is tightly regulated: PSA-NCAM levels are high during brain development but there is a progressive reduction until adulthood (see Rutishauser et al., 1996; Bonfanti; 2006 and Gascon et al., 2007a for review).

The synthesis of PSA in the Golgi compartment is catalyzed by two resident polysialyltransferases, **ST8SiaII** (also known as STX) and **ST8SiaIV** (also known as PST). Both enzymes are strongly expressed during prenatal development and this expression is dramatically downregulated after the perinatal period. During adulthood the expression of ST8SiaII and ST8SiaIV is low, but the later is more abundant than the former (Nakayama et al., 1996; Kojima et al., 1996; Hildebrandt et al., 1998 and 2008). PSA has been found also on other proteins: the α-subunit of the rat brain voltage-sensitive sodium channel (Zuber et al., 1992), SynCAM (Galuska et al., 2010), podocalyxin (Vitureira et al., 2010) and the polysialyltransferases St8SiaII and St8SiaIV, which are autopolysialylated in vivo (Close and Colley; 1998). However, NCAM is the principal carrier of PSA in the nervous system, where it has a fundamental role (see Rutishauser 1996 and 2008 for review).

Carboxyl groups give their peculiar biochemical characteristics and negative charge to PSA, attracting water and ionic molecules. This large hydrated volume inhibits cell-cell apposition (steric impediment), which prevents both the homotypic and the heterotypic binding of NCAM (**figure 8**) (Yang et al., 1992). Therefore, the post-translational addition of PSA on NCAM increases the range and magnitude of

intermembrane repulsion by increasing the nonspecific repulsive force between cells (Johnson et al., 2005). These **anti-adhesive properties** of PSA-NCAM are particularly evident during neuronal migration. This molecule is expressed by neural precursors migrating from the subventicular zone (SVZ) to the olfactory bulb by a mechanism in which the cells move forward in a stream by using each other as a substrate and PSA-NCAM enhances the cycles of adhesion and de-adhesion (Rousselot et al., 1995; Petridis et al., 2004). PSA-NCAM expression also participates in the axophilic migration of luteinizing hormone releasing neurons to the forebrain (Yoshida et al., 1999). Moreover, PSA-NCAM plays a permissive role in axon guidance, reducing the fasciculative interactions between axons and allowing them to respond more effectively to a variety of extrinsic signals and to reach their target, both in the peripheral and in the central nervous systems (see Rutishauser and Landmesser, 1996; Kiss and Rougon, 1997 ; Brusés and Rutishauser; 2001; Rutishauser 2008 for review).

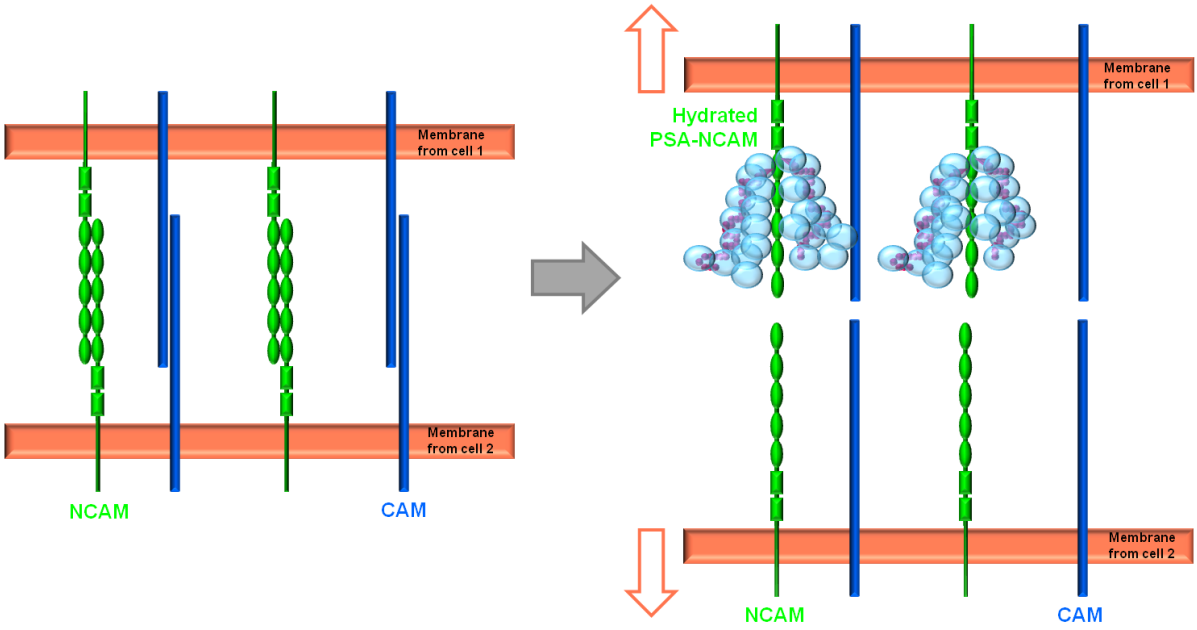

Figure 8. Illustration showing the anti-adhesive proprieties of the PSA-NCAM molecule. NCAM can be post-translationally modified by the addition of polysialic acid (PSA). PSA is negatively charged and rapidly becomes hydrated (**right**) (see also figure 7), preventing both the homotypic and heterotypic binding of NCAM by a steric impediment and, therefore, increasing the non-specific repulsive force between cells. Abbreviations: CAM, cell adhesion molecule, NCAM, neural cell adheshion molecule, PSA-NCAM, polysialylated for of the NCAM.

Multiple lines of evidence implicate NCAM in synaptic functions and suggest a role of PSA-NCAM in **synaptic strength modulation** (see Dalva et al. 2007; Dityatev et al. 2008, for review). There are several mechanisms by which PSA-NCAM might regulate synaptic strength. One possibility is suggested by the finding that

neuronal activity increases the expression PSA-NCAM on the cell surface (Muller et al. 1996; Kiss et al. 1994; Schuster et al. 1998), and enzymatic removal of PSA (by Endo-N, see **figure 7**) or its blockade with antibodies, prevents LTP, LTP-associated formation of perforated synapses and LTD in the CA1 region of the hippocampus (Becker et al., 1996; Muller et al., 1996; Dityatev et al., 2004). Hippocampus-dependent spatial learning protocols increase the expression levels of PSA-NCAM (Venero et al. 2006) and mice deficient in one of the two polysialyltransferases St8SiaII or St8SiaIV show normal basal synaptic transmission but defects in LTP and LTD in CA1 (Eckhardt et al., 2000; Angata et al., 2004). Functionally, PSA weakens homophilic NCAM interactions (Rutishauser 1996 and 2008), indicating that PSA–NCAM might mediate a downregulation of adhesion that is a prerequisite for structural changes that underlie plasticity. In this model, PSA linkage acts as a switch between structural stability and plasticity; however, this model has not been verified. PSA–NCAM might also indirectly regulate synaptic plasticity through interactions with other synaptic proteins. Currently, NCAM and PSA–NCAM have been shown to interact with a large number of molecules or signalling pathways that regulate aspects of LTP including AMPARs (Vaithianathan et al. 2004), NMDARs (Hoffman et al. 1998), brain-derived neurotrophic factor (BDNF)–tyrosine receptor kinase B (TrkB) signaling (Muller et al. 2000), the spectrin-based scaffold (Wechsler and Teichberg, 1998; Sytnyk et al., 2002; Sytnyk et al., 2006), the fibroblast growth factor (FGF) receptor (Cambon et al. 2004) and the non-receptor tyrosine kinase Fyn (Beggs et al. 1997). Unfortunately, in most of these cases, a direct link between the interactions and LTP has not been demonstrated. The exception is BDNF–TrkB signalling, where defects in LTP caused by enzymatic PSA removal are rescued by exogenous treatment with BDNF, indicating that PSA-dependent defects in LTP are due to decreased BDNF signaling (Muller et al. 2000). Nevertheless, the numerous interactions between NCAM and LTP-influencing pathways show that NCAM is a multifunctional protein capable of influencing synaptic plasticity at multiple levels (Dalva et al. 2007).

PSA expression is also important in the development and function of the **immune system**. For instance, human NK cells modulate NCAM expression and its degree of polysialylation according to their activation state (Drake et al., 2008; Drake et al; 2009).

PSA and NCAM have also a prominent role in **oncology**. These two molecules have been found in different human cancers, including small-cell lung carcinomas and multiple myeloma (Miyahara et al., 2001; Suzuki et al., 2005).

5. PSA-NCAM, ST8SiaII AND ST8SiaIV EXPRESSION IN THE ADULT mPFC

As we have commented before, although PSA-NCAM levels are very high during the embryonic and early postnatal development of the mammalian brain, the expression of this molecule during adulthood is restricted to brain regions that display a high degree of neuronal plasticity, including the mPFC (Bonfanti, 2006; Varea et al. 2005; Varea et al. 2007c; Varea et al. 2009).

In the frontal cortex of rodents, PSA-NCAM begins to be highly expressed at embryonic day 14 (E14) and its level of expression remains very high from this moment until postnatal day 5 (P5), when it starts rapidly to decrease. At P21, PSA-NCAM expression in the mPFC reaches similar levels to those found during adulthood and they continue stable until old age (Seki and Arai, 1991; Probstmeier et al. 1994; Kurosawa et al. 1997; Oltmann-Norden et al. 2008; Varea et al. 2005; Varea et al., 2009).

PSA-NCAM expression has been described in neurons and neuropil elements in the adult mPFC of both rodents (Varea et al. 2005; Gómez-Climent et al. 2010) and humans (Varea et al. 2007c). PSA-NCAM expressing cells in the rodent mPFC mainly show a multipolar morphology and they are found in all regions (IL, PrL, Cg1 and Cg2) and layers (I-VI) within the mPFC, although their density in deep layers (V-VI) is higher than in layers I-III (Varea et al. 2005; Gómez-Climent et al. 2010).

The changes observed in PSA-NCAM expression during mPFC development are in accordance with changes in the mRNA levels of both ST8SiaII and ST8SiaIV polysialyltransferases. The expression of ST8SiaII in the mPFC is very high from E14 to P5, when it dramatically begins to decrease until P14, when its level is similar to that in the adult cortex. By contrast, the decrease in ST8SiaIV expression from P5 onwards is very low and, although ST8SiaII mRNA levels are two-fold higher than those of the ST8SiaIV during embryonic and early postnatal development, ST8SiaIV is the major polysialyltransferase of the adult brain (Kurosawa et al. 1997; Angata et al. 1997; Hildebrandt et al. 1998; Ong et al. 1998; Galuska et al. 2006; Oltmann-Norden et al. 2008). Analysis of single polysialyltransferase knockout mice has revealed that ST8SiaIV is solely responsible for PSA-NCAM expression in mature

interneurons and in most regions of cortical neuropil. By contrast, ST8SiaII is the major polysialyltransferase in immature neurons of the paleocortex layer II and the hippocampal subgranular zone (Nacher et al., 2010).

5.1. Neurochemical phenotype of PSA-NCAM expressing cells in the adult mPFC

PSA-NCAM expression in the rodent mPFC can only be found in mature neurons that are not recently generated. No astrocytes, oligodendrocytes, microglial cells or pyramidal neurons are found to express this molecule. Most PSA-NCAM expressing neurons are interneurons and belong to different subpopulations, attending their co-expression of calcium binding proteins (CB, CR and PV) or neuropeptides (cholecystokinin, CCK; vasointestinal neuropeptide, VIP; neuropeptide-Y, NPY; and somatostatin, SST). Regarding the expression of calcium-binding proteins, PSA-NCAM immunoreactive neurons in the mPFC mainly co-expressed CB and rarely CR or PV. PSA-NCAM/CB double immunoreactive cells were most frequently found in deep layers (V-VI), although they could also be observed in layers II and III. The highest percentage of co-localization of PSA-NCAM expressing cells with neuropeptides was found when studying SST. These double-labeled neurons were mainly located in deep layers of both prelimbic and cingulate cortices. The co-localization with NPY, CCK and VIP was lower than that of SST. PSA-NCAM/NPY double labeled neurons were located most frequently in deep layers, especially in the cingulated cortex (Varea et al. 2005; Gómez-Climent et al. 2010). The phenotype of PSA-NCAM expressing neurons in the mPFC of adult humans (Varea et al., 2007c), mice (Gómez-Climent et al. 2010) and cats (Varea et al., unpublished results) is very similar to the phenotype described for these neurons in the mPFC of adult rats (Varea et al. 2005; Gómez-Climent et al. 2010).

6. PSYCHIATRIC AND NEUROLOGICAL DISEASES

Impairments of dopaminergic neurotransmission affecting mPFC function are implicated in the pathogenesis of several psychiatric disorders such as schizophrenia and major depression (Waxman, 2005). In Parkinson's disease, the dopaminergic system is severely affected; not only there is a massive death of dopaminergic neurons in the SN (responsible of motor symtoms), but also in the VTA, which has been related to the cognitive deficits and depressive symtoms frequently found in

these patients (Dubois and Pillon 1997; Zesiewicz and Hauser 2002). Decreased levels of D2R have been found in the mPFC of both human and animal models of schizophrenia (Knable et al. 2001; Zhang et al. 2010), major depression (Knable et al. 2001) and Parkinson's disease (Kaasinen et al. 2003).

During recent years, increasing evidences indicate that, in addition to neurochemical alterations, changes in the structure and connectivity of neurons in the mPFC may also underlie the pathogenesis of these diseases and that pharmacological treatments may revert these changes by enhancing the plasticity of neuronal connections (Sairanen et al. 2007; Varea et al., 2007a; Lewis and Gonzalez-Burgos, 2008; Solis et al., 2007). This findings support the **"neuroplastic hypothesis of depression"** and extent it to other psychiatric and neurological diseases (Duman, 2002; Castren, 2004; Castren, 2005) (**figure 9**).

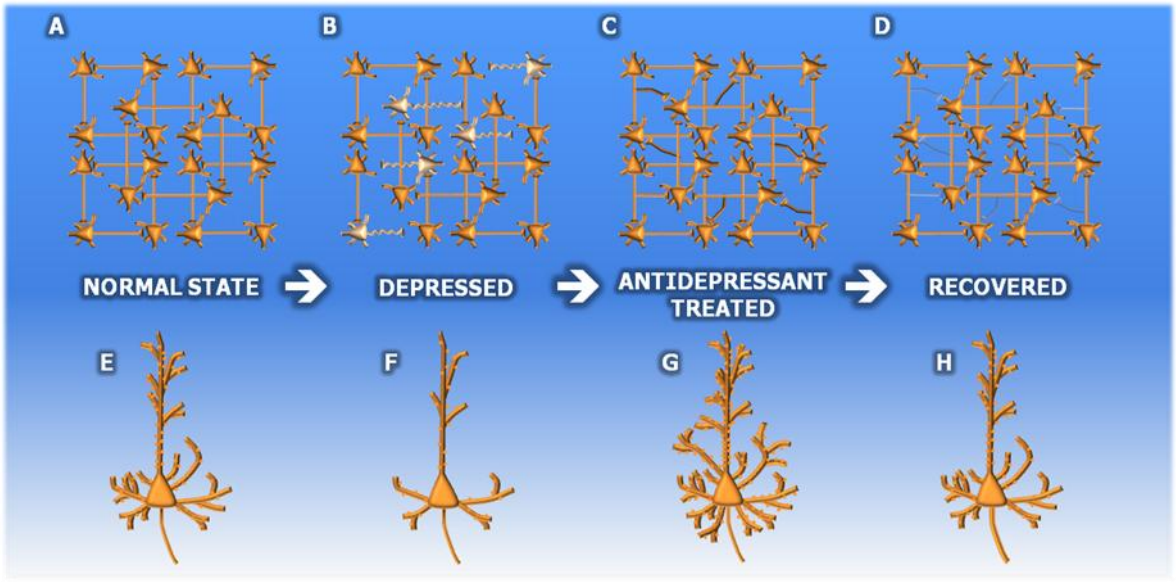

Figure 9. The "neuroplastic" hypothesis of depression. (A-E) In the healthy brain, information is processed in partially overlapping neural networks. **(B-F)** In depression, information processing in some networks may not function properly. Pyramidal neurons in the mPFC reduced their dendritic tree and spine number **(C-G)** Antidepressant treatment may enhance connectivity in neural networks. **(D-H)** Activity-dependent pruning of synapses selects out and stabilizes the active synapses and networks, and pyramidal neuron structure is then recovered. Illustrations based on Castren, 2004 and 2005, Radley et al., 2004.

Although most of the studies on neuronal structural plasticity have been focused on principal neurons (**figure 9**), there is abundant evidence that, in these psychiatric and neurological disorders, interneurons and cortical inhibitory networks show abnormalities and therefore, the neuronal plasticity of inhibitory networks may also be affected (Benes and Berretta, 2001; Daskalakis et al., 2007; Rajkowska et al., 2007; Lanoue et al. 2010).

PSA-NCAM is a good candidate to mediate these structural changes, especially in interneurons. In fact, *ncam1* and *st8siaII* are candidate susceptibility genes for schizophrenia and a long standing record links disregulation of NCAM to the pathophysiology of several neuropsychiatric disorders (for review, Vawter, 2000; Brennaman and Maness, 2008).

Chapter 2

OBJECTIVES

The **main objectives** of this thesis are to study the influence of dopaminergic neurotransmission on the neuronal plasticity of prefrontocortical circuits and to evaluate whether changes in the expression of the polysialylated form of the neural cell adhesion molecule (PSA-NCAM) are responsible for these neuroplastic changes. From these two main objectives, derive the subsequent **specific objectives**:

1. To map the distribution and analyze the morphology of PSA-NCAM expressing cells in the mPFC of adult rats.

2. To map the distribution of PSA-NCAM expressing elements in the mPFC neuropil and to characterize the neurochemical phenotype of those elements located surrounding the soma of pyramidal neurons in this cortical region.

3. To study the expression of D2R in PSA-NCAM expressing neurons in the mPFC, as well as the spatial relationship between these cells and dopaminergic terminals in this region.

4. To analyze the effects of a lesion on the mesocortical dopamine pathway and the effects of chronic treatments with D2R agonists and antagonists on the expression of PSA-NCAM and other molecules related to synapses and inhibitory neurotransmission in the mPFC.

5. To study in different time points the expression of plasticity-related genes in the mPFC during a chronic treatment with a D2R agonist.

6. To evaluate the effects of the enzymatic depletion of PSA from NCAM on the remodeling of inhibitory networks and pyramidal neurons in the mPFC and its influence on the neuroplastic changes induced by chronic treatment with D2R agonists.

Chapter

3

MATERIAL AND METHODS

1. ANIMALS

One hundred and fourteen male Sprague-Dawley rats (3 months-old, Harlan Interfauna Iberica S.L., Barcelona, Spain) were used in this doctoral thesis as follows: (i) 8 rats, to analyze the distribution PSA-NCAM expressing cells and neuropil; (ii) 4 rats, to analyze the phenotype of PSA-NCAM expressing puncta surrounding pyramidal cell somata; (iii) 4 rats, to study the relationship between PSA-NCAM neurons and D2R or dopaminergic fibers; (iv) 10 rats, for the dopamine depletion experiment (6-OHDA lesion); (v) 10 rats, for the D2R antagonist treatment (haloperidol); (vi) 12 rats, for the D2R agonist treatment (PPHT); (vii) 36 rats, for PPHT treatment destined to gene expression study; (viii) 24 rats, for PPHT treatment after PSA depletion; and (ix) 6 rats, to confirm the specificity of primary antibodies by western blot analysis (**figure 10**).

Transgenic mice pups [GIN, Tg (*gad*-GFP)-45704Swn] of postnatal day 8 (P8) were used for preparation of mPFC organotypic cultures. These animals express the green fluorescent protein (GFP) under the promoter of the *gad* gene (codifies the enzyme responsible for the synthesis of the inhibitory neurotransmitter GABA). Adult mice were purchased from Jackson laboratories (Bar Harbor, Maine, USA) and mice pups were obtained in our animal facility (**figure 10**).

1.1. General housing conditions and bioethical issues

Rats were housed in groups of three or four and were allowed to habituate to our facilities at least one week prior to the start of the experiments.

Pregnant mice were housed alone and mice pups were kept with their mothers until being used.

Animals were maintained in a temperature- and humidity-controlled environment and on a 12 h light/dark cycle with food and water available *ad libitum*.

All animal experimentation was conducted in accordance with the Directives 86/609/EEC and 2010/63/EU of the European Communities Council of November 24th 1986 and September 22nd 2010, respectively, on the protection of animals used for scientific purposes and was approved by the Committee on Bioethics of the Universitat de València. Every effort was made to minimize the number of animals used and their suffering.

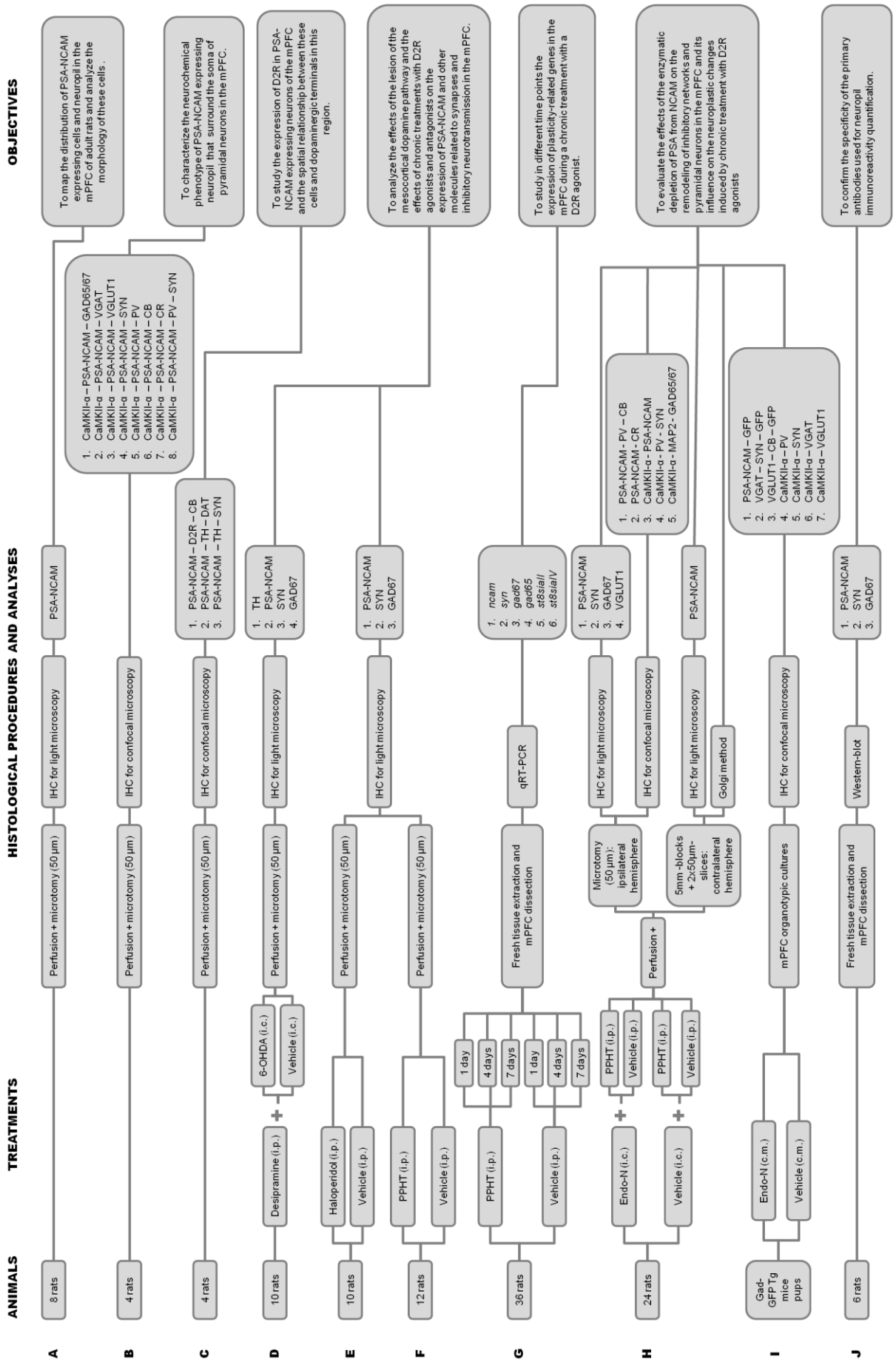

Figure 10. Scheme summarizing the animals, treatments, procedures and analyses used in this thesis. Abbreviations: c.m., culture medium; i.c., intracranial injection; i.p., intraperitoneal injection; IHC, immunohistochemistry. For antibodies abbreviations, please see table 1 or the abbreviation list on page xviii-xix.

2. PHARMACOLOGICAL TREATMENTS *IN VIVO*

2.1. 6-hydroxydopamine lesions of Ventral Tegmental Area

Ten rats were pre-treated with the norepinephrine uptake blocker, desipramine hydrochloride [25 mg/kg in 0.9% NaCl, intraperitoneal (i.p; Sigma-Aldrich)] to prevent destruction of noradrenergic nerve terminals. Thirty minutes later, they were deeply anaesthetized (5 mg/g xylazine and 0.5 ml/kg ketamine i.p.) and placed in a stereotaxic instrument (David Kopf Instruments, Tujunga, CA). A 10 µl Flexifil tapertip syringe (World Precision Instruments Inc.; Sarasota, FL) was then positioned in the VTA using the following coordinates from the atlas of Paxinos and Watson (Paxinos and Watson, 2007): Bregma – 6.00 mm, Lateral ± 0.60 mm, Deep – 8.20 mm. The needle was left in position for 1 minute and then 2 µl of 6-hydroxydopamine hydrobromide (6-OHDA, Sigma-Aldrich, 2 µg/µl in 0.9% NaCl) were injected over a 2 minutes period into one hemisphere. After the injection was completed, the needle was left in place for another 2 minutes to reduce reflux of the solution into the track of the injection needle and then withdrawn. The contralateral hemisphere was used as a control and received 2 µl of vehicle solution (0.9% NaCl) in the VTA following the same procedure. After recovery from anaesthesia, rats were returned to their cages in the colony room and were perfused transcardially 7 days later. The lesion of TH expressing somata in the VTA of the 6-OHDA injected hemisphere was confirmed by microscopic observation of a subset of sections processed for TH immunohistochemistry (see section **5.1** and **figures 10** and **11**).

2.2. Haloperidol treatment

Rats were randomly separated in 2 groups (n=5) and received either the D2R antagonist haloperidol (Sigma-Aldrich, 0.5 mg/kg/day in 0.1 N acetic acid, pH 5-6) or the vehicle solution (0.1 N acetic acid). Treatments were administered i.p. once daily for 26 consecutive days (MacDonald et al., 2005). Body weight was measured before the onset of the treatment (day 0), after 13 days of i.p injections and at the end of the treatment (day 26). Animals were perfused transcardially 24 hours after the last injection (**figure 10**).

2.3. PPHT treatment

The selective D2R agonist 2-(N-Phenethyl-N-propyl) amino-5-hydroxytetralin hydrochloride (PPHT, Sigma-Aldrich, 1.5 mg/kg/day in 0.9% NaCl) was administered to 6 rats (treated group), once daily for 7 consecutive days (Sugahara and Shiraishi, 1998). Rats from control group (n=6) received saline i.p. injections following the same procedure. Animals were weighted at the beginning (day 0), in the middle (day 4) and at the end (day 7) of pharmacological treatment, and were perfused transcardially the day after the last i.p. injection (**figure 10**).

2.4. PPHT treatment for gene expression study

Thirty-six rats were randomly assigned to 6 experimental groups (n=6) and were i.p. injected once daily either with PPHT (1,5 mg/kg/day in 0,9% NaCl; Sigma-Aldrich) or saline (0,9% NaCl) for 1, 4 or 7 consecutive days. Body weight was measured before the onset of treatments, in the middle of the experiment and at the end, and rats were sacrificed by decapitation 24 hours after the last injection in order to obtain fresh tissue (**figure 10**).

2.5. Endo-N and PPHT combined treatment

Twenty-four rats were deeply anaesthetized and received unilaterally a stereotaxic injection (see section **2.1**) of either the enzime Endo-N-acetylneuraminidase (Endo-N; 1 µl; 369 U/µl in glycerol; AbCys, Paris, France) or the vehicle solution (1 µl; 0.9% NaCl and glycerol 1:1) in the secondary motor cortex (Bregma + 1,70 mm, Lateral ± 1,00 mm, Deep – 0,80 mm; Paxinos and Watson, 2007). The Endo-N is a phage enzyme that specifically cleaves α-2,8-linked N-acetylneuraminic acid polymers with minimum chain length of 8 (see **chapter 1**, **figure 7**). It diffuses rapidly throughout the brain and removes all detectable PSA within 1 day for 3-4 weeks (Vimr et al., 1984; Hallenbeck et al., 1987). The contralateral hemisphere did not receive any injection because pilot experiments demonstrated that Endo-N also diffuses to contralateral mPFC.

Seven days later, rats which had received Endo-N (n=12) were randomly separated in 2 groups (n=6) and were administered intraperitoneally either PPHT or saline for 7 days as described in section **2.3**. The same procedure was followed for rats which had received intracranial vehicle injection (n=12). Body weight was

measured in the day of surgery (day 0), before the onset of pharmacological treatment (day 7), in the middle of pharmacological treatment (day 10) and at the end of the experiment (day 14). Animals were perfused transcardially 24 hours after the last i.p. injection (**figure 10**).

3. HISTOLOGICAL PROCEDURES

3.1. Perfusion and microtomy techniques

Rats, except those treated as described in section **2.4**, were perfused transcardially under deep chloral hydrate anesthesia, first for 1 minute with NaCl 0.9 % and then for 30 minutes with 4% paraformaldehyde in phosphate buffer (PB) 0.1 M, pH 7.4. Thirty minutes after perfusion, brains were extracted from the skull and their hemispheres were separated.

All brain hemispheres, except those destined to Golgi impregnation (contralateral hemispheres of rats described in section **2.5**), were cryoprotected with 30% sucrose in cold PB 0.1 M (4ºC) for 48 hours and then cut in 50 μm-thick coronal sections with a freezing-sliding microtome (Leica SM2000R, Leica, Nussloch, Germany). Slices were collected in 10 subseries and stored at –20 ºC in a cryoprotective solution until used (30% glycerol, 30% ethylene glycol in PB 0.1M).

Brain hemispheres destined to Golgi impregnation were washed in cold PB 0.1 M (4ºC) for one day and then cut in 5-mm-thick coronal blocks. Two 50 μm-thick coronal sections from all slices containing mPFC were obtained with a vibratome (Leica VT 1000E, Leica, Nussloch, Germany) in order to check whether Endo-N also diffused to contralateral mPFC (see section **5.1**). Blocks were then impregnated by Golgi method as described below (see section **6**).

See a summarizing scheme in **figure 10**.

3.2. Fresh tissue extraction and dissection of mPFC

Rats treated as described in section **2.4** were sacrificed by decapitation using a guillotine. Brains were immediately removed from the skull and placed on Petri dishes filled with cold sterile PB. Under a stereo microscope (SZX7; Olympus) the overlying pia was removed and coronal cuts were made to remove portions of the rostral and caudal poles. The mPFC from the left and right cortices were dissected with a micro scalpel and then stored on separated eppendorfs. Tissue was frozen in

liquid nitrogen and kept at -80ºC until used. The whole procedure was performed at cold temperature and under RNAse-free conditions to prevent RNA degradation.

4. MEDIAL PREFRONTAL CORTEX SLICE CULTURES

4.1. Preparation of slice cultures

P8 transgenic mice pups [GIN, Tg (*gad*-GFP) 45704Swn] were decapitated and their brains were removed from the skull under sterile conditions. Brains were placed into Petri dishes filled with cold (4º C) sterile dissecting medium [1% glucose (0.5 gr/mL, MERCK), 0,2% penicillin/streptomycin, 0,1% hexamycin, 0,5% L-glutamin, 0,05% fungizone (GIBCO) in GBSS (Life Technologies)]. The overlying pia was gently removed and coronal cuts were made to remove portions of the rostral and caudal poles, leaving the frontoparietal region intact. The right and left cortices were cut simultaneously in the coronal plane at a thickness of 350 µm with a McIlwain^{TM} Tissue Chopper. Slices were then transferred into dissecting medium and separated gently by agitation.

Slices containing mPFC were placed on moistened translucent membranes of tissue culture inserts (0.4 µm, Millicell-CM, Millipore, Bedford, MA, USA) and immersed in 1 mL of Serum-OPTIMEM culture medium [25% heat inactivated horse serum, 25% HBSS, 50% Optimem-1 (GIBCO) supplemented with 10 µL/mL glucose (0,5 gr/mL, MERCK)]. Three slices were cultured in the same insert and six inserts were placed together in six-well plates. To ensure that slices from control and treated group were cultured under identical conditions, three inserts from each plate were designated as “control group” and other three, to “treated group”.

Cultures were stored in a humid atmosphere at 36°C, in 5% CO_2 for 14 days (HERAcell® 150i, Thermo Scientific) and culture medium was changed twice a week.

4.2. Delivery of Endo-N

After 12 days *in vitro* (DIV 12), 2 U/mL of the enzyme Endo-N was added to the culture medium in slices from treated group, whereas slices from control group received the same amount of vehicle solution (glycerol) in their culture medium. Two days before (DIV 14), slices were fixed as described below (section **4.3**).

4.3. Histological processing of slices

Slices were fixed by immerse the inserts for 30 minutes in a solution of 4% paraformaldehyde in 0.1M phosphate buffer (PB; pH 7.4) and then washed with PB intensively. Because pilot experiments had demonstrated that our mPFC slices used to decrease their thickness to 150-200 µm, tissue was not cut in thinner sections before being processed for the immunohistochemistry.

In order to separate the slices that had been cultured in the same insert, insert membranes were cut surrounding each slice and then slices were stored at 4ºC fully immersed in PB 0.1M.

5. IMMUNOHISTOCHEMICAL STUDY

All the antibodies employed in this doctoral thesis and its dilutions and incubation conditions can be found in **Table 1**. For each experiment, all the studied sections passed through all procedures simultaneously to minimize any difference from immunohistochemical staining itself. To avoid any bias in the analysis, all slides were coded prior to the analysis and the codes were not broken until the experiment was finished.

5.1. Immunohistochemistry for conventional light microscopy

Tissue was processed "free-floating" for immunohistochemistry using the avidin-biotin-peroxidase (ABC) method as follows. Fifty µm-thick sections were first treated for 1 minute with an antigen unmasking solution (0.01 M citrate buffer, pH 6) at 100ºC. After cooling down sections to room temperature, they were incubated with 3% H_2O_2 in phosphate buffered saline (PBS) for 10 minutes to block endogenous peroxidase activity. After this, sections were treated for 1 hour with 10% normal donkey serum (NDS; Jackson ImmunoResearch Laboratories, West Grove, PA) in PBS with 0.2% Triton-X100 (Sigma-Aldrich, St. Louis, MO) and then, they were incubated with the appropriate primary antibody (**table 1**) in PBS with 0.2% Triton-X-100 and 5% NDS.

Next, sections were incubated for 1 hour with the right biotinilated secondary antibody (**table 1**) in PBS with 0.2% Triton-X-100 and 5% NDS, followed by a 30 minutes treatment with an avidin-biotin-peroxidase complex in PBS (ABC; Vector Laboratories, Peterborough, UK). Color development was achieved by incubating

with 3,3'- diaminobenzidine tetrahydrochloride (DAB; Sigma-Aldrich) and 0.033% H_2O_2 for 4 minutes.

Finally, sections were mounted on slides, dried for one day at room temperature, dehydrated with ascending alcohols and rinsed in xilol. After this, sections were coverslipped using Eukitt mounting medium.

PSA-NCAM immunohistochemistry was performed in tissue from control rats (to describe PSA-NCAM expression in mPFC neuropil and cells) and from rats described in **2.1, 2.2, 2.3** and **2.5**, to analyze effects of each treatment on PSA-NCAM expression in the mPFC or the effectiveness of Endo-N (**2.5**).

SYN and GAD67 immunohistochemistry was performed in brain sections from **2.1, 2.2, 2.3** and **2.5** experiments, in order to study how treatments affected the mPFC neuropil expression of those proteins.

Tissue from **2.1** experiment containing VTA, was processed for TH immunohistochemistry in order to confirm the lesion (**figure 11**).

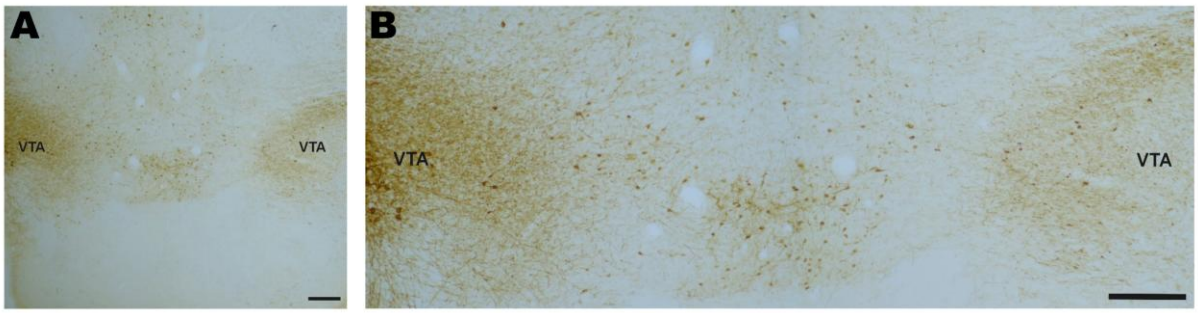

Figure 11. (A,B) Microphotographs comparing the TH immunoreactivity in the Ventral Tegmental Area (VTA) of a 6-OHDA-treated hemisphere (A and B, right) with its contralateral vehicle-treated (control) hemisphere (A and B, left). Observe a lower intensity in the 6-OHDA injected VTA when compared with the control VTA. Brain section. located at Bregma -5,00 mm (coordinates derived from the atlas of Paxinos and Watson, 2007) Scale bar: 250 µm.

Brain sections from animals treated as described in **2.5** were processed for VGLUT1 immunohistochemistry to study the effect of the treatment on VGLUT1 neuropil expression.

A summarizing scheme of these procedures can be found in **figure 10**.

5.2. Immunohistochemistry for confocal microscopy

In general, tissue was processed "free-floating" for immunohistochemistry as described above (section **5.1**) but omitting the endogenous peroxidase block. Sections were incubated with a cocktail of two, three or four primary antibodies and then with the appropriate fluorescent secondary antibodies (**table 1**). Finally, sections

were mounted on slides and coverslipped using DakoCytomation fluorescent mounting medium (Dako North America Inc., Carpinteria, CA).

When it was necessary to use two primary antibodies generated in mouse in the same immunohistochemisty, sections were first processed for one of them (primary and secondary antibody) and next, they were incubated with the other primary antibody generated in mouse. After that, sections were treated for 2 h with an excess of unconjugated goat anti-mouse IgG Fab fragments (1:100; Jackson ImmunoResearch Laboratories, West Grove, PA) in order to be recognized before by an anti-goat fluorescent secondary antibody, avoiding crossing reactions (Lewis Carl et al. 1993).

“Goat anti-mouse IgG subclass 1 specific” was used for the detection of anti-CaMKII-α primary antibody when other primary antibody generated in mouse was also being used. Because this secondary antibody was conjugated with biotin, the Avidin, NeutrAvidin®, Texas Red® conjugate (1:200, Molecular Probes) or streptavidin, Alexa Fluor ® 488 conjugate were used before to detect biotin (see table 1).

To analyze the neurochemical phenotype of PSA-NCAM expressing puncta surrounding pyramidal neuron somata in the mPFC, triple immunostainings in brain sections from control rats were performed. PSA-NCAM and CaMKII-α (pyramidal neuron marker) were labeled in all of them and additionally markers of inhibitory elements (GAD65/67), synapses (SYN), inhibitory (VGAT) or excitatory (VGLUT1) synapses and interneuron subpopulations (PV, CR, CB). A quadruple immunostaining (CaMKII-α - PSA-NCAM - PV - SYN) was also performed in order to know whether perisomatic puncta co-expressing PSA-NCAM and PV corresponded to synapses.

Brain sections from control rats were also used in order to study whether PSA-NCAM neurons co-expressed dopamine D2R (PSA-NCAM – D2R – CB triple immunostaining) and whether they showed dopaminergic fibers close to their somata (PSA-NCAM – TH – DAT and PSA-NCAM – TH – SYN triple immunostainings).

In tissue from rats described in section **2.5**, we performed the following immunostainings: PSA-NCAM - PV - CB and PSA-NCAM - CR (to analyze the neurochemical phenotype of PSA-NCAM expressing neurons after treatment); CaMKII-α - PSA-NCAM, CaMKII-α - PV - SYN and CaMKII-α - MAP2 - GAD65/67 (to

study perisomatic and/or peridendritic innervations of mPFC pyramidal neurons after treatment).

Medial prefrontal cortex slice cultures from Gad-GFP transgenic mice (section **4**) were immunostained as follows: PSA-NCAM – GFP (to check Endo-N efficiency and to study its effects on the density of dendritic spines in GFP expressing interneurons); VGAT – SYN – GFP and VGLUT1 – CB – GFP (to study the effects on the neuropil expression of these proteins); CaMKII-α – PV, CaMKII-α – SYN, CaMKII-α – VGAT and CaMKII-α – VGLUT1) (to study perisomatic innervations of mPFC pyramidal neurons after treatment).

See a summarizing scheme in **figure 10**.

Table 1. Primary and secondary antibodies

Primary antibodies (abbreviated names)	**Host**	**Isotype**	**Dilution**	**Incubation**	**Company**	**References**
Anti-CB	Rabbit	IgG	1:2000	O/N, 4ºC	Swant	Hédou et al., 2002
Anti-CR	Rabbit	IgG	1:2000	O/N, 4ºC	Swant	Schwaller et al., 1993
Anti-CaMKII-α	Mouse	IgG1	1:500	36 h, 4ºC	Abcam	Benson et al., 1992
Anti-DAT	Rat	IgG2a	1:200	O/N, 4ºC	Chemicon-Millipore	Freed et al., 1995
Anti-D2R	Rabbit	IgG	1:200	O/N, 4ºC	Chemicon-Millipore	Brock et al., 1992
Anti-GAD67	Mouse	IgG2a	1:500	O/N, 4ºC	Chemicon-Millipore	Varea et al., 2005
Anti-GAD65/67	Rabbit	IgG	1:1000	O/N, 4ºC	Chemicon-Millipore	Benagiano et al., 2007
Anti-GFP	Chicken	IgY	1:1000	O/N, 4ºC	Chemicon-Millipore	Kain et al., 1995
Anti-MAP2	Mouse	IgG1	1:2000	O/N, 4ºC	Sigma-Aldrich	Riederer and Matus, 1985
Anti-PSA-NCAM	Mouse	IgM	1:700	36 h, 4ºC	Abcys	Theodosis et al, 1991
Anti-PV [1]	Rabbit	IgG	1:2000	O/N, 4ºC	Swant	Miettinen et al., 1996
Anti-PV [2]	Guinea pig	IgG	1:2000	36 h, 4ºC	Synaptic Systems	www.sysy.com
Anti-SYN [3]	Mouse	IgG1	1:500	O/N, 4ºC	Sigma-Aldrich	Devoto and Barnstable, 1989
Anti-SYN	Rabbit	IgG	1:1000	O/N, 4ºC	Chemicon-Millipore	Hanaya et al., 2007
Anti-TH	Mouse	IgG1	1:200	O/N, 4ºC	Chemicon-Millipore	Höckfelt et al., 1977
Anti-VGAT	Rabbit	IgG	1:1000	O/N, 4ºC	Synaptic Systems	Takamori et al.,2000
Anti-VLUT1	Guinea pig	IgG	1:2000	O/N, 4ºC	Chemicon-Millipore	Melone et al., 2005

Secondary antibodies	**Host**	**Label**	**Dilution**	**Incubation**	**Company**
Anti-Chicken IgY	Donkey	DyLight™488	1:400	1 h, 25ºC	Jackson immunoResearch
Anti-Guinea pig IgG	Donkey	Biotin-SP	1:400	1 h, 25ºC	Jackson immunoResearch
Anti-Guinea pig IgG	Donkey	Cy™5	1:400	1 h, 25ºC	Jackson immunoResearch
Anti-Mouse IgM	Donkey	Biotin-SP	1:400	1 h, 25ºC	Jackson immunoResearch
Anti-Mouse IgM	Goat	Alexa Fluor® 555	1:400	1 h, 25ºC	Molecular Probes
Anti-Mouse IgG	Donkey	Biotin-SP	1:400	1 h, 25ºC	Jackson immunoResearch
Anti-Mouse IgG [4]	Goat	Unconjugated	1:100	2 h, 25ºC	Jackson immunoResearch
Anti-Mouse IgG1 [4]	Goat	Biotin-SP	1:400	2 h, 25ºC	Jackson immunoResearch
Anti-Rabbit IgG	Donkey	Alexa Fluor® 488	1:400	1 h, 25ºC	Molecular Probes
Anti-Rabbit IgG	Donkey	Alexa Fluor® 647	1:400	1 h, 25ºC	Molecular Probes
Anti-Rat IgG	Donkey	Alexa Fluor® 488	1:400	1 h, 25ºC	Molecular Probes
Anti-Rat IgG	Goat	Alexa Fluor® 647	1:400	1 h, 25ºC	Molecular Probes

[1] Used in CaMKIIα - PSA-NCAM - PV triple immunohistochemistry.

[2] Used in CaMKIIα - PSA-NCAM - SYN- PV quadruple immunohistochemistry.

[3] Used in SYN immunohistochemistry for light microscopy.

[4] Used in multiple-labeling experiments for the detection of a primary antibody generated in mouse when other primary antibody generated in mouse was also being used. For instance, we have used anti-mouse IgG1 for the detection of anti-CaMKIIα and then, the Avidin-NeutrAvidin®- Texas Red® conjugate (1:200, Molecular Probes) or streptavidin-Alexa Fluor ® 488 conjugate were used before to detect biotin.

Abbreviations: CB, calbindin-D28k; CR , calretinin; CaMKIIα, α subunit of the Ca^{2+} /calmodulin dependent protein kinase II; DAT, dopamine transporter; D2R, dopamine D2 receptor; GAD67, 67 kDa isoform of the glutamate decarboxilase enzime, GAD65/67, both 65 and 67 kDa isoforms of the glutamate decarboxilase enzyme; GFP, green fluorescent protein; MAP2, Microtubule associated protein 2; PSA-NCAM, polysialylated form of de neural cell adhesion molecule; PV, parvalbumin; SYN, synaptophysin; TH, tyrosine hydroxylase; VGAT, vesicular γ-aminobutyric acid (GABA) transporter; VGLUT1, vesicular glutamate transporter 1.

6. GOLGI METHOD

In rats treated as described in section **2.5**, contralateral hemispheres relatives to the side of the injection were cut into 5-mm thick coronal blocks (section **3.1**) and processed by Golgi-Colonnier method (Colonnier, 1964) with some modifications described before (Guirado et al. 2009). In brief, blocks were post-fixed with 3% potassium dichromate and 5% glutaraldehyde for 7 d at 4ºC and then impregnated with 0.75% silver nitrate solution for 48 hours. Blocks were then cut into 150 µm-thick coronal sections with a vibratome, dehydrated with ascending alcohols and mounted with epoxy resin between two coverslips.

To avoid any bias in the analysis, the slides were coded and the code was not broken until the analysis was completed.

7. GENE EXPRESSION STUDY

7.1. RNA isolation

Frozen brain tissues from rats described in section **2.4** were homogenized in tubes containing TriPure reagent (Roche Applied Science, Indianapolis, IN) and total RNA was obtained by means of a one-step sample homogenization/lysis procedure. TriPure Isolation Reagent disrupted cells and denatured endogenous nucleases. Then, chloroform was added to the sample and the mixture was centrifuged. This step separates the sample into three phases: a colorless aqueous (upper) phase, a white interphase and a red organic (lower) phase. The upper phase was placed in a separate tube and RNA was recovered from it by isopropanol precipitation. Finally, RNA was isolated by alcohol precipitation steps.

Purified total RNA was eluted in RNase-free water and stored at -80 ºC. RNA concentration and purity was measured in a spectrophotometer at 260 nm and 260/280nm, respectively (Eppendorf BioPhotometer plus; Eppendorf AG, Hamburg, Germany).

7.2. cDNA synthesis by RT-PCR

Reverse transcription (RT) reactions were performed as follows: 2 µl oligo dTplus [10 pmol] were hybridized to 1 µl of total RNA (100ng/µl) in 10,5 µl volume by heating up to 65 ºC for 10 min. First strand cDNA was then synthesised by incubating

the hybridized RNA at 43 ºC for 60 min with dGTP, dTTP, dCTP, dATP (1 mM each),1 µl Expand reverse transcriptase (50 U/ µl), 0,5 µl Protector RNAse inhibitor (40 U/µl), 2 µl 1,4-dithio-DL-threitol (DTT, 100 mM) in 20 µl Buffer for Expand reverse transcriptase. All products were purchased from Roche Applied Science. cDNA reactions were then diluted fivefold in nuclease-free water.

The quality of cDNA was checked by agarose gel electrophoresis after PCR amplification. Only the former small amplicon but not the latter larger amplicon was detected in all samples on the agarose gel electrophoresis, demonstrating no contamination of samples with genomic DNA (data not shown).

7.3. DNA oligonucleotide primers

Specific primers to rat *gad67, gad65, ncam, st8siaII, st8siaIV* and *syn* genes were designed from public sequences, which were obtained from Ensembl data base using “Primer 3” free software. Primers were designed between exons to avoid DNA contamination. The sequence of primers for the reference gene (*ywhaz*) was obtained from Bonefeld et al. 2008. See **table 2**, for further details.

All DNA oligonucleotide primers were custom synthetized by Metabion international AG (Martinsried, Germany).

Table 2. DNA oligonucleotide primers

Rat target gene	Primers	Sequence (5’ →3’)	Amplicon size[(1)]
gad65	Forward	CTGCTTCTGGTTTGTACCTCCT	122
	Reverse	CCATTGTGGTCCCATACTCC	
gad67	Forward	CTGGAGCTGGCTGAATACCT	120
	Reverse	TCGGAGGCTTTGTGGTATGT	
ncam	Forward	AACGGACTCCAAACCATGAC	123
	Reverse	CTGGCTTTGCTTCTGACTCC	
st8siaII	Forward	GGCAACTCAGGAGTCTTGCT	123
	Reverse	GTCAGTCTTGAGGCCCACAT	
st8siaIV	Forward	CCTTCATGGTCAAAGGAGGA	125
	Reverse	CCAGTAACCTCTGACCGCAT	
syn	Forward	CTATGGGCAGCAAGGCTATG	120
	Reverse	CAGGCCTTCTCTTGAGCTCTT	
ywhaz	Forward	TTGAGCAGAAGACGGAAGGT	136
	Reverse	GAAGCATTGGGGATCAAGAA	

[(1)] Amplicon length in base pairs.

7.4. Real-time quantitative RT-PCR

The amplification reactions were performed in triplicate in 10 µl SYBR Green PCR master mix 2X (Applied Biosystems), 4 µl cDNA (50ng) and 1 µl forward and reverse primers (240 nM each; see table 2) and 5 µl of water for a total volume of 20 µl. The termocycler was an ABI PRISM 7700 Sequence Detector (Applied Biosystems). The cycling parameters were 95 ºC 15 s, 60 ºC 1 min for 40 cycles, after one initial step at 95 ºC, 10 min, which was set to activate the AmpliTaq Gold polymerase.

Ct (cycle threshold) values were calculated by the StepOne Software v2.0 (Applied Biosystems) from fluorescence readings, and these values were converted into copy number per copy number of reference gene (*ywhaz*). Primer specificity was checked by analyzing the dissociation curve method according to the Applied Biosystems protocol.

8. ANALYSIS OF RESULTS

8.1. Body weight analysis

In rats described in sections **2.2-2.5**, body weight differences across the different time points were calculated, and data were analyzed by unpaired Student's t-tests or one-way ANOVA tests followed by multiple pair-wise comparisons with Bonferroni's correction.

8.2. Quantification of neuropil immunoreactivity

This study was performed in brain sections from rats treated as described in sections **2.1, 2.2, 2.3 and 2.5** and processed for PSA-NCAM, SYN, GAD67 or VGLUT1 immunohistochemistry for conventional light microscopy (section **5.1**) in order to analyze treatment effect on the neuropil expression of those proteins.

From each immunostaining, three sections per animal were selected randomly from the following coordinate intervals [IL: Bregma 2.70 to 2.20 mm; PrL: Bregma 3.70 to 2.20 mm; Cg: Bregma 1.70 to -0.26 mm (Paxinos and Watson, 2007)]. Sections were examined with an Olympus CX41 microscope under bright-field illumination, homogeneously lighted and digitalized using a CCD camera. Photographs to the different areas and layers were taken at 20X magnification. A

Nissl stain in alternate series of sections was used for determining layer and area boundaries within mPFC regions, based on cytoarchitectural differences across these layers and areas (**figure 12**).

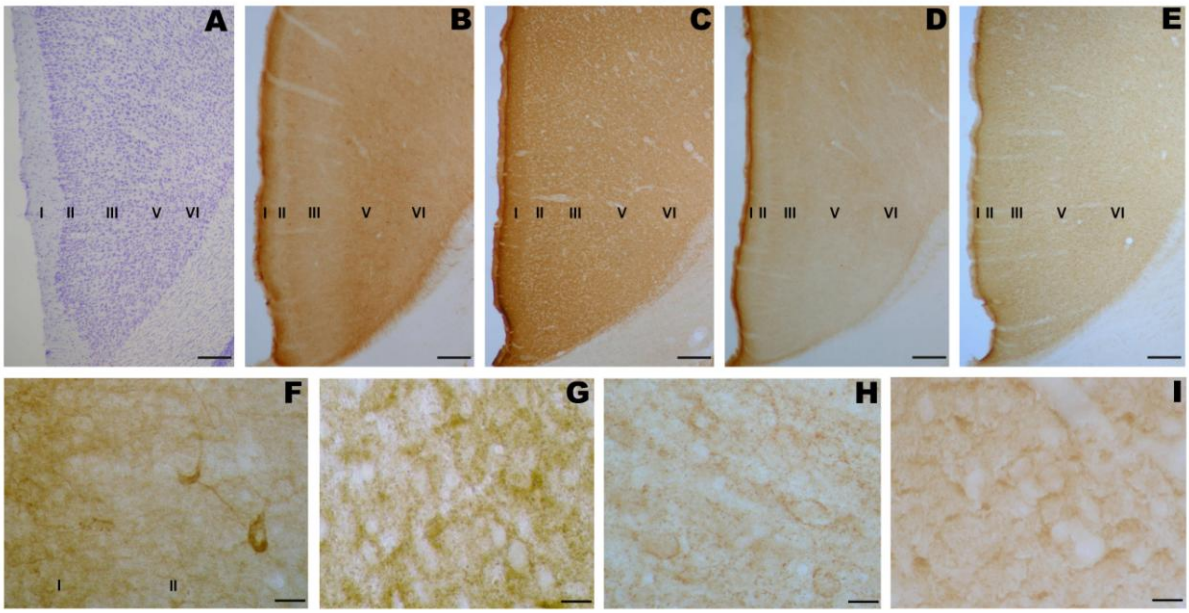

Figure 12. Panoramic and detailed views of the rat cingulate cortex showing the distribution of PSA-NCAM (B, F), SYN(C, G), GAD67 (D, H) and VGLUT1 (E, I) immunoreactivity in the neuropil. (A) A Nissl stain (cresyl violet) is used for determining layer boundaries within mPFC regions, based on cytoarchitectural differences across these layers. (F) Detailed view of PSA-NCAM immunoreactivity in layer I and II of the rat cingulate cortex. PSA-NCAM expressing neurons can be observed in layer II. Detailed view of (F) SYN GAD67 (G) and VGLUT1 immunoreactivity in layer III of the cingulate cortex. Scale bars: 250 µm for A-E and H-I; 20 µm for F-I. Roman numbers indicate cortical layers.

Grey levels were converted to optical densities (OD) using Image J software (NIH). Means were determined for each experimental group and data were subjected to paired Student's t-test followed by Bonferroni's correction (6-OHDA experiment, section **2.1**) or to repeated-measures ANOVA (for the rest of experiments) using the SPSS software package (version 17).

In repeated measures ANOVA, region (IL, PrL, Cg1 and Cg2) and layer (I, II, III, V, VI) were considered as within-subjects variables (repeated measures variables) and treatment (Haloperidol, Control; PPHT, Control; Endo-N/PPHT, Endo-N/Control Control/PPHT, Control/Control), as between-subjects variable. The sphericity assumption in repeated measures variables and the homogeneity of variances in between-subjects variable were first assessed by means of the Mauchly's test of sphericity and the Levene's test for homogeneity of variances. Levene's test indicated that there were homogeneity of variances in between-subjects variable ($p>0.05$) in all cases. The assumption of sphericity in repeated measures variables (Mauchly's test) was violated ($p<0.05$) for the main effect of layer and for the region x

layer interaction for PSA-NCAM, SYN, GAD67 and VGLUT1 neuropil immunoreactivity, as well for the main effect of region for PSA-NCAM, GAD67 and VGLUT1. Therefore, degrees of freedom on the univariate repeated measures ANOVA test were adjusted using Greenhouse-Geisser correction for those variables. For all protein neuropil expression, ANOVA test showed significant main effects of treatment, region and layer ($p<0.05$, see results section), so multiple pair wise-comparisons with Bonferroni's correction were performed for each immunostaining in order to evaluate treatment effect on mPFC. The three-way interaction (region x layer x treatment) on the repeated measures ANOVA test was also significant for all protein neuropil expression ($p<0.05$, see results section). Multiple pair-wise comparison with Bonferroni's correction were performed in each case, in order to analyze in which specific layer from each region inside the mPFC there were differences between groups (see results section).

8.3. Estimation of the total number of PSA-NCAM expressing somata

This quantification was performed in brain sections from the Endo-N/PPHT combined treatment experiment (section **2.5**) processed for PSA-NCAM immunohistochemistry for conventional light microscopy (section **5.1**). Since Endo-N intracranial injection results in an absolute absence of PSA-NCAM immunoreactive neurons in the mPFC (see **figure 49** in **chapter 6**, section **1.2**), only non-Endo-N injected animals were analyzed.

The number of PSA-NCAM expressing neurons within the different layers and regions of mPFC was estimated using a modified version of the fractionator method (West, 1993), as described before (Nacher et al. 2002; Varea et al. 2007a). PSA-NCAM expressing somata covering 100% of the sample area were counted, that is, within each 50 µm-thick section, all labeled cells found in the selected region (infralimbic, prelimbic, dorsal cingulate and ventral cingulate cortices) and layer (I, II, III, V and VI). The fractionator sampling scheme refers to the methodology of examining one out of every ten brain sections. Thus, our modification of the optical dissector combined with a 1:10 fractionator sampling is truly a modification of the optical fractionator method. One from 10 systematic-random series of sections covering the whole rostral to caudal extension of mPFC was viewed on an Olympus CX41 microscope. Cell somata were identified and counted with a 40X objective. Cells appearing in the upper focal plane were omitted to prevent counting cell caps.

Means were determined for each experimental group (Control/PPHT, Control/Control) within each region and layer from the mPFC area. The normality of the variables and homogeneity of variances were first assessed by means of the Shapiro-Wilk´s normality test and the Levene's test for homogeneity of variances. These tests showed that all the variables followed a normal distribution ($p > 0.05$) and all samples had equal variances ($p>0.05$). Data were then subjected to unpaired Student's t-test statistical analysis followed by Bonferroni's correction.

8.4. Observation and quantification of multiple-labeled fluorescent cells

Sections double or triple labeled for PSA-NCAM and different markers (section **5.2**) were observed under a confocal microscope (Leica TCS-SPE) using a 63X oil objective. PSA-NCAM expressing cells were first identified using conventional fluorescence microscopy and then, z-series of optical sections (1 µm apart) covering all its three-dimensional extension were obtained using sequential scanning mode. These stacks were processed with LSM 5 image software. In each immunostaining, fifty PSA-NCAM immunoreactive neurons per animal inside the mPFC [from Bregma + 3,20 mm to - 1,40 mm (Paxinos and Watson, 2007)] were randomly selected to determine the co-expression of PSA-NCAM and each marker. Percentages of co-localization were determined for each animal and means ± S.E.M. were calculated.

In tissue from animals described in section **2.5.**, the data were subjected to unpaired Student's t-test statistical analysis (Control/PPHT vs. Control/Control) followed by Bonferroni's correction.

8.5. Quantification of perisomatic/peridendritic puncta of mPFC pyramidal neurons

8.5.1. Co-localization of perisomatic PSA-NCAM expressing puncta and different markers

Sections triple or quadruple labeled for CaMKII-α, PSA-NCAM and different markers (section **5.2**) were mainly observed as described above (section **8.4**) but with some differences. From each animal and immunostaining, fifty CaMKII-α expressing neurons from mPFC layers III and V and displaying triangular-shaped soma were randomly selected by conventional fluorescence microscopy. Z-series of optical sections (0.5 µm apart) were acquired using sequential scanning mode and

stacks were processed with LSM 5 Image Browser software at 4X-Zoom magnification. The soma profile of these neurons was drawn and puncta placed within an area 0.5 µm distal from the edge of this profile were analyzed. A puncta was defined as having an area not smaller than 0.15 and not larger than 2.5 μm^2 (Di Cristo et al., 2007). The co-localization of PSA-NCAM and each of the different markers was analyzed on five consecutive confocal planes from each selected neuron, in which the penetration of both antibodies was optimal. The percentage of puncta co-expressing PSA-NCAM and each marker was obtained for each neuron and mean ± S.E.M was determined. Puncta density values were also determined for each marker and expressed as number of puncta per micron of soma perimeter.

8.5.2. Analysis and comparison of perisomatic puncta density after Endo-N/PPHT combined treatments or Endo-N delivery in vitro

For this purpose, we used brain sections from rats treated with Endo-N and/or PPHT (section **2.5**) or slices from mPFC organotypic cultures (section **4**), which were triple immunostained for CaMKII-α and other markers (see **5.2**). Tissue was observed and analyzed as described above (**8.5.1**) but in this case, six pyramidal neurons per slice were analyzed as we will describe below for other analyses.

Values of puncta density for PSA-NCAM, GAD65/67, PV, SYN or VGAT were obtained from each neuron and expressed as number of puncta per micron of soma perimeter. For each experimental group, mean ± S.E.M. was determined and the resulting values were analyzed by one-way ANOVA with the number of neurons as the “n”. Significant effects were further analyzed by Student-Newman-Keuls post-hoc test. In Endo-N and/or PPHT treated animals, the percentage of PV puncta co-expressing SYN was also obtained from each neuron and analyzed following the same procedure.

8.5.3. Analysis and comparison of GAD65/67 peridendritic puncta density after Endo-N / PPHT treatments.

In general, GAD65/67 immunoreactive puncta were observed and analyzed as described before (section **8.5.2**) but in this case, neurons should follow these features in order to be suitable for the study: (i) they must express both CAMKII-α and MAP2, (ii) their soma shape must be unequivocally pyramidal (iii) we should be able to follow clearly the apical dendrite until 200 µm from the soma. The profile of

these apical dendrites was drawn and puncta were counted using LSM 5 Image Browser Software as described above (section **8.5.1**). Values of puncta density were expressed as the number of puncta per micron of dendrite length. For each experimental group, mean ± S.E.M. was determined and the resulting values were analyzed by one-way ANOVA with the number of neurons as the "n". Significant effects were further analyzed by Student-Newman-Keuls post-hoc test.

8.6. Analysis of dendritic spine density in mPFC pyramidal neurons after Endo-N / PPHT treatments

Dendritic spine density was analyzed following a previously described methodology (Magariños et al., 1996; Guirado et al. 2009) in rat tissue processed by Golgi-Colonnier method (section **6**). From each animal, six pyramidal neurons from layers III and V inside mPFC area were randomly selected. In order to be suitable for dendritic spine analysis, neurons should follow these features: (i) they must display complete Golgi impregnation of the apical dendrite, (ii) the cell type must be identifiable and (iii) the minimum length of the apical dendrite must be 200 µm from the soma. Each neuron was traced at 1000x magnification using a light microscope with a camera lucida drawing tube attachment (Nikon, Japan) and spines were quantified in four successive segments of 50 µm distances up to a total length of 200 µm. Overall spine density values or densities per segment were expressed as number of spines/µm length. For each experimental group, mean ± S.E.M. was determined and the resulting values analyzed by one-way ANOVA with the number of neurons as the "n". Significant effects were further analyzed by Student-Newman-Keuls post-hoc test.

8.7. Analysis of dendritic spine density in cultured GAD-GFP expressing interneurons after Endo-N delivery *in vitro*

From each slice, six GFP-expressing neurons located in mPFC layer III were examined by confocal microscopy at 100X magnification. In order to be analyzed, neurons had to fulfill the following features: (1) the measured dendrite must not be truncated, (2) dendrite length must be greater than 180 µm, and (3) the soma must be located at least 30 µm deep from the surface of the tissue. These cells were first identified using conventional fluorescence microscopy and then, Z-series of optical sections (0.1 µm apart) covering all its three-dimensional extension were acquired

using sequential scanning mode. Stacks were processed with LSM 5 Image Browser software at 4X-Zoom magnification and spines were quantified in three successive segments of 60 μm distances up to a total length of 180 μm. Spine density values (overall or per segment) were expressed as number of spines/μm length. For each experimental group, mean ± S.E.M. was determined and the resulting values were analyzed by unpaired Student's t-test with the number of neurons as the "n".

8.8. Estimation and comparison of neuropil puncta density after Endo-N delivery *in vitro*

The density of neuropil puncta expressing Gad-GFP, VGAT, VGLUT1, SYN or CB was analyzed in mPFC, layer III. From each immunostaining, slices from the same rostral-caudal level were examined under a confocal microscope (Leica TCS SPE) using a 100X oil objective. Z-series of optical sections (0.5 μm apart) were obtained using sequential scanning mode and processed with LSM 5 Image software. The values of acquisition settings, such as the laser intensity percentage, gain and offset were identical for each stack taken from the same area. Subsequently, confocal images, in which the same level of antibody penetrability was observed, were chosen from each stack. Then, the background fluorescence of each image was subtracted. Due to the density and proximity of puncta, these were divided into three size groups: from 4 to 22 pixels, from 23 to 33 pixels and from 34 to infinite. This last group was not taken into account, since it only represented fibrillar processes. Then, images were normalized and thresholded and puncta were counted automatically using ImageJ software. All slides were coded prior to analysis and the codes were not broken until the experiment was finished. Means ± S.E.M were determined for each experimental group and data were subjected to unpaired Student's t-test.

8.9. Gene expression data analysis

The analysis of gene expression in rats treated as described in **2.4**, was performed by means of the "$2^{-\Delta\Delta C_T}$ method" (Livak et al., 2001) where,

$\Delta\Delta C_T = (C_{T,\text{target gene}} - C_{T,\text{ reference gen}})_{\text{exp. group}} - (C_{T,\text{target gene}} - C_{T,\text{ reference gen}})_{\text{control group}}$

The resulting values were subjected to one-way ANOVA with Bonferroni's correction.

9. SPECIFICITY OF PRIMARY ANTIBODIES

The specificity of all the primary antibodies employed in our study has been tested and confirmed by their commercial providers using western blot analysis of rat brain homogenates. In addition, the commercial providers and/or previous studies have tested them by immunohistochemistry in paraformaldehyde fixed rat brains (see references on **table 1**). All these antibodies showed a regional and cellular immunolabeling distribution comparable to that of their respective antigens with the same or other equally selective antisera. In order to confirm that some of the immunostaining was not produced by the secondary antibodies or by the immunohistochemical protocol, we have omitted primary antibodies or have substituted them by normal donkey serum. These controls resulted in a complete absence of immunostaining in every case.

In addition, we performed western blot analysis to confirm the specificity of the primary antibodies used for neuropil immunoreactivity quantification (**figure 13**). Six male Sprague-Dawley rats (3 months old) were sacrificed by decapitation, their brains were removed and their mPFC were dissected out. Samples were immediately frozen in liquid nitrogen and kept at -80ºC until use. For protein extraction, tissue was homogenized in 1% NP40, 0.1% SDS, 0.5% Sodium deoxycholate, 150 mM NaCl and 50 mM Tris-HCl (pH 8.0) containing a mixture of protease inhibitors (Sigma). Samples were kept in rotation at 4ºC for 2 hours and then, centrifugated at 12000 rpm and 4ºC for 20 minutes. Supernatant was assessed for the amount of protein using Bradford reagent (Sigma) at 595 nm with BSA as the standard. Protein extract was boiled for 1 minute in reducing electrophoresis buffer and then, samples containing 20 µg of protein were resolved on 8% (for PSA-NCAM western blot) or 10% (for SYN and GAD67 western blot) SDS-polyacrylamide gels at 32 mA, 250 V for 2 hours. Prestained broad-range protein ladders (Fermentas International Inc, Canada, USA) were included to measure molecular weight of individual bands. The proteins were transferred overnight at 20 V, 350 mA at 4ºC onto nitrocellulose sheets (BioRad Laboratories, Hercules, CA, USA). After saturation of the nonspecific sites with 5% non-fat dry milk in TBS-T (50 mM Tris-HCl pH 7.4, 150 mM NaCl, 0.1% Tween-20), the blots were incubated at room temperature for 2 hours with antisera directed against PSA-NCAM (1:1000), SYN (1:2000) or GAD67 (1:1000). Membranes were then washed and incubated with horseradish peroxidase-conjugated goat anti-

mouse IgM (1:3000; Sigma) or goat anti-mouse IgG (1:2500; Sigma), respectively, in blocking buffer for 1 h at room temperature. Immunoreactive bands were detected with the enhanced chemiluminescence system, ECL (Amersham Pharmacia, Piscataway, NJ, USA) exposing later the blots to Kodak XAR-5 film (Sigma). Control for PSA-NCAM western blot (lane 2) was performed treating samples containing 20 µg of mPFC protein with 1 µl of EndoN (Abcys). Controls for SYN and GAD67 immunoblotting (lane 2) were carried out using the same amount of total protein isolated from rat liver tissue instead of mPFC tissue. Since PSA-NCAM western blot rendered a wide band probably due to different polysialylation levels, we have also tested the specificity of the anti-PSA antibody using sections from control male rats injected intracerebrally with EndoN (Abcys), an enzyme that depletes exclusively PSA from NCAM. In these sections, no immunostaining could be detected in the mPFC.

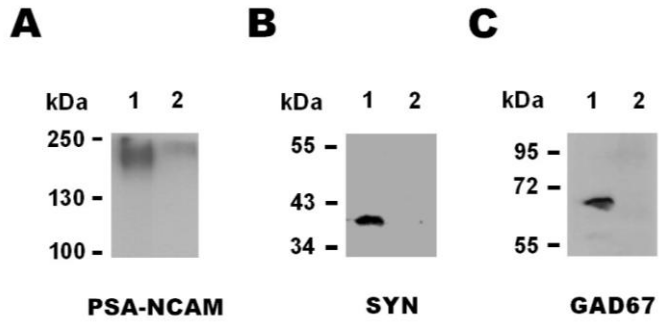

Figure 13. Representative immunoblots of total protein isolated from rat mPFC tissue (lane 1) showing specific immunoreactivity for (A) PSA-NCAM, (B) SYN and (C) GAD67. Molecular weight markers are indicated, and demonstrate that the observed bands migrate at the expected weight of approximately (A) 180–220°kDa for PSA-NCAM, (B) 38 kDa for synaptophysin and (C) 67 kDa for GAD67. Lane 1 = 20 µg of rat mPFC total protein; lane 2 (A) = 20 µg of rat mPFC total protein treated with 1 µl of Endo-N; lane 2 (B, C) = 20 µg of total protein isolated from rat liver tissue.

Chapter 4

RESULTS (I)

PSA-NCAM expression in the mPFC of adult rats

1. PSA-NCAM EXPRESSING CELLS IN THE ADULT mPFC

1.1. Distribution and morphology of PSA-NCAM expressing cells

PSA-NCAM expressing somata were found in all the regions [Infralimbic cortex (IL), prelimbic cortex (PrL), dorsal cingulate cortex (Cg1) and ventral cingulate cortex (Cg2)] and all the layers (I, II, III, V and VI) of the mPFC (**figure 14**). They were more abundant in deep layers (V-VI) than in layers II–III and their presence in layer I was scarce.

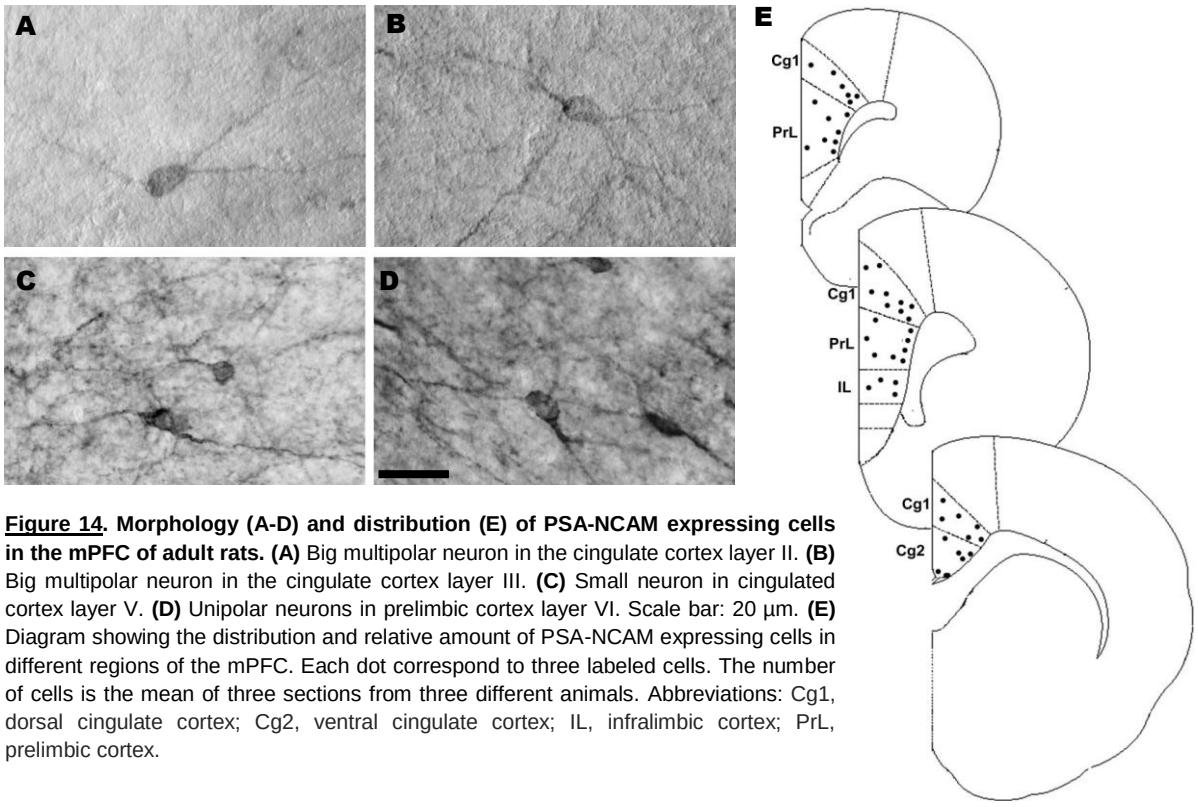

Figure 14. Morphology (A-D) and distribution (E) of PSA-NCAM expressing cells in the mPFC of adult rats. (A) Big multipolar neuron in the cingulate cortex layer II. **(B)** Big multipolar neuron in the cingulate cortex layer III. **(C)** Small neuron in cingulated cortex layer V. **(D)** Unipolar neurons in prelimbic cortex layer VI. Scale bar: 20 µm. **(E)** Diagram showing the distribution and relative amount of PSA-NCAM expressing cells in different regions of the mPFC. Each dot correspond to three labeled cells. The number of cells is the mean of three sections from three different animals. Abbreviations: Cg1, dorsal cingulate cortex; Cg2, ventral cingulate cortex; IL, infralimbic cortex; PrL, prelimbic cortex.

PSA-NCAM expressing cells from layer I, were middle-sized (soma diameter aprox. 20 µm) with a rounded soma. In layers II and III, two types of PSA-NCAM immunoreactive cells could be observed: a) frequently found small cells (soma diameter < 20 µm) with fusiform morphology and b) scarce large cells (soma diameter 30–40 µm), frequently multipolar, showing immunoreactivity in their somata and proximal processes (**figure 14 A, B**). In layers V and VI, there were also two types of PSA-NCAM immunoreactive cells: a) scarce large multipolar cells (similar to those described in layer III), and b) more abundant small cells showing only a single process (**figure 14 C, D**). Large cells were found mainly in layer V, whereas small cells appeared equally in layer V and VI. All the regions of mPFC showed this cellular

distribution pattern. The only difference among regions was the presence of a layer of highly stained big cells in the upper limit of layer V in the infralimbic cortex. Big multipolar cells resembled those described in the piriform cortex layer III (Nacher et al., 2002a) and the hippocampal “non-granule” PSA-NCAM immunoreactive neurons (Nacher et al., 2002c).

Confocal microscopic analysis showed that PSA-NCAM immunoreactivity in cells was located in the periphery and appeared absent from the central region of the cytoplasm and the nucleus (please, see **figure 16 C, D1-2, F1-3** in section **2.2**).

2. PSA-NCAM EXPRESSION IN THE mPFC NEUROPIL

2.1. Distribution of PSA-NCAM expression in the neuropil

In the PrL and IL cortices the intensity of PSA-NCAM neuropil staining was higher than that of the Cg1 and Cg2 cortices.

All regions within the mPFC showed a moderate intensity of staining in layer I, nearly lack of staining in layer II, weak staining in layer III and intense staining in layers V–VI (**figure 15**).

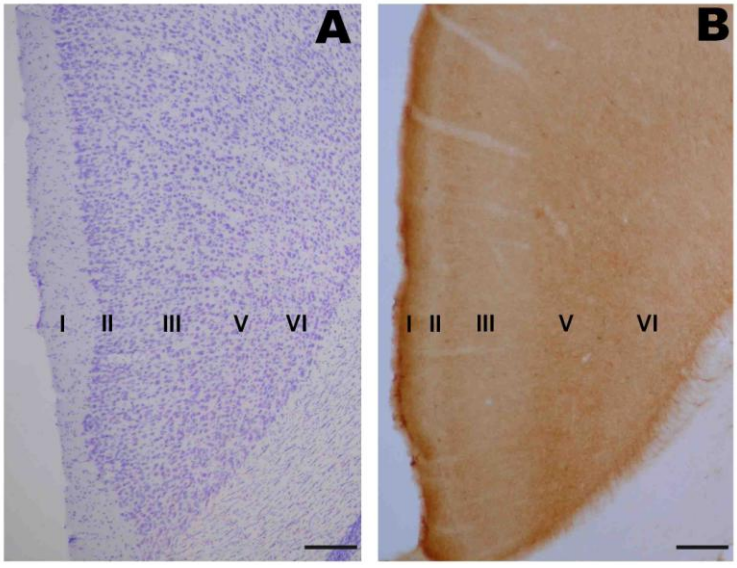

Figure 15. Panoramic views of the rat cingulated cortex showing the laminated distribution of PSA-NCAM expression in the neuropil. (A) Cresyl violet staining. **(B)** PSA-NCAM immunostaining, showing a moderate intensity of staining in layer I, nearly lack of staining in layer II, weak staining in layer III and intense staining in layers V–VI. Roman numbers indicate cortical layers. Scale bar: 250 µm.

2.2. Pyramidal neuron somata are surrounded by PSA-NCAM expressing puncta

Pyramidal neurons in the mPFC of adult rats do not express PSA-NCAM (Gomez-Climent et al. 2010) but some PSA-NCAM expressing puncta, particularly in layers III and V, were found delineating the profiles of the soma and the juxtasomatic portion of the principal apical dendrite of mPFC pyramidal neurons. The mean density of these puncta was 0.368 ± 0.014 puncta/µm of soma perimeter (**figure 16**).

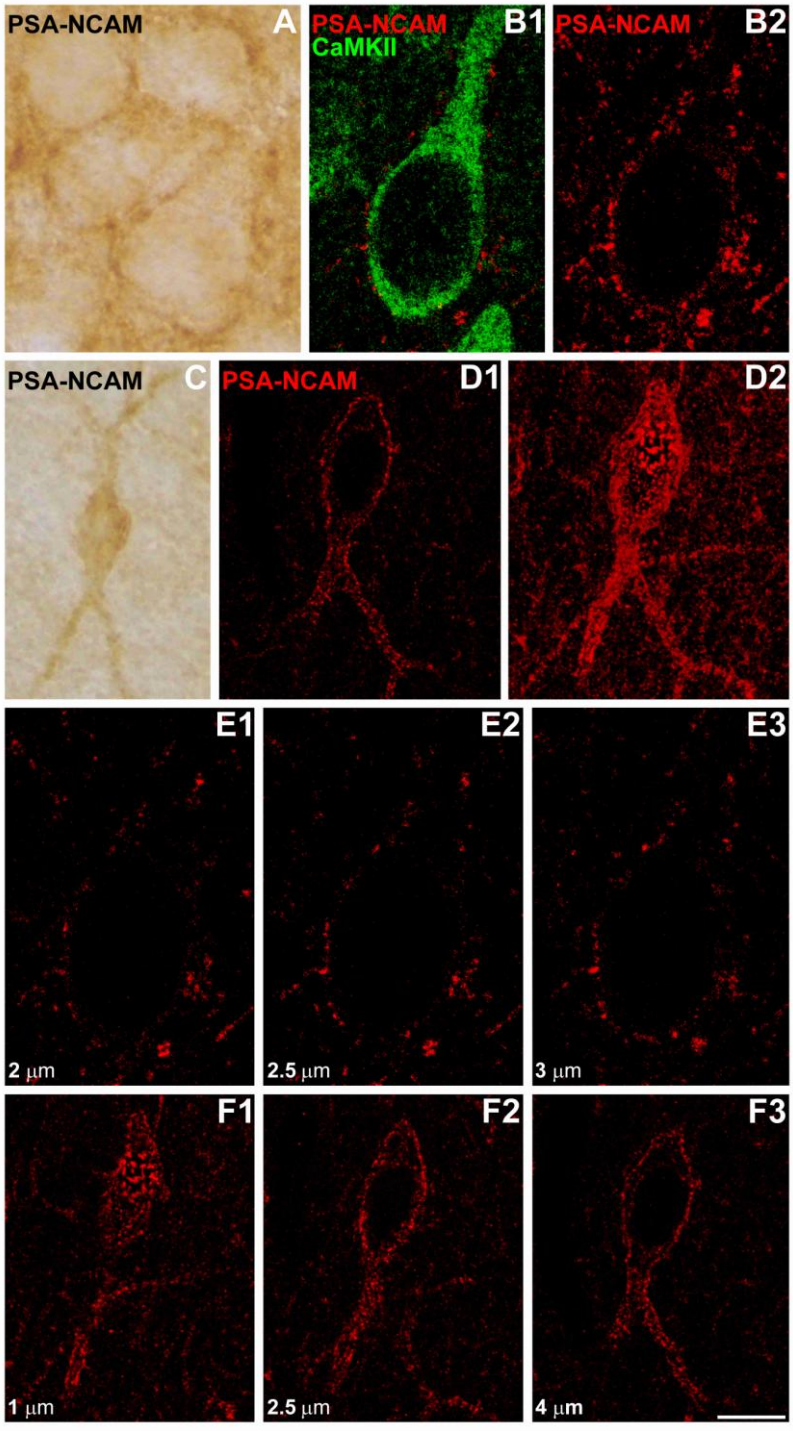

Figure 16. PSA-NCAM immunostaining in interneurons and surrounding pyramidal neurons in the rat cingulate cortex, layer V. (**A)** Pyramidal neuron, conventional optical microscopy with DAB immunostaining. Note the presence of several immunoreactive puncta surrounding non-labeled somata. **(B)** Pyramidal neuron, laser confocal microscopy with fluorescent immunostaining. **B1** is a single confocal plane where the soma shows CAMKII expression (a marker of principal neurons), and it is surrounded by external PSA-NCAM immunoreactive puncta. **B2** is a 2D projection of ten consecutive focal planes located 0.5 µm apart. (**C & D)** For comparative purposes we also show microphotographs of a PSA-NCAM expressing neuron in the cingulate cortex, as revealed with conventional optical microscopy with DAB immunostaining (C) and laser confocal microscopy with fluorescent immunostaining (D). D1 is a single confocal plane and D2 is a 2D projection of ten consecutive focal planes located 0.5 µm apart. **(E & F)** Three selected consecutive confocal planes from the 2D projections shown in B2 and D2 respectively. Scale bar: 10 µm for A, B, D and F; 6.5 µm for C and 11.5 µm for E.

2.2.1. *Most PSA-NCAM expressing perisomatic puncta on mPFC pyramidal neurons express inhibitory or synaptic markers*

PSA-NCAM expressing perisomatic puncta mainly co-expressed markers of inhibitory elements or synapses, such as GAD65/67 (36.073 ± 2.704%; **table 3**, **figure 17 A)** or VGAT (38.363 ±1.005%; **table 3, figure 17 B**) and rarely co-expressed VGLUT1 (2.545±0.461%; **table 3, figure 17 C**), a marker of excitatory synapses. The synaptic vesicle protein SYN was also frequently found in PSA-NCAM expressing perisomatic puncta (34.338 ± 1.858%; **table 3, figure 17 D**).

Because PSA-NCAM expressing perisomatic puncta were shown to be mainly inhibitory, the co-expression in these puncta of the interneuron subpopulation markers PV, CR and CB was also studied. This analysis revealed that the highest percentage of co-localization occurred with PV (40.621 ± 1.469%; **table 3, figure 18 A**), whereas the co-localization with CR (2.890 ± 0.087%; **table 3, figure 18 C**) or CB (2.415 ± 0.039%; **table 3, figure 18 D**) was very low. The density of PV expressing perisomatic puncta was substantially higher than that of puncta expressing CB or CR (see **table 3**).

In order to know whether perisomatic puncta co-expressing PSA-NCAM and PV corresponded to synapses, we analyzed the co-localization of these molecules with SYN. Surprisingly, despite the high percentage of co-localization of PSA-NCAM with either PV or SYN in the perisomatic region (see above) and the high density of puncta co-expressing PV and SYN (**table 3**), only 1.990 ± 0.138 % of PSA-NCAM puncta co-expressed both PV and SYN (**table 3, figure 18 B2**). These triple labeled puncta were present in a very low density (0.007± 0.001puncta/µm of soma perimeter; **table 3**).

Table 3. Puncta surrounding pyramidal neurons somata in the mPFC

Puncta immunoreactive for:	Puncta density (puncta/μm)[(a)]	Co-localization percentage (%)[(b)]
PSA-NCAM	0.368 ± 0.014	
GAD65/67	0.330 ± 0.040	
VGAT	0.565 ± 0.003	
VGLUT1	0.171 ± 0.006	
SYN	0.604 ± 0.072	
CB	0.027 ± 0.001	
CR	0.052 ± 0.008	
PV	0.402 ± 0.021	
PV– SYN	0.319 ± 0.017	
PSA-NCAM – GAD65/67	0.093 ± 0.018	36.073 ± 2.704
PSA-NCAM – VGAT	0.184 ± 0.006	38.363 ± 1.005
PSA-NCAM – VGLUT1	0.004 ± 0.001	2.545 ± 0.461
PSA-NCAM – SYN	0.163 ± 0.013	34.328 ± 1.858
PSA-NCAM – CB	0.010 ± 0.001	2.415 ± 0.039
PSA-NCAM – CR	0.010± 0.001	2.890 ± 0.087
PSA-NCAM –PV	0.179 ± 0.004	40.621 ± 1.469
PSA-NCAM – PV – SYN	0.007± 0.001	1.990 ± 0.138
GAD65/67 – PSA-NCAM	0.093 ± 0.018	28.114 ± 2.891
VGAT – PSA-NCAM	0.184 ± 0.006	32.948 ± 0.869
VGLUT1 – PSA-NCAM	0.004 ± 0.001	1.923 ± 0.423
SYN –PSA-NCAM	0.163 ± 0.013	26.831 ± 0.908
CB – PSA-NCAM	0.010 ± 0.001	42.977 ± 3.690
CR – PSA-NCAM	0.010± 0.001	20.624 ± 1.122
PV – PSA-NCAM	0.179 ± 0.004	43.331 ± 3.622

(a) Puncta density data are expressed as mean ± s.e.m. of puncta expressing the named marker/s per micron of soma perimeter.

(b) Co-localization percentage of puncta expressing the first named marker which also expresses the second or second and third named marker/s (i.e. PSA-NCAM – GAD65/67 co-localization percentage: percentage of PSA-NCAM expressing puncta which also express GAD65/67). Data are expressed as mean± s.e.m.

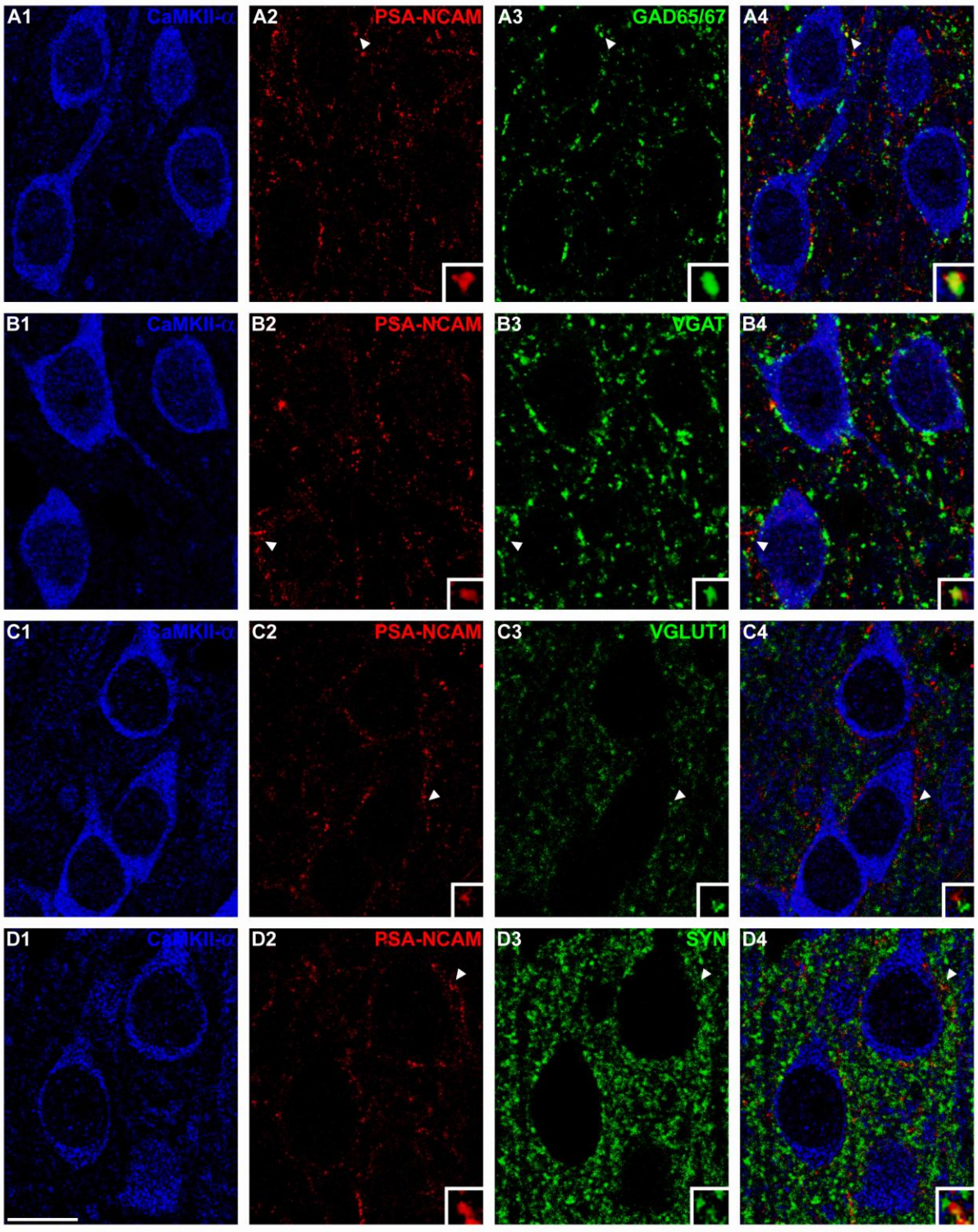

Figure 17. Confocal microscopic analysis of the neurochemical phenotype of PSA-NCAM immunoreactive puncta surrounding pyramidal cell somata in mPFC. (A) PSA-NCAM-expressing puncta co-localizing with GAD67 in the perisomatic region of CaMKII-α expressing neurons. **(B)** PSA-NCAM / VGAT double-labeled puncta surrounding CaMKII-α immunoreactive neurons. **(C)** Lack of co-localization between perisomatic PSA-NCAM-expressing puncta and VGLUT1-expressing puncta. **(D)** Perisomatic puncta co-expressing PSA-NCAM and SYN. All the images in this figure are taken from single confocal planes. Scale bar: 10 µm. Insets in the images are 5X enlargements of puncta marked with arroheads.

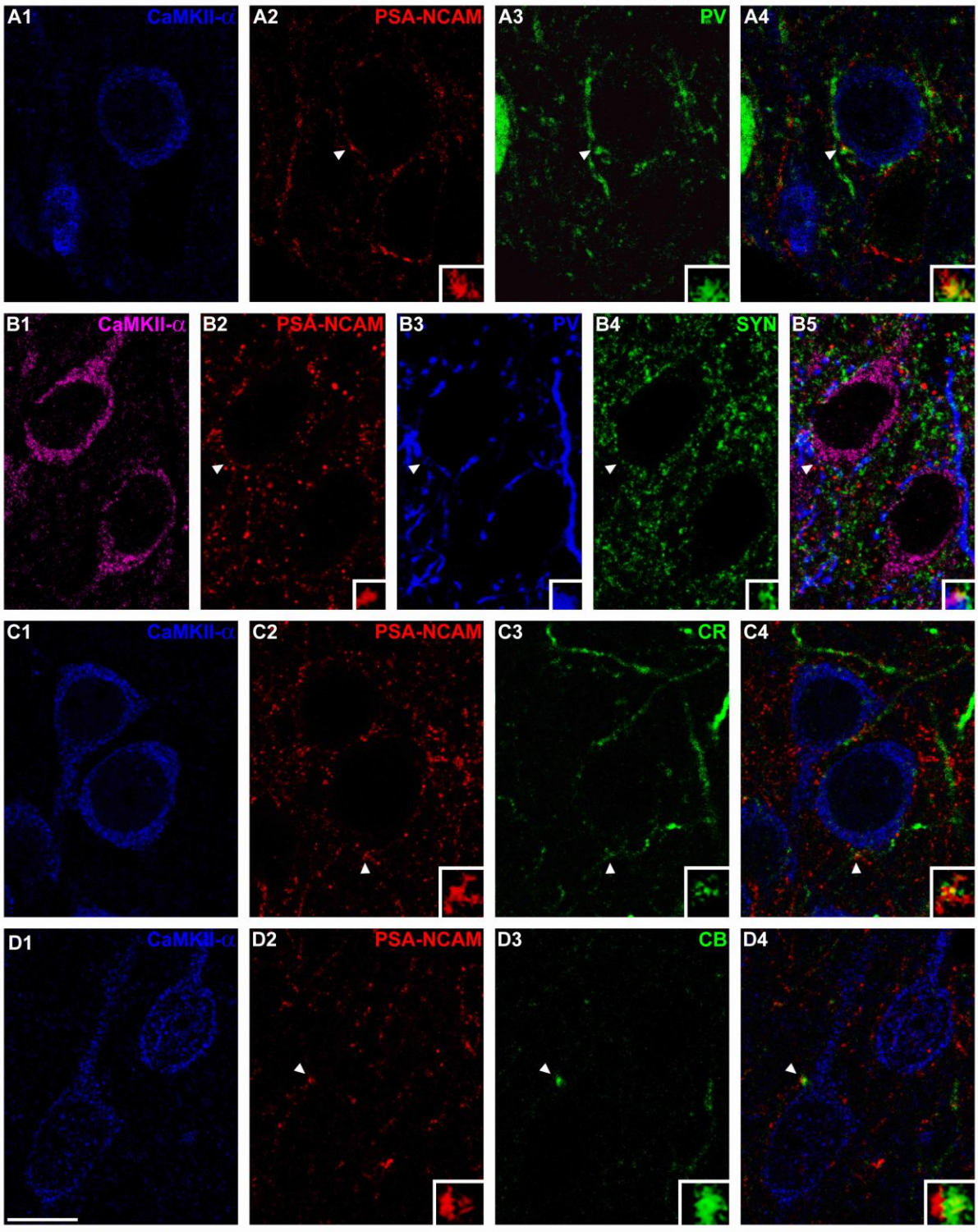

Figure 18. Confocal microscopic analysis of the co-expression of PV, CR and CB in PSA-NCAM immunoreactive puncta surrounding pyramidal cell somata in mPFC. (A) PSA-NCAM-expressing puncta co-localizing with PV immunoreactive puncta in the perisomatic region of a neuron expressing CaMKII-α. (B) Very few perisomatic PSA-NCAM immunoreactive puncta co-expressed both PV and SYN. (C) PSA-NCAM immunoreactive puncta co-expressing CR surrounding CaMKII-α expressing neurons. (D) Observe a CB-expressing puncta close to a PSA-NCAM expressing puncta in the perisomatic region of a pyramidal neuron. All the images in this figure are taken from single confocal planes. Scale bar: 10 µm. Insets in the images are 5X enlargements of puncta marked with arrowheads.

3. RELATIONSHIP BETWEEN PSA-NCAM EXPRESSING NEURONS AND DOPAMINERGIC INNERVATION IN THE ADULT mPFC

3.1. PSA-NCAM expressing interneurons co-express dopamine D2 receptors

Confocal microscopic analysis of brain sections triple immunostained for PSA-NCAM, dopamine D2 receptors (D2R) and calbindin (CB) revealed that 76 ± 3 % of PSA-NCAM immunoreactive cells in the mPFC co-expressed the D2R. Moreover, 86 ± 4 % of these double labeled cells were calbindin expressing interneurons (**figure 19 A1-4**).

3.2. Dopaminergic fibers in the mPFC are closely apposed to PSA-NCAM expressing neurons

In order to analyze the spatial relationship between PSA-NCAM expressing neurons and dopaminergic terminals in the mPFC, we performed a double immunohistochemistry for PSA-NCAM and Tyrosine hydroxylase [TH, the enzyme that catalyzes the conversion of the amino acid tyrosine to L-dihydroxy-phenylalanine (L-DOPA), the precursor for dopamine, which, in turn, is a precursor for norepinephrine]. Fibers containing TH were denser in layers I-III and they were sparse in the inner layers. Many TH immunoreactive fibers and puncta were observed in close apposition to PSA-NCAM expressing neurons (**figure 19 B & C**). Triple immunohistochemistry for PSA-NCAM, TH and SYN revealed that some of these PSA-NCAM/TH immunoreactive puncta also expressed SYN (**figure 19 D & E**).

Because TH expressing fibers could be dopaminergic or norepinephrinergic (see TH definition above), a triple immunostaining for PSA-NCAM, TH and the dopamine transporter (DAT) was performed to confirm that TH fibers observed close to PSA-NCAM interneurons were dopaminergic. Many TH/DAT double-labeled fibers and puncta were observed close to PSA-NCAM expressing neurons (**figure 19 F & G**).

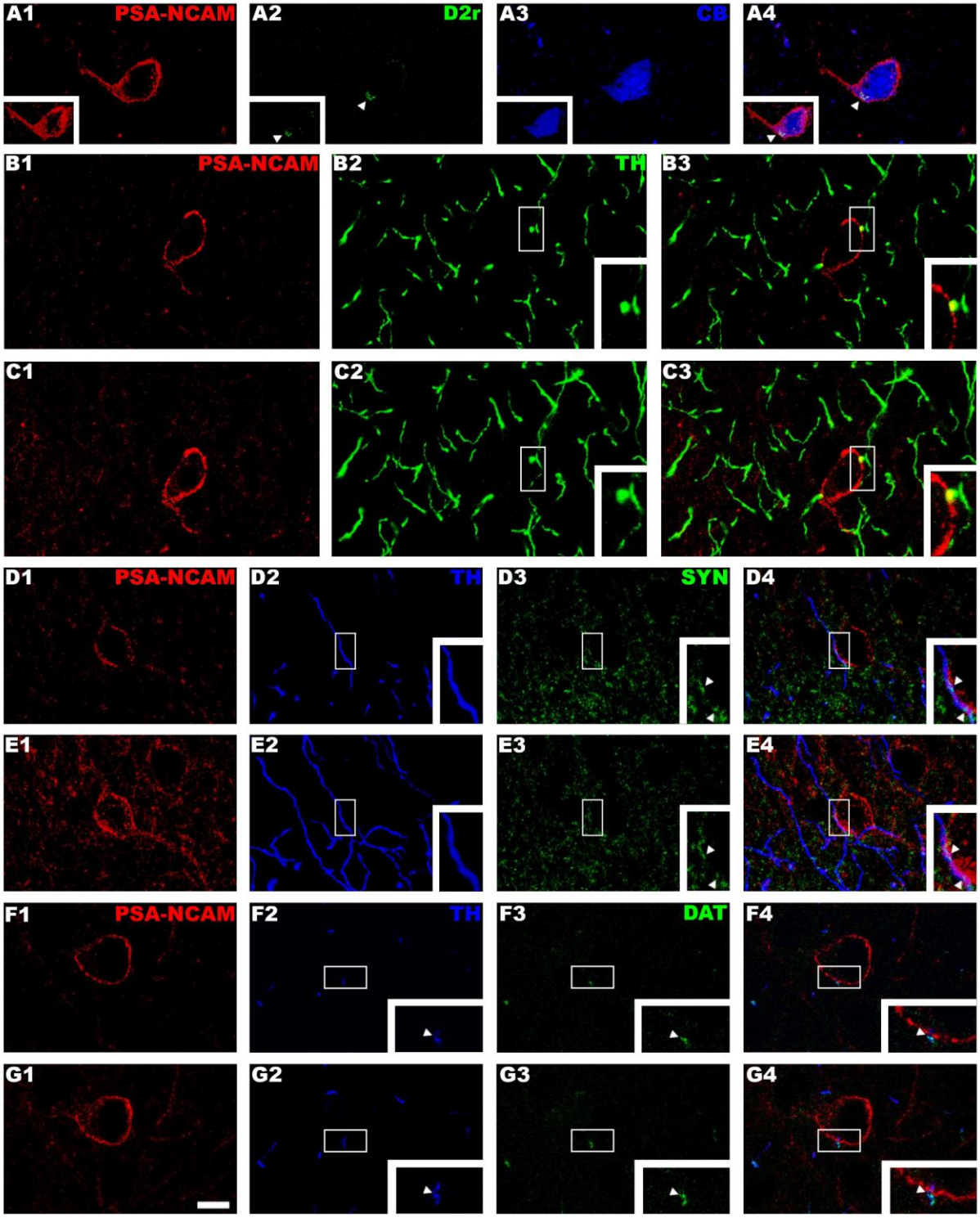

Figure 19. Confocal microscopic analysis of PSA-NCAM immunoreactive neurons and dopaminergic fibers in the mPFC. A: Triple PSA-NCAM/D2R/CB immunohistochemistry in the cingulate cortex layer III. Note the presence of D2R expression (arrowhead) in the cytoplasm of the PSA-NCAM/CB expressing somata. **B & C:** PSA-NCAM immunoreactive neuron in the cingulate cortex layer V. Observe TH puncta apposed to the neuronal somata. A detailed view of the squared section can be observed in the insert. **D & E:** Cingulate cortex layer III. Triple PSA-NCAM/TH/SYN immunohistochemistry. Note that the TH immunoreactive fiber contacting the PSA-NCAM expressing soma co-expresses synaptophysin (squared area in D2-4 & E2-4 and arrowheads in inserted images). **F & G:** PSA-NCAM immunoreactive neuron in cingulate cortex layer III. Observe the colocalization between TH and DAT fibers and the presence of a TH/DAT immunoreactive puncta in close apposition to the neuronal somata (squared area in F2-4 & G2-4 and arrowhead in inserted images. **C**, **E** and **G** are 2D projections of reconstructions of the focal planes shown in B1-3, D1-4 and F1-4, respectively, and its previous and subsequent focal planes located 1 µm apart. Scale bar: 10 µm. PSA-NCAM: polysialylated form of the neural cell adhesion molecule; D2R: dopamine D2 receptor; CB: calbindin; TH: tyrosine hydroxylase; SYN: synaptophysin; DAT: dopamine transporter.

Chapter 5

RESULTS (II)

Manipulation of dopaminergic neurotransmission: effects on the neuronal structural plasticity of the rat mPFC

1. THE LESION OF THE DOPAMINE MESOCORTICAL PATHWAY DECREASES THE EXPRESSION OF PLASTICITY-RELATED PROTEINS

1.1. PSA-NCAM expression in the mPFC neuropil decreases after 6-OHDA lesion

6-OHDA injection induced a statistically significant decrease in PSA-NCAM expression in the mPFC neuropil, when comparing 6-OHDA-treated hemispheres with vehicle-injected (control) hemispheres (p=0.042; **figure 20**).

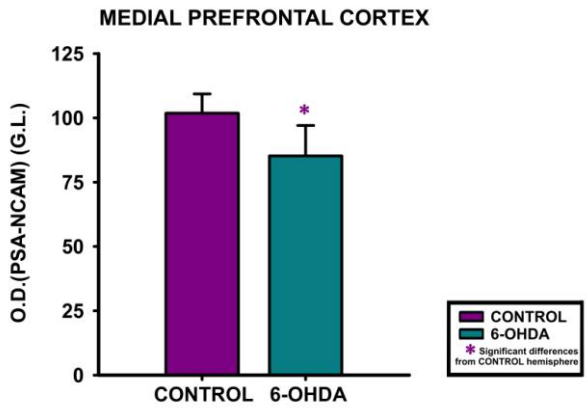

Figure 20. Graph representing the changes in the intensity of PSA-NCAM neuropil immunoreactivity in the mPFC when comparing 6-OHDA-treated hemispheres with contralateral vehicle-treated hemispheres (control). Asterisk in 6-OHDA bar indicate a statistically significant difference from control hemisphere after paired Student's t-test followed by Bonferroni's correction [p<0.05(*)]. Abbreviations: 6-OHDA, 6-hydroxydopamine hydrobromide; G.L., grey level; IR, immunoreactivity; O.D., optic density.

This downregulation was also found to be statistically significant (p<0.05) in all regions (IL, PrL, Cg1 and Cg2) and layers (I, II, III, V, VI) of the mPFC, with the exception of IL layer II, where only a trend toward a decrease in PSA-NCAM expression could be observed (**figure 21**).

For comparative purposes we also analyzed the expression of PSA-NCAM in a subcortical region, the ventral thalamic nucleus, and in a cortical region outside the mPFC, the endopiriform nucleus. No statistically significant variations in the optic density of PSA-NCAM immunoreactivity could be observed in these regions (p=0.4559 and p=0.2361, respectively; **figure 22**).

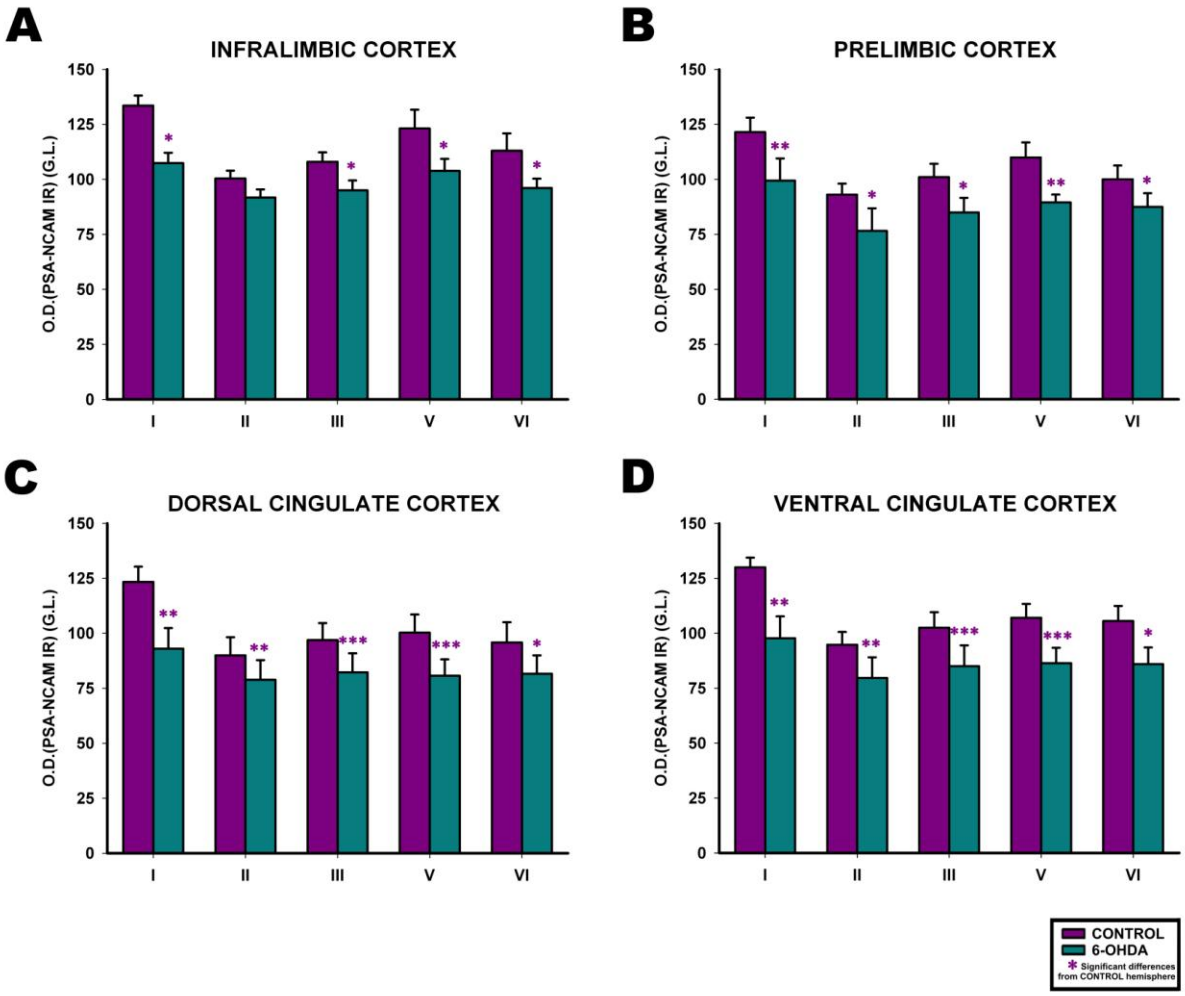

Figure 21. Graphs representing the changes in the intensity of PSA-NCAM neuropil immunoreactivity in the infralimbic (A), prelimbic (B), dorsal cingulate (C; Cg1) and ventral cingulate (D; Cg2) cortices when comparing 6-OHDA-treated hemispheres with contralateral vehicle-treated hemispheres (control). Asterisks in 6-OHDA bars indicate statistically significant differences from control hemisphere after paired Student's t-test followed by Bonferroni's correction; $p<0.05$ (*), $p<0.01$ (**), $p<0.001$ (***). Abbreviations: 6-OHDA, 6-hydroxydopamine hydrobromide; G.L., grey levels; IR, immunoreactivity; O.D., optic density. Roman numbers indicate cortical layers.

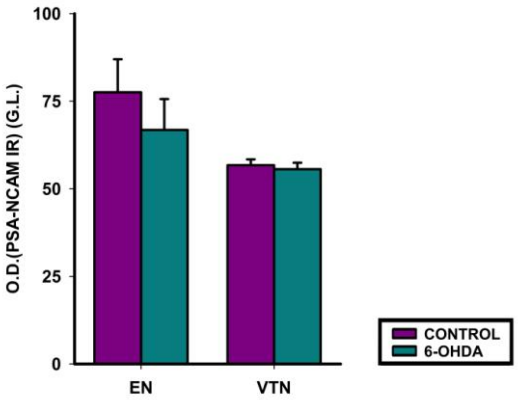

Figure 22. Graph showing no changes in the intensity of PSA-NCAM neuropil immunoreactivity in the endopiriform (EN) and ventral thalamic nuclei (VTN) after 6-OHDA lesion. Comparison between 6-OHDA-treated hemispheres and their contralateral vehicle-treated hemispheres. No statistically significant differences were found after paired Student's t-test followed by Bonferroni's correction. Abbreviations: 6-OHDA, 6-hydroxydopamine hydrobromide; EN, endopiriform nucleus; G.L., grey levels; IR, immunoreactivity; O.D., optic density; VTN, ventral thalamic nucleus.

1.2. 6-OHDA lesion decreases SYN neuropil expression in the mPFC

SYN expression in the mPFC neuropil decreased after dopamine cortical depletion (p<0.0001; **figure 23**).

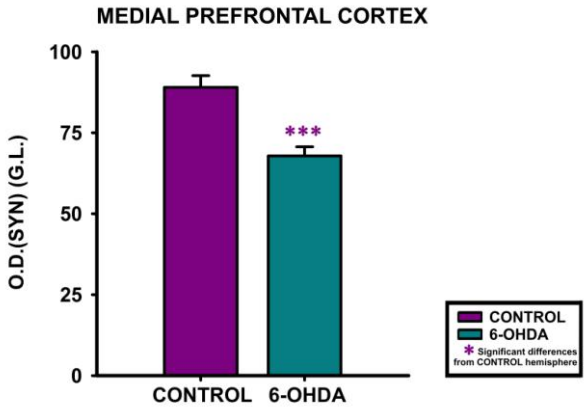

Figure 23. Graph showing the changes in the intensity of SYN neuropil immunoreactivity in the mPFC when comparing 6-OHDA-treated hemispheres with contralateral vehicle-treated hemispheres (control). Asterisk in 6-OHDA bar indicate a statistically significant difference from control hemisphere after paired Student's t-test followed by Bonferroni's correction [p<0.001(***)]. Abbreviations: 6-OHDA, 6-hydroxydopamine hydrobromide; G.L., grey level; IR, immunoreactivity; O.D., optic density.

Statistically significant decreases in SYN expression could also be observed in all regions (IL, PrL, Cg1 and Cg2) and layers (I, II, III, V, VI) of the mPFC (see **figure 24** for further details).

Neither the ventral thalamic nucleus nor the endopiriform nucleus showed statistically significant variations in the optic density of SYN immunoreactivity (p=0.6573 and p=0.5814, respectively; **figure 25**).

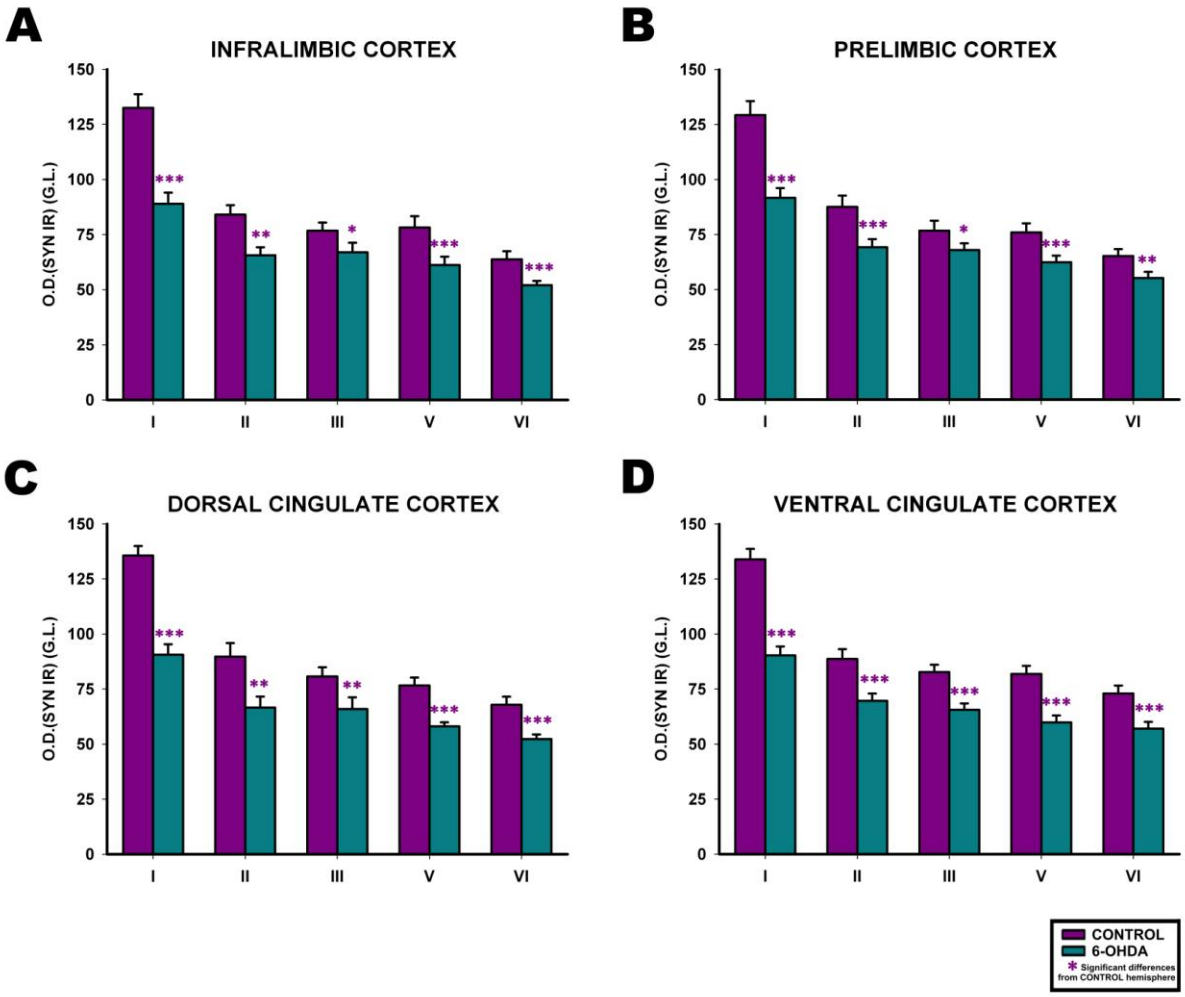

Figure 24. Graphs representing the changes in the intensity of SYN neuropil immunoreactivity in the infralimbic (A), prelimbic (B), dorsal cingulate (C; Cg1) and ventral cingulate (D; Cg2) cortices when comparing 6-OHDA-treated hemispheres with contralateral vehicle-treated hemispheres (control). Asterisks in 6-OHDA bars indicate statistically significant differences from control hemisphere after paired Student's t-test followed by Bonferroni's correction; $p<0.05$ (*), $p<0.01$ (**), $p<0.001$ (***). Abbreviations: 6-OHDA, 6-hydroxydopamine hydrobromide; G.L., grey levels; IR, immunoreactivity; O.D., optic density. Roman numbers indicate cortical layers.

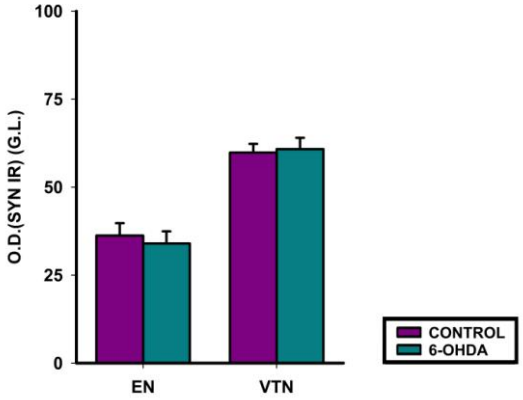

Figure 25. Graph showing no changes in the intensity of SYN neuropil immunoreactivity in the endopiriform (EN) and ventral thalamic nuclei (VTN) after 6-OHDA lesion. Comparison between 6-OHDA-treated hemispheres and their contralateral vehicle-treated hemispheres. No statistically significant differences were found after paired Student's t-test followed by Bonferroni's correction. Abbreviations: 6-OHDA, 6-hydroxydopamine hydrobromide; EN, endopiriform nucleus; G.L., grey levels; IR, immunoreactivity; O.D., optic density; VTN, ventral thalamic nucleus.

1.3. GAD67 expression in the mPFC neuropil decreases after 6-OHDA lesion

The lesion of the dopamine mesocortical pathway induced a significant decrease in GAD67 neuropil expression in the mPFC (p=0.002; **figure 26**).

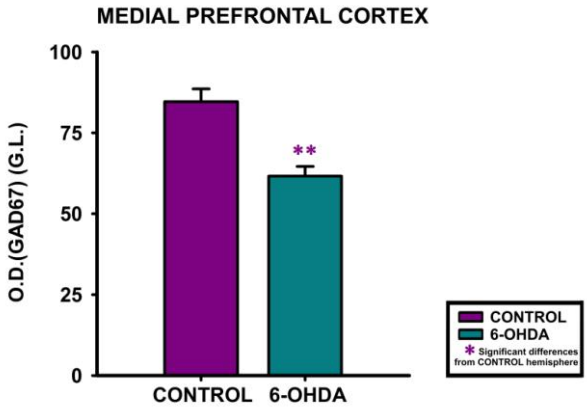

Figure 26. Graph showing the changes in the intensity of GAD67 neuropil immunoreactivity in the mPFC when comparing 6-OHDA-treated hemispheres with contralateral vehicle-treated hemispheres (control). Asterisk in 6-OHDA bar indicate a statistically significant difference from control hemisphere after paired Student's t-test followed by Bonferroni's correction [p<0.01(**)]. Abbreviations: 6-OHDA, 6-hydroxydopamine hydrobromide; G.L., grey level; IR, immunoreactivity; O.D., optic density.

This reduction was also statistically significant in all layers of the Cg2; layers I, III, V and VI of the IL and PrL; and layers I, III and V of the Cg1 (**figure 27**). The other layers in the four regions of the mPFC did not show statistically significant changes in GAD67 neuropil expression, although a clear trend towards a decrease could be observed in all of them.

The optic density of GAD67 immunoreactivity did not show statistically significant variations after 6-OHDA lesion neither in the ventral thalamic nucleus nor in the endopiriform nucleus (p=0.2327 and p=0.3656, respectively; **figure 28**).

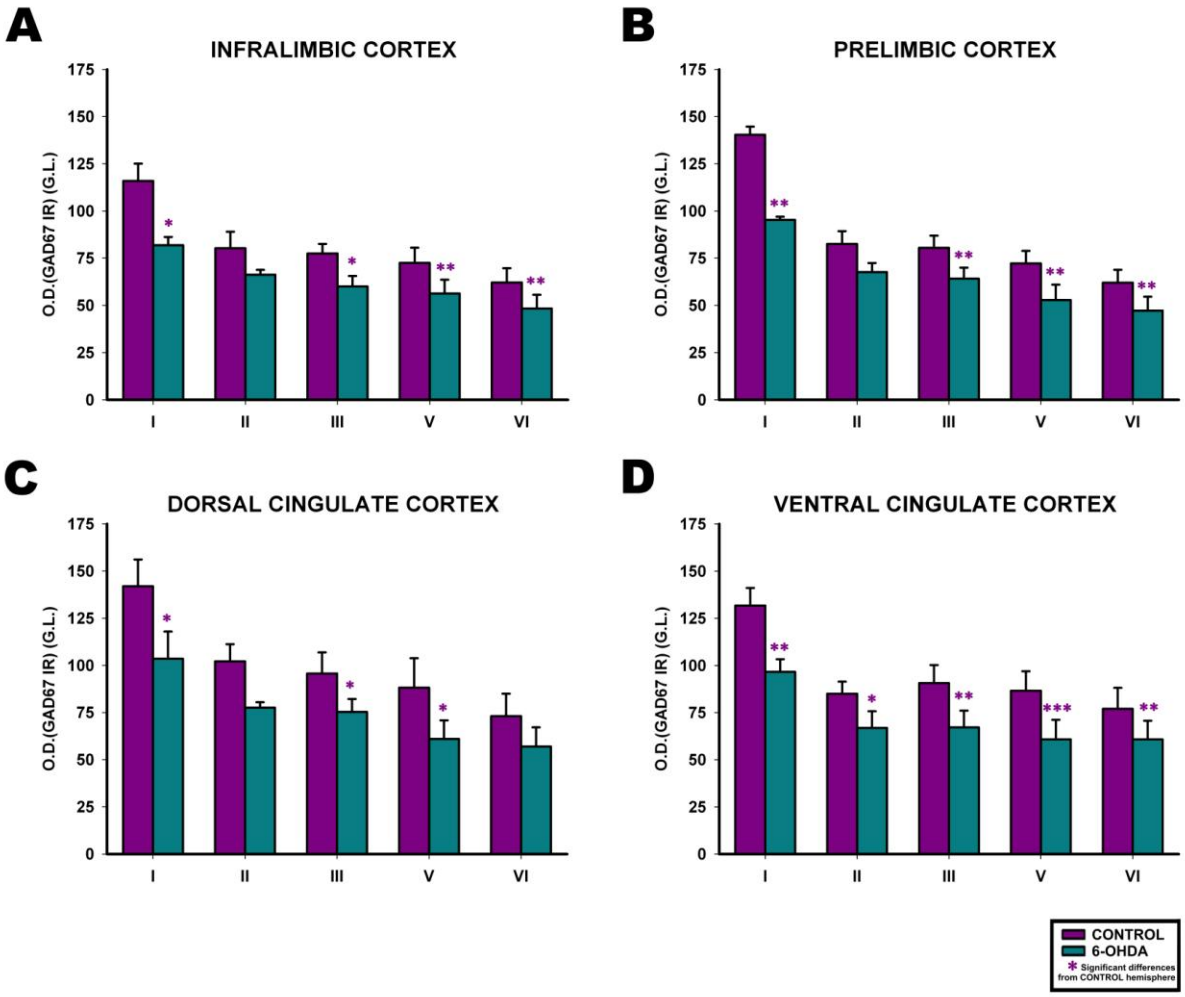

Figure 27. Graphs representing the changes in the intensity of GAD67 neuropil immunoreactivity in the infralimbic (A), prelimbic (B), dorsal cingulate (C; Cg1) and ventral cingulate (D; Cg2) cortices when comparing 6-OHDA-treated hemispheres with contralateral vehicle-treated hemispheres (control). Asterisks in 6-OHDA bars indicate statistically significant differences from control hemisphere after paired Student's t-test followed by Bonferroni's correction; $p<0.05$ (*), $p<0.01$ (**), $p<0.001$ (***). Abbreviations: 6-OHDA, 6-hydroxydopamine hydrobromide; G.L., grey levels; IR, immunoreactivity; O.D., optic density. Roman numbers indicate cortical layers.

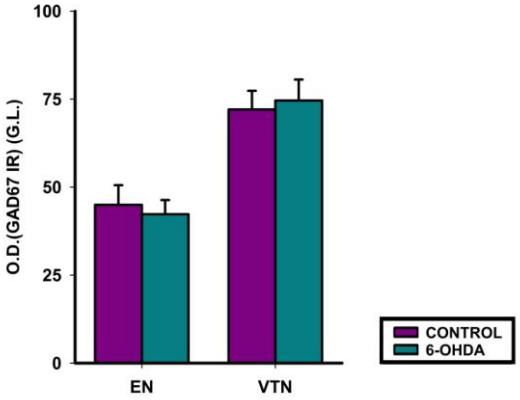

Figure 28. Graph showing no changes in the intensity of GAD67 neuropil immunoreactivity in the endopiriform (EN) and ventral thalamic nuclei (VTN) after 6-OHDA lesion. Comparison between 6-OHDA-treated hemispheres and their contralateral vehicle-treated hemispheres. No statistically significant differences were found after paired Student's t-test followed by Bonferroni's correction. Abbreviations: 6-OHDA, 6-hydroxydopamine hydrobromide; EN, endopiriform nucleus; G.L., grey levels; IR, immunoreactivity; O.D., optic density; VTN, ventral thalamic nucleus.

2. HALOPERIDOL, A DOPAMINE D2R ANTAGONIST, DECREASES THE EXPRESSION OF PLASTICITY-RELATED PROTEINS IN THE ADULT mPFC.

2.1. Body weight gain is not affected by haloperidol

Body weight was measured before the onset of the treatment (day 0), after 13 days of i.p injections and at the end of the treatment (day 26). All animals increased their body weight during the experiment but no statistically significant differences on body weight gain could be observed between groups in any of the time-periods analyzed (from day 0 to 26th day: p=0.8654; from day 0 to 13th day: p=0.4485; from 13th to 26th day: p=0.1584).

2.2. PSA-NCAM expression in the mPFC neuropil decreases after haloperidol treatment

Twenty-six days of haloperidol treatment induced a statistically significant decrease in PSA-NCAM neuropil expression in the rat mPFC (p<0.0001; **figure 29**), that could also observed in layers I and III of the IL, and layers I, III and V of the PrL, Cg1 and Cg2. A trend towards a decrease could be observed in PSA-NCAM expression in the remaining layers (**figure 30**).

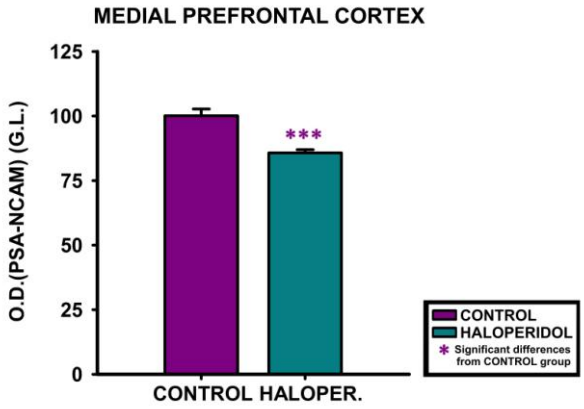

Figure 29. Graph showing the changes in the intensity of PSA-NCAM neuropil immunoreactivity in the mPFC after chronic haloperidol treatment. Asterisks in haloperidol bar indicate a statistically significant difference from control group after univariate repeated measures ANOVA [p<0.001(***)] followed by Bonferroni's correction. Abbreviations: G.L., grey level; HALOPER, haloperidol; IR, immunoreactivity; O.D., optic density.

Haloperidol treatment also induced a statistically significant decrease in PSA-NCAM expression in the ventral thalamic nucleus (p=0.0331) but no significant variations were detected in the endopiriform nucleus (p=0.2606; **figure 31**).

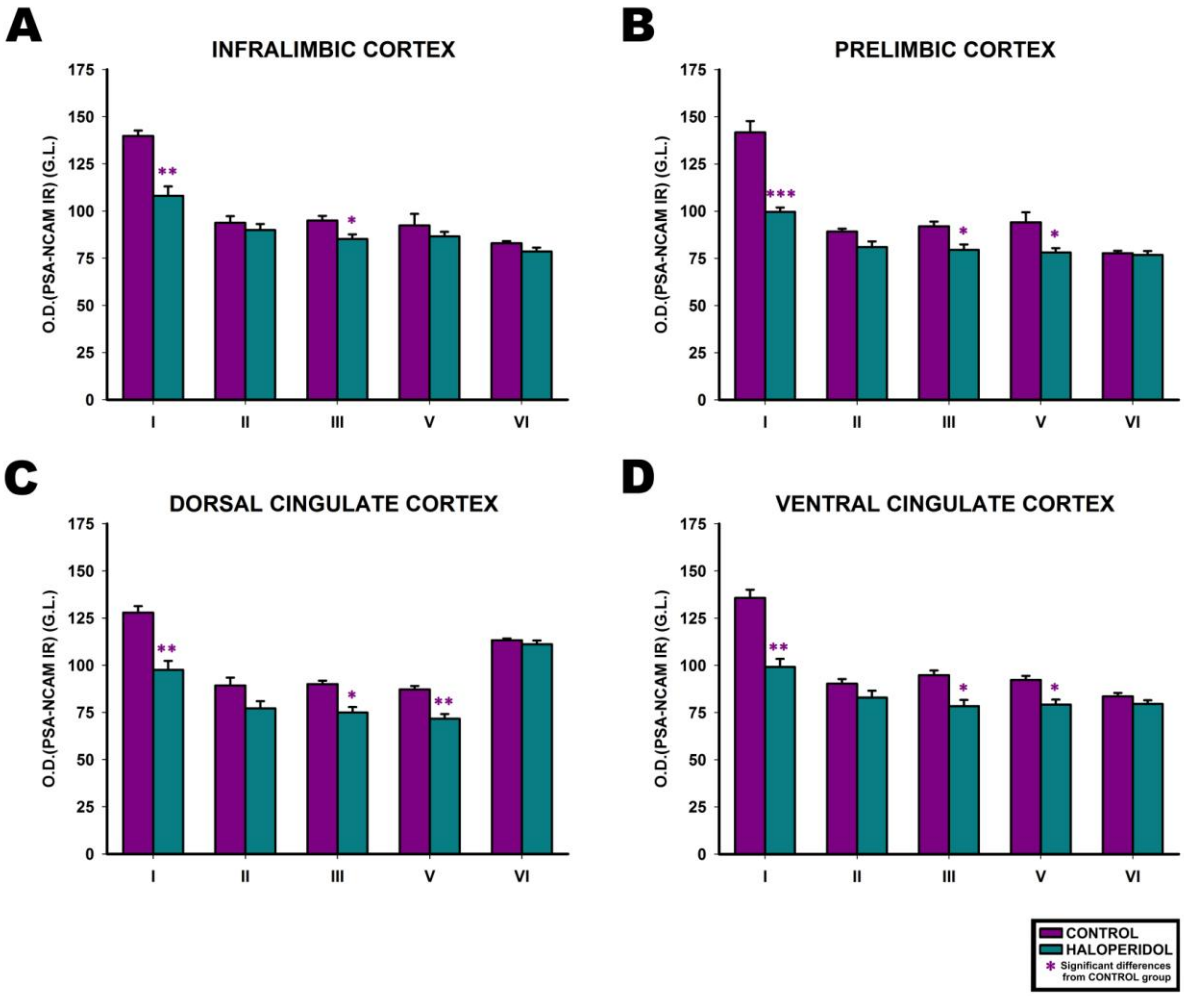

Figure 30. Graphs showing the changes in the intensity of PSA-NCAM neuropil immunoreactivity in the infralimbic (A), prelimbic (B), dorsal cingulate (C; Cg1) and ventral cingulate (D; Cg2) cortices after chronic haloperidol treatment. Asterisks in bars indicate statistically significant differences between groups after univariate repeated measures ANOVA followed by multiple pair-wise comparisons with Bonferroni's correction; $p<0.05$ (*), $p<0.01$ (**), $p<0.001$ (***). Abbreviations: G.L., grey levels; IR, immunoreactivity; O.D., optic density. Roman numbers indicate cortical layers.

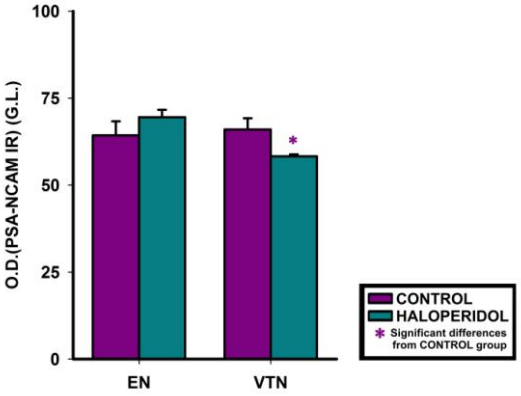

Figure 31. Graph showing changes in the intensity of PSA-NCAM neuropil immunoreactivity in the endopiriform (EN) and ventral thalamic nuclei (VTN) after chronic haloperidol treatment. Asterisks in bars indicate statistically significant differences between groups after unpaired Student's t-test followed by Bonferroni's correction [$p<0.05$ (*)]. Abbreviations: EN, endopiriform nucleus; G.L., grey levels; IR, immunoreactivity; O.D., optic density; VTN, ventral thalamic nucleus.

2.3. SYN neuropil expression decreases after haloperidol treatment in the mPFC

A statistically significant decrease in SYN expression could be observed after pharmacological treatment with haloperidol in the mPFC neuropil ($p<0.0001$; **figure 32**). Several layers of the IL, PrL, Cg1 and Cg2 also showed statistically significant decreases in SYN neuropil immunoreactivity (see **figure 33** for further details).

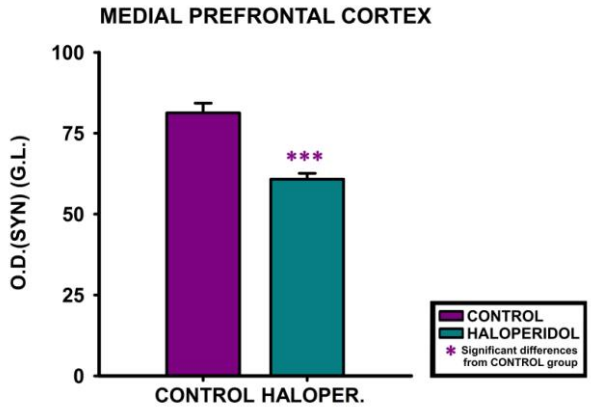

Figure 32. Graph showing the changes in the intensity of SYN neuropil immunoreactivity in the mPFC after chronic haloperidol treatment. Asterisks in haloperidol bar indicate a statistically significant difference from control group after univariate repeated measures ANOVA [$p<0.001$(***)] followed by Bonferroni's correction. Abbreviations: G.L., grey level; HALOPER, haloperidol; IR, immunoreactivity; O.D., optic density.

Neither the ventral thalamic nucleus ($p=0.2089$) nor the endopiriform nucleus ($p=0.4701$) showed significant variations in the optic density of SYN immunoreactivity (**figure 34**).

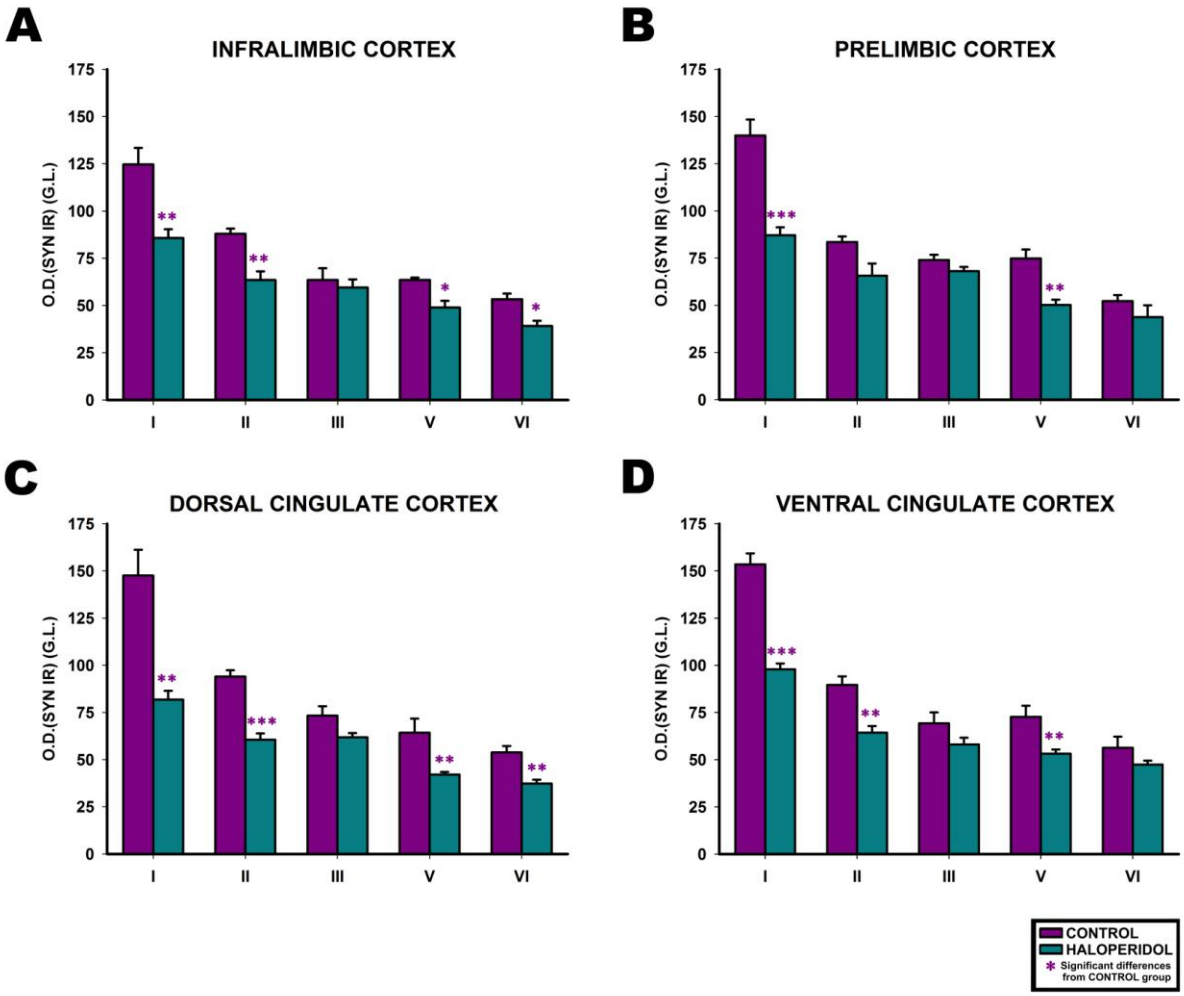

Figure 33. Graphs showing the changes in the intensity of SYN neuropil immunoreactivity in the infralimbic (A), prelimbic (B), dorsal cingulate (C; Cg1) and ventral cingulate (D; Cg2) cortices after chronic haloperidol treatment. Asterisks in bars indicate statistically significant differences between groups after univariate repeated measures ANOVA followed by multiple pair-wise comparisons with Bonferroni's correction; p<0.05 (*), p<0.01 (**), p<0.001 (***). Abbreviations: G.L., grey levels; IR, immunoreactivity; O.D., optic density. Roman numbers indicate cortical layers.

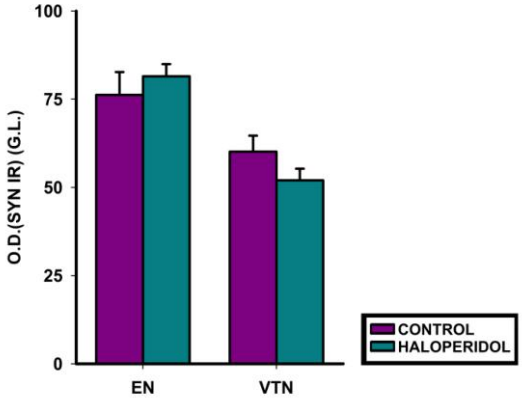

Figure 34. Graph showing changes in the intensity of SYN neuropil immunoreactivity in the endopiriform (EN) and ventral thalamic nuclei (VTN) after chronic haloperidol treatment. No statistically significant differences between groups were found after unpaired Student's t-test followed by Bonferroni's correction. Abbreviations: EN, endopiriform nucleus; G.L., grey levels; IR, immunoreactivity; O.D., optic density; VTN, ventral thalamic nucleus.

2.4. GAD67 expression in the mPFC decreases after haloperidol treatment

A significant decrease in GAD67 expression could be observed after haloperidol treatment in the mPFC neuropil ($p<0.0001$; **figure 35**), that is also statistically significant in many layers of IL, PrL, Cg1 and Cg2 (see **figure 36**).

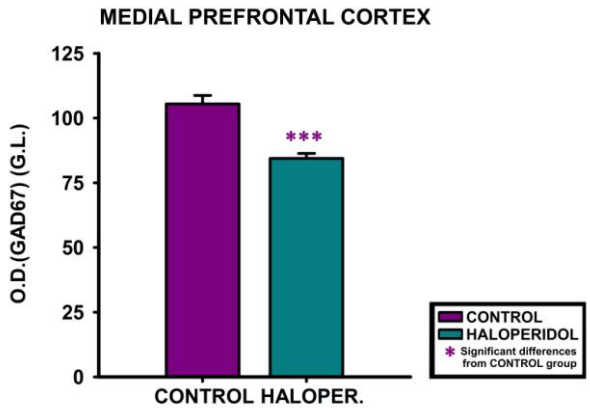

Figure 35. Graph showing the changes in the intensity of GAD67 neuropil immunoreactivity in the mPFC after chronic haloperidol treatment. Asterisks in haloperidol bar indicate a statistically significant difference from control group after univariate repeated measures ANOVA [p<0.001(***)] followed by Bonferroni's correction. Abbreviations: G.L., grey level; HALOPER, haloperidol; IR, immunoreactivity; O.D., optic density.

GAD67 neuropil expression did not show statistically significant variations after haloperidol treatment neither in the ventral thalamic nucleus ($p=0.9407$) nor in the endopiriform nucleus ($p=0.3403$) (**figure 37**).

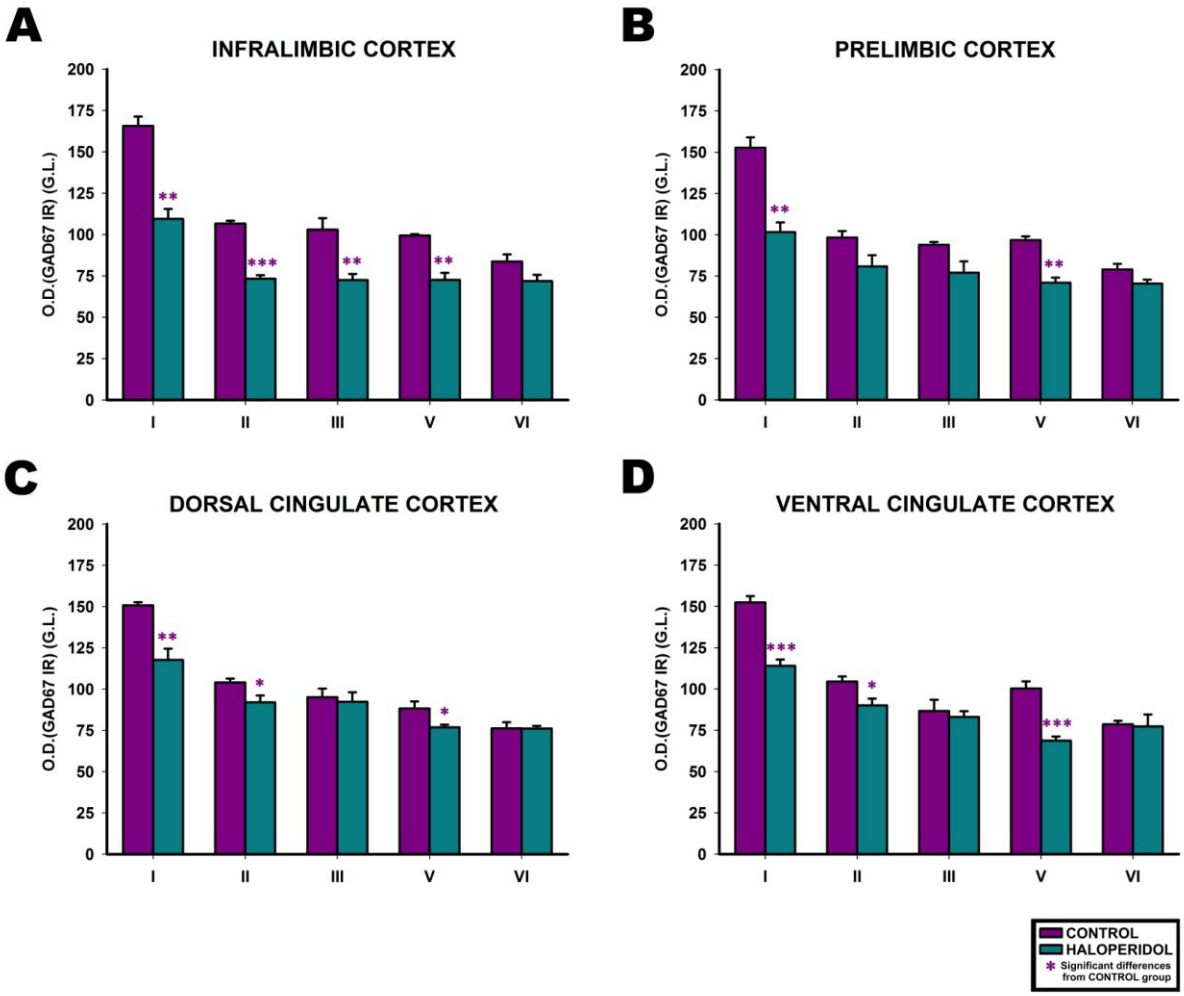

Figure 36. Graphs showing the changes in the intensity of GAD67 neuropil immunoreactivity in the infralimbic (A), prelimbic (B), dorsal cingulate (C; Cg1) and ventral cingulate (D; Cg2) cortices after chronic haloperidol treatment. Asterisks in bars indicate statistically significant differences between groups after univariate repeated measures ANOVA followed by multiple pair-wise comparisons with Bonferroni's correction; p<0.05 (*), p<0.01 (**), p<0.001 (***). Abbreviations: G.L., grey levels; IR, immunoreactivity; O.D., optic density. Roman numbers indicate cortical layers.

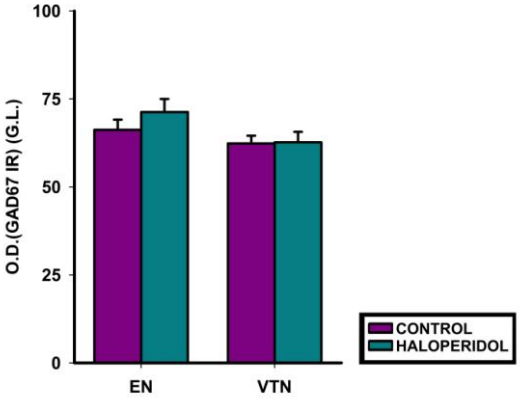

Figure 37. Graph showing changes in the intensity of GAD67 neuropil immunoreactivity in the endopiriform (EN) and ventral thalamic nuclei (VTN) after chronic haloperidol treatment. No statistically significant differences between groups were found after unpaired Student's t-test followed by Bonferroni's correction. Abbreviations: EN, endopiriform nucleus; G.L., grey levels; IR, immunoreactivity; O.D., optic density; VTN, ventral thalamic nucleus.

3. PPHT, A DOPAMINE D2R AGONIST, INCREASES THE EXPRESSION OF PLASTICITY-RELATED PROTEINS IN THE ADULT mPFC.

3.1. PPHT induces a decrease on body weight gain

Animals were weighted at the beginning (day 0), in the middle (day 4) and at the end (day 7) of pharmacological treatment. Body weight gain in animals treated with PPHT was significantly lower than in control animals in all the time-periods analyzed (from day 0 to 7th day: p=0.0004; from day 0 to 4th day: p=0.0105; from 4th to 7th day: p=0.0349).

3.2. PSA-NCAM expression in the mPFC neuropil increases after PPHT treatment

After seven days of PPHT treatment, significant increases in PSA-NCAM neuropil expression could be observed in the mPFC (p<0.0001; **figure 38**). This upregulation was statistically significant in all layers (I, II, III, V and VI) within all regions (IL, PrL, Cg1 and Cg2) of the mPFC (**figure 39**).

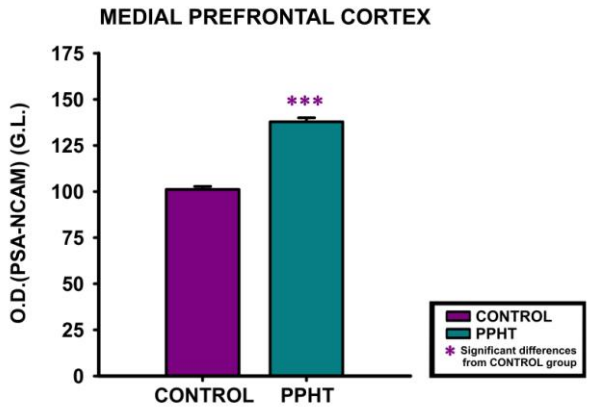

Figure 38. Graph showing the changes in the intensity of PSA-NCAM neuropil immunoreactivity in the mPFC after PPHT treatment. Asterisks in haloperidol bar indicate a statistically significant difference from control group after univariate repeated measures ANOVA [p<0.001(***)] followed by Bonferroni's correction. Abbreviations: G.L., grey level; IR, immunoreactivity; O.D., optic density; PPHT, 2-(N-Phenethyl-N-propyl)-amino-5-hydroxytetralin hydrochloride.

PPHT treatment also induced a significant increase in PSA-NCAM neuropil expression in the ventral thalamic nucleus (p=0.0114). By contrast, no significant variations (p=0.7343) were detected in the endopiriform nucleus (**figure 40**).

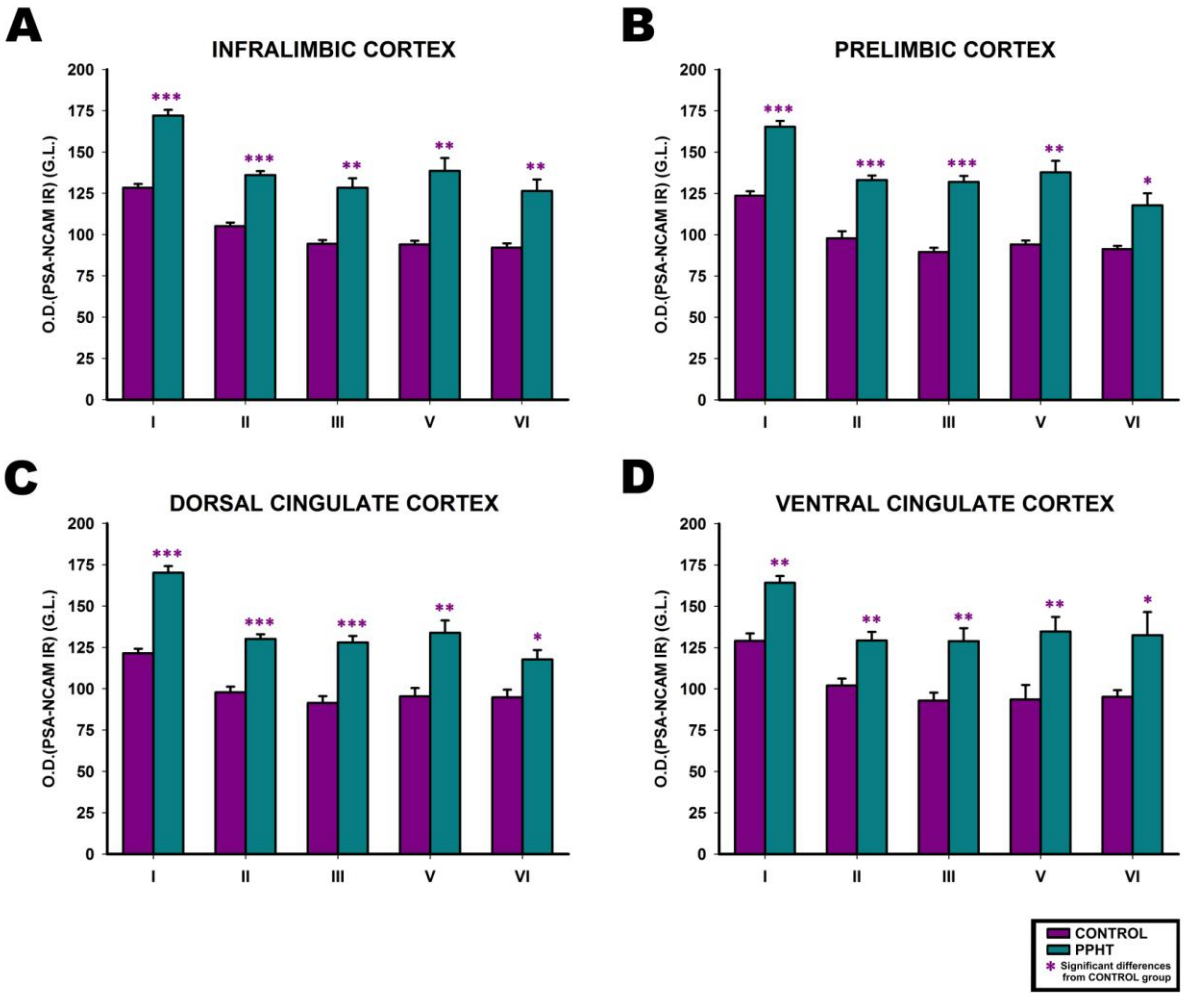

Figure 39. Graphs showing the changes in the intensity of PSA-NCAM neuropil immunoreactivity in the infralimbic (A), prelimbic (B), dorsal cingulate (C; Cg1) and ventral cingulate (D; Cg2) cortices after PPHT treatment. Asterisks in bars indicate statistically significant differences between groups after univariate repeated measures ANOVA followed by multiple pair-wise comparisons with Bonferroni's correction; p<0.05 (*), p<0.01 (**), p<0.001 (***). Abbreviations: G.L., grey levels; IR, immunoreactivity; O.D., optic density; PPHT, 2-(N-Phenethyl-N-propyl)-amino-5-hydroxytetralin hydrochloride. Roman numbers indicate cortical layers.

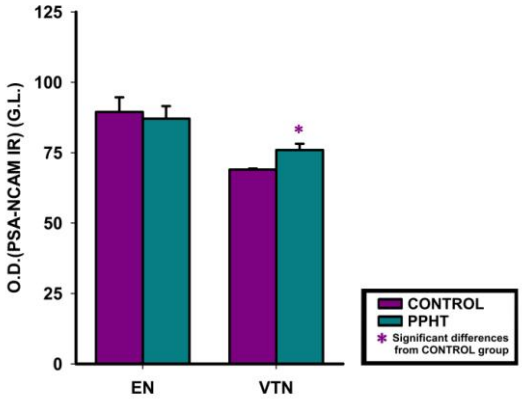

Figure 40. Graph showing changes in the intensity of PSA-NCAM neuropil immunoreactivity in the endopiriform (EN) and ventral thalamic nuclei (VTN) after PPHT treatment. Asterisks in bars indicate statistically significant differences between groups after unpaired Student's t-test followed by Bonferroni's correction [p<0.05 (*)]. Abbreviations: EN, endopiriform nucleus; G.L., grey levels; IR, immunoreactivity; O.D., optic density; PPHT, 2-(N-Phenethyl-N-propyl)-amino-5-hydroxytetralin hydrochloride; VTN, ventral thalamic nucleus.

3.3. SYN neuropil expression in the mPFC increases after PPHT treatment

PPHT treatment induced statistically significant increases in SYN expression in the mPFC neuropil ($p<0.0001$; **figure 41**). With the exception of layer II in the ventral and dorsal cingulate cortices, all layers in all regions of the mPFC showed statistically significant increases in SYN neuropil expression (**figure 42).**

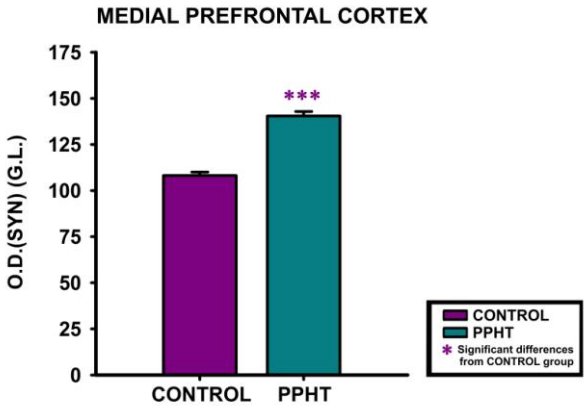

Figure 41. Graph showing the changes in the intensity of SYN neuropil immunoreactivity in the mPFC after PPHT treatment. Asterisks in haloperidol bar indicate a statistically significant difference from control group after univariate repeated measures ANOVA [p<0.001(***)] followed by Bonferroni's correction. Abbreviations: G.L., grey level; IR, immunoreactivity; O.D., optic density; PPHT, 2-(N-Phenethyl-N-propyl)-amino-5-hydroxytetralin hydrochloride.

Neither the ventral thalamic nucleus ($p=0.8341$) nor the endopiriform nucleus ($p=0.3948$) showed significant variations in the optic density of SYN immunoreactivity (**figure 43**).

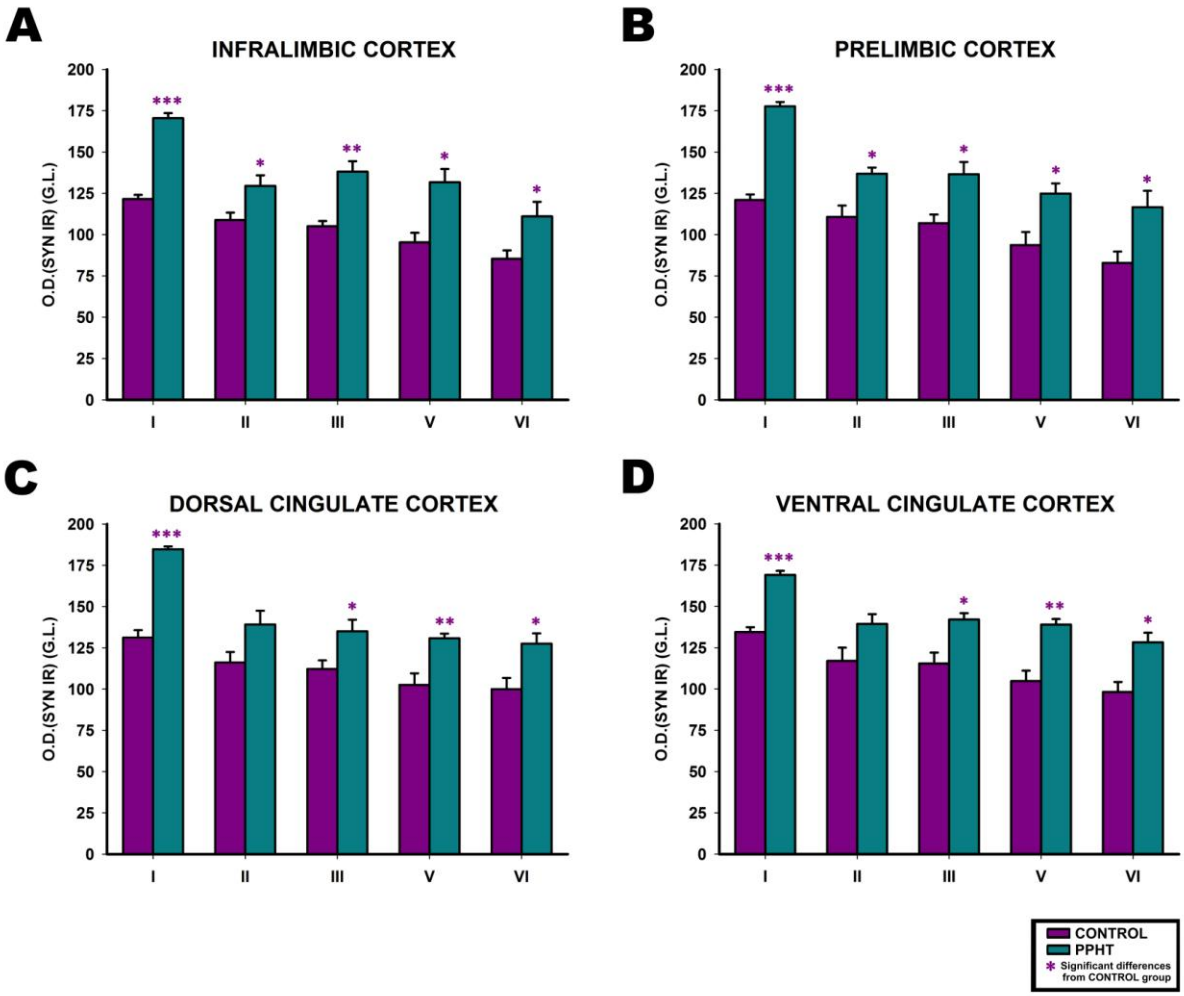

Figure 42. Graphs showing the changes in the intensity of SYN neuropil immunoreactivity in the infralimbic (A), prelimbic (B), dorsal cingulate (C; Cg1) and ventral cingulate (D; Cg2) cortices after PPHT treatment. Asterisks in bars indicate statistically significant differences between groups after univariate repeated measures ANOVA followed by multiple pair-wise comparisons with Bonferroni's correction; p<0.05 (*), p<0.01 (**), p<0.001 (***). Abbreviations: G.L., grey levels; IR, immunoreactivity; O.D., optic density; PPHT, 2-(N-Phenethyl-N-propyl)-amino-5-hydroxytetralin hydrochloride. Roman numbers indicate cortical layers.

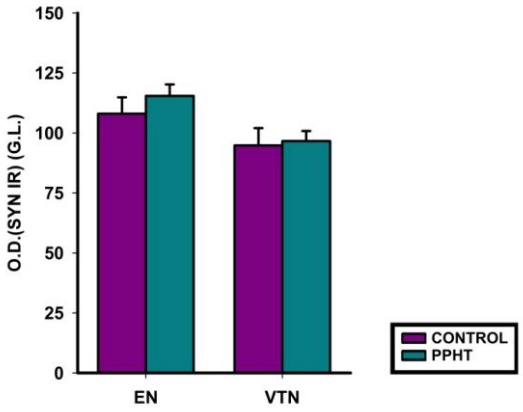

Figure 43. Graph showing changes in the intensity of SYN neuropil immunoreactivity in the endopiriform (EN) and ventral thalamic nuclei (VTN) after PPHT treatment. No statistically significant differences between groups were found after unpaired Student's t-test followed by Bonferroni's correction. Abbreviations: EN, endopiriform nucleus; G.L., grey levels; IR, immunoreactivity; O.D., optic density; PPHT, 2-(N-Phenethyl-N-propyl)-amino-5-hydroxytetralin hydrochloride; VTN, ventral thalamic nucleus.

3.4. PPHT treatment increases GAD67 neuropil expression in mPFC

Statistically significant increases in GAD67 neuropil expression in the mPFC could be observed after PPHT treatment ($p<0.0001$; **figure 44**). This significant upregulation could be observed in most layers of all regions (IL, PrL, Cg1 and Cg2) in the mPFC (see **figure 45** for further details).

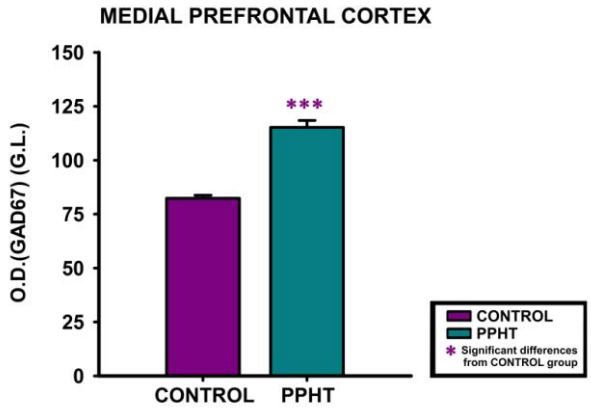

Figure 44. Graph showing the changes in the intensity of GAD67 neuropil immunoreactivity in the mPFC after PPHT treatment. Asterisks in haloperidol bar indicate a statistically significant difference from control group after univariate repeated measures ANOVA [p<0.001(***)] followed by Bonferroni's correction. Abbreviations: G.L., grey level; IR, immunoreactivity; O.D., optic density; PPHT, 2-(N-Phenethyl-N-propyl)-amino-5-hydroxytetralin hydrochloride.

The optic density of GAD67 immunoreactivity did not show statistically significant variations after PPHT treatment neither in the ventral thalamic nucleus ($p=0.3720$) nor in the endopiriform nucleus ($p= 0.2743$) (**figure 46**).

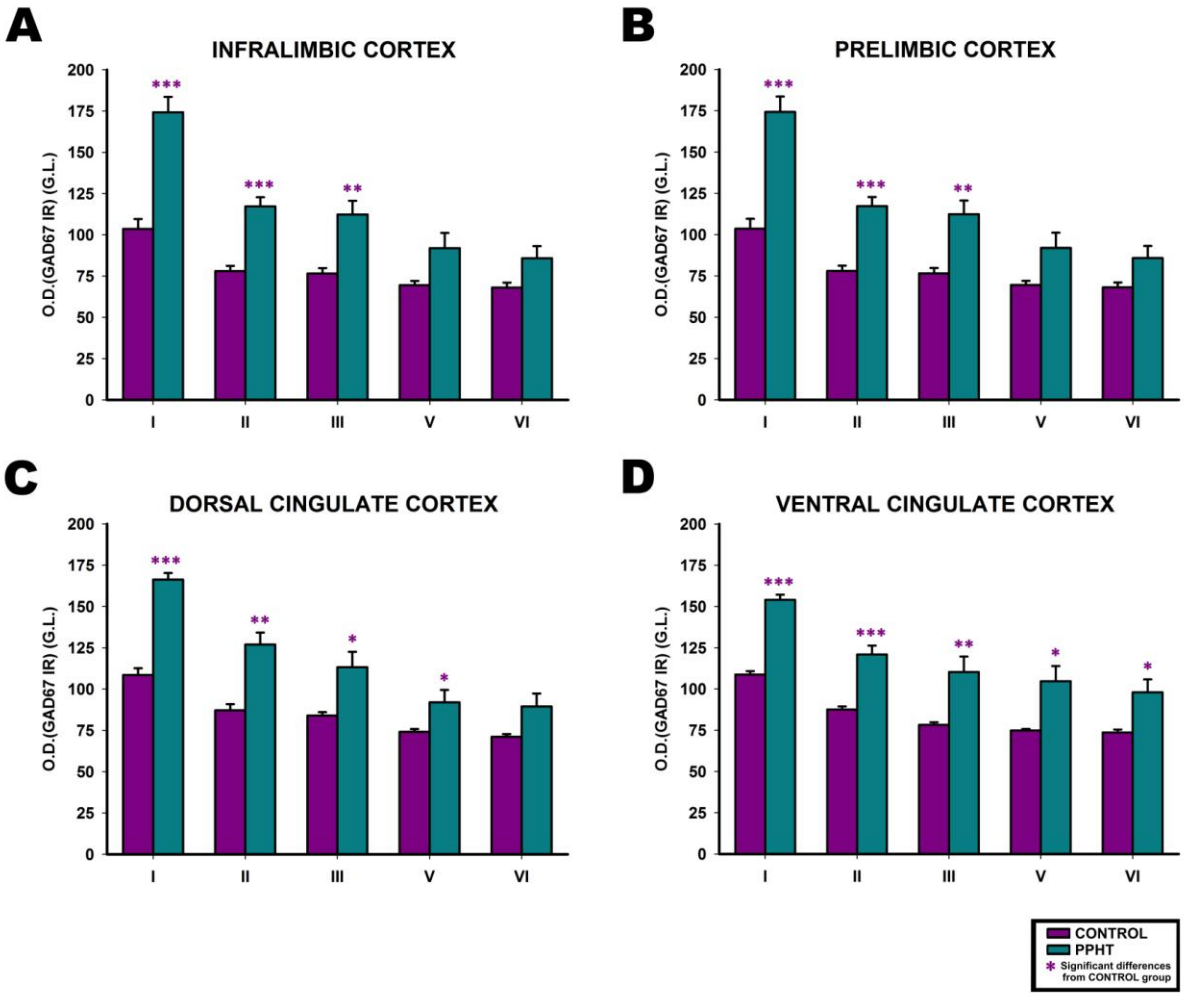

Figure 45. Graphs showing the changes in the intensity of GAD67 neuropil immunoreactivity in the infralimbic (A), prelimbic (B), dorsal cingulate (C; Cg1) and ventral cingulate (D; Cg2) cortices after PPHT treatment. Asterisks in bars indicate statistically significant differences between groups after univariate repeated measures ANOVA followed by multiple pair-wise comparisons with Bonferroni's correction; p<0.05 (*), p<0.01 (**), p<0.001 (***). Abbreviations: G.L., grey levels; IR, immunoreactivity; O.D., optic density; PPHT, 2-(N-Phenethyl-N-propyl)-amino-5-hydroxytetralin hydrochloride. Roman numbers indicate cortical layers.

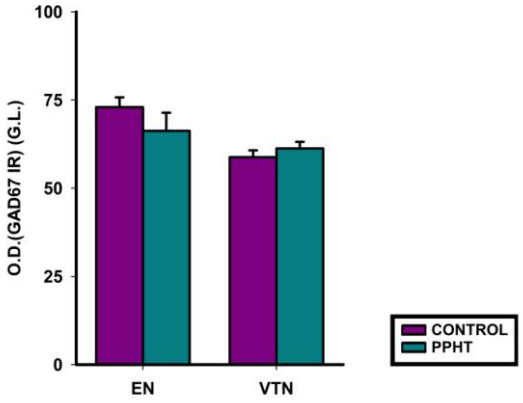

Figure 46. Graph showing changes in the intensity of GAD67 neuropil immunoreactivity in the endopiriform (EN) and ventral thalamic nuclei (VTN) after PPHT treatment. No statistically significant differences between groups were found after unpaired Student's t-test followed by Bonferroni's correction. Abbreviations: EN, endopiriform nucleus; G.L., grey levels; IR, immunoreactivity; O.D., optic density; PPHT, 2-(N-Phenethyl-N-propyl)-amino-5-hydroxytetralin hydrochloride; VTN, ventral thalamic nucleus.

4. TEMPORAL DIFFERENCES IN THE EXPRESSION OF PLASTICITY-RELATED GENES DURING PPHT TREATMENT IN THE mPFC

4.1. Body weight decreases after acute or chronic PPHT treatment

At the end of the experiment, all PPHT-treated groups showed statistically significant decreases in their body weights when compared with their respective control group (1 day-treatment group: p=0.0026; 4 days-treatment group: p=0.0005; 7 days-treatment group: p=0.0030). In particular, these decreases took place during the first half of the treatment (from day 0 to 2nd day in the 4 days-treatment group: p=0.0018; from day 0 to 4th day in the 7 days-treatment group: p=0.0009). After that, PPHT-treated animals increased their body weight similar to controls (from 2nd to 4th day in the 4 days-treatment-group: p=0.2668; from 4th to 7th day in the 7 days-treatment group: p=0.2442).

4.2. Time-course changes in mPFC gene expression during PPHT treatment

4.2.1. Expression of polysialyltransferase genes st8siaII and st8siaIV

After 1 day of PPHT treatment, *st8siaII* and *st8siaIV* mRNA levels in the mPFC did not significantly differ from those of the control group (**figure 47 A**). Four days of treatment significantly increased *st8siaIV* gene expression (p=0.047; fold increase=1.26) but did not change *st8siaII* mRNA levels (**figure 47 B**). At the end of the experiment (7th day), the expression of both polysialyltransferase genes did not show statistically significant differences when compared with that of the control group (**figure 47 C**) (**table 4**).

Table 4. qRT-PCR results in the mPFC of PPHT-treated rats vs. control

	1 day		4 days		7days	
	Δ	***p-value***	Δ	***p-value***	Δ	***p-value***
ncam	0.8950	0.6257	0.9264	0.4911	**0.5020**	**0.0002**
syn	0.8846	0.6587	1.0981	0.5942	0.8751	0.7912
gad67	1.0179	0.9178	**1.3210**	**0.0492**	0.5090	0.1601
gad65	1.1526	0.4574	**1.4093**	**0.0418**	1.3675	0.3327
st8siaII	0.9024	0.7450	1.3486	0.1943	1.3784	0.4832
st8siaIV	0.9655	0.8820	**1.2622**	**0.0470**	1.9053	0.1240

Δ, fold change in mRNA levels in PPHT-treated animals relative to control animals. Information in bold represents significant changes ($p<0.05$) after unpaired Student's t-test followed by Bonferroni's correction.

4.2.2. Ncam gene expression

No statistically significant changes were found in *ncam* gene expression after 1 or 4 days of PPHT treatment but a significant 0.5-fold decrease in *ncam* mRNA level was observed after 7 days of treatment (p=0.0002) (**figure 47**) (**table 4**).

4.2.3. Syn gene expression

No statistically significant changes were found in s*yn* gene expression after 1, 4 or 7 days of PPHT treatment (**figure 47**) (**table 4**).

4.2.4. Expression of glutamate decarboxylase genes gad65 and gad67

Both gad65 and gad67 genes only were found to increase their expression after 4 days of PPHT treatment (gad65: p=0.0418, fold increase=1.4; gad67: p=0.0492, fold increase=1.3). The expression of both genes did not change after 1 or 7 days of treatment (**figure 47**) (**table 4**).

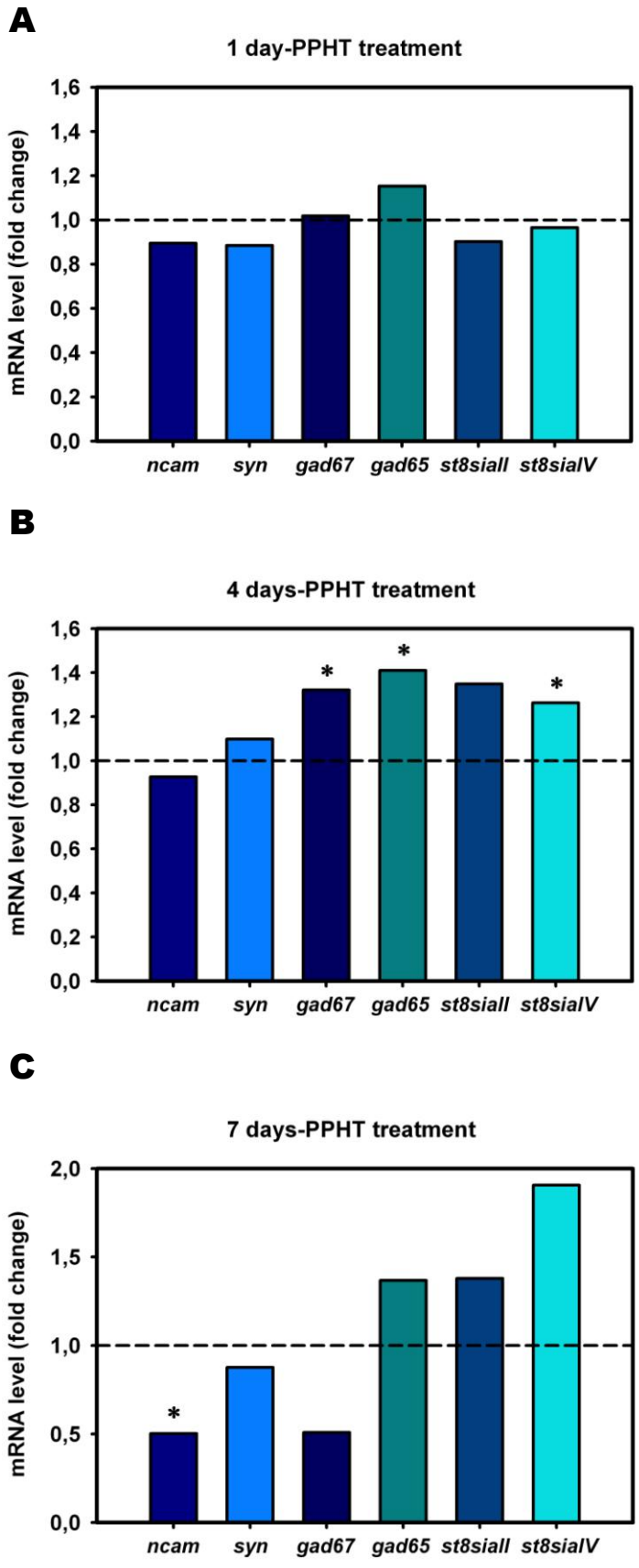

Figure 47. Time-course changes of ncam, syn, gad65, gad67, siaII and sia IV gene expression after 1 day (A), 4 days (B) and 7 days (C) of PPHT treatment in the mPFC of adult rats. Bars indicate fold change values on mRNA level when compare the treated and the control group in each time point. Asterisks in bars indicate statistically significant differences from the control group in unpaired Student's t-test followed by Bonferroni correction: $p<0.05$ (*), $p< 0.01$(***), $p<0.001$(***).

Chapter 6

RESULTS (III)

Effects of PSA depletion on the remodeling of inhibitory networks and pyramidal neurons in the mPFC and its influence on the neuroplastic changes mediated by D2R agonists

1. DOPAMINE D2 RECEPTORS AND POLYSIALIC ACID PARTICIPATE IN THE REMODELING OF INHIBITORY NETWORKS AND PYRAMIDAL NEURONS IN THE mPFC

1.1. Body weight loss after PPHT treatment

From the day of surgery (day 0) to the onset of pharmacological treatment (day 7), no statistically significant differences were found on body weight between groups (p=0.087). After PPHT treatment (from 7^{th} to 14^{th} day), animals showed a significant weight loss when compared with non-PPHT treated ones (Endo-N/PPHT vs. Endo-N/Control: p<0.0001; Control/PPHT vs. Control/Control: p=0.0246). These decreases on body weight took place specifically from 7^{th} to 10^{th} day (EndoN/PPHT vs. Endo-N/Control: p<0.0001; Control/PPHT vs. Control/Control: p=0.005); from day 10^{th} to 14^{th}, all groups increased equally their body weight (p=0.322).

All the results that will be shown in the following sections (from **1.2** to **1.6**) are summarized in **table 5.**

1.2. Endo-N injection blocks PPHT-induced increases in SYN and GAD67 expression in the mPFC neuropil, and reduces VGLUT1 expression

In consonance with our previous results (see **chapter 5**, section **3.2-3.4**), seven days of PPHT treatment induced statistically significant increases in PSA-NCAM (p<0.001), SYN (p=0.003) and GAD67 (p<0.001) expression in the mPFC neuropil. These effects of PPHT on SYN and GAD67 expression were prevented when PSA was removed one week before the onset of the PPHT treatment [Control/Control vs. Endo-N/PPHT: p=1.000 (SYN), p=0.139 (GAD67); Endo-N/Control vs. Endo-N/PPHT: p=1.000 (SYN and GAD67)] (**figure 48 A-C**). PSA-NCAM expression in the mPFC remained undetectable 14 days after Endo-N injection (**figure 49**).

VGLUT1 expression in the neuropil was not affected by PPHT treatment, neither in the presence nor in the absence of PSA (Control/Control vs. Control/PPHT or Endo-N/Control vs. Endo-N/PPHT: p=1.000) (**figure 48 D**).

Endo-N administration by itself did not induce changes in GAD67 or SYN expression, but decreased VGLUT1 expression in the mPFC neuropil [Endo-

N/Control vs. Control/Control: p=1.000 for GAD67 and SYN, p=0.028 for VGLUT1) (**figure 48 B-D**).

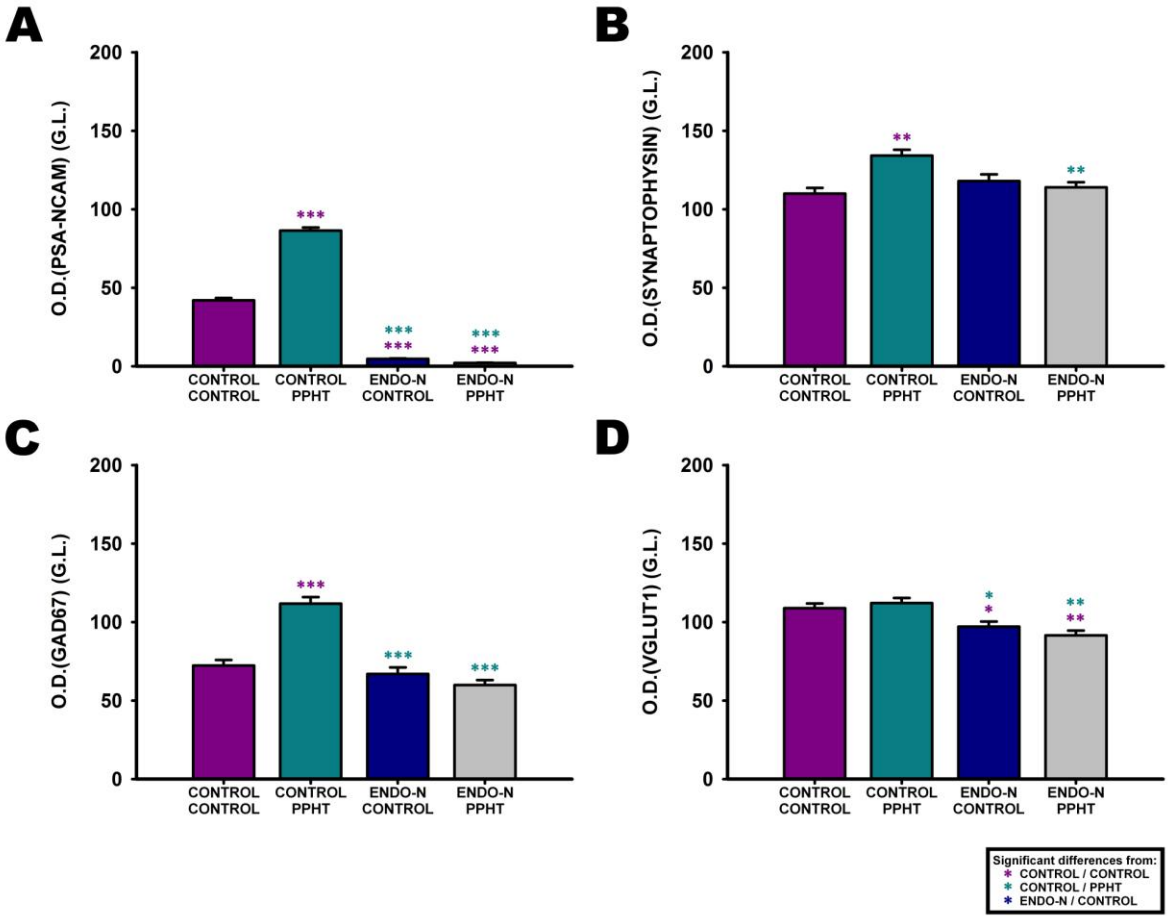

Figure 48. Graphs showing changes in the expression of PSA-NCAM (A), SYN (B), GAD67 (C) and VGLUT1 (D) in the mPFC neuropil after Endo-N or PPHT treatments and their combination. Asterisks in bars indicate statistically significant differences between groups (see graph legend) after univariate repeated measures ANOVA followed by multiple pair-wise comparisons with Bonferroni's correction; p<0.05 (*), p<0.01 (**), p<0.001 (***).Abbreviations: Endo-N, Endo-N-acetylneuraminidase; G.L., grey levels; IR, immunoreactivity; O.D., optic density; PPHT, 2-(N-Phenethyl-N-propyl)-amino-5-hydroxytetralin hydrochloride.

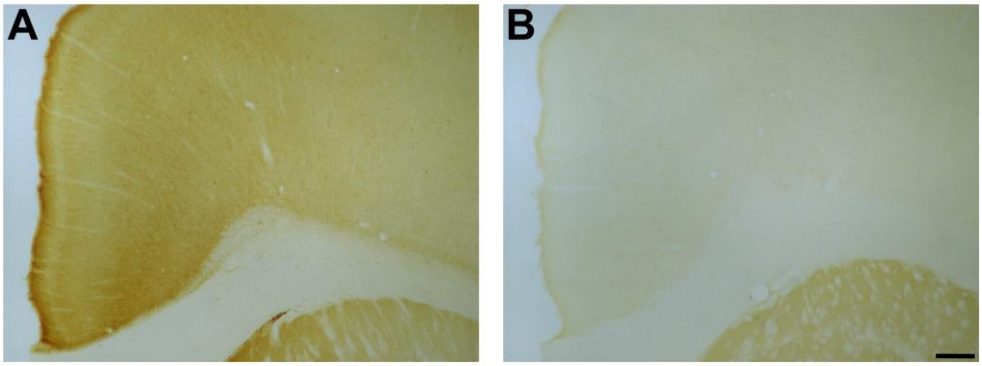

Figure 49. Microphotographs showing PSA-NCAM immunostaining in control (A) and Endo-N treated rats (B). Note in panel B the lack of PSA-NCAM expression in the cingulate cortex, but not in the striatum. Scale bar: 100 μm.

The effects described above for PSA-NCAM, SYN, GAD67 and VGLUT1 expression, considering the whole mPFC neuropil, were also observed in most layers of every region within the mPFC (IL, PrL, Cg1 and Cg2) (**figure 50-53**).

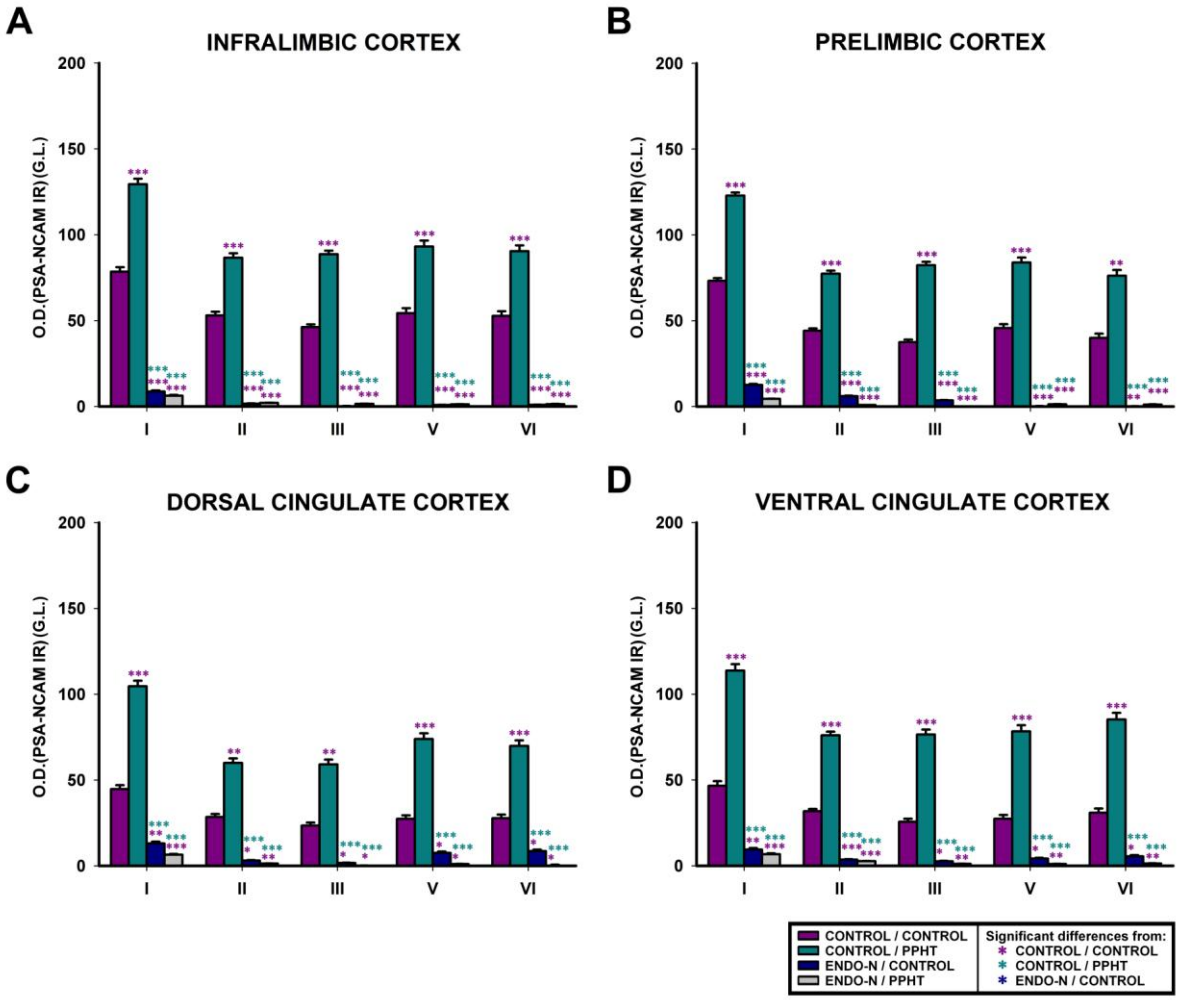

Figure 50. Graphs representing the changes in PSA-NCAM neuropil expression after Endo-N and/or PPHT treatments. (A) Infralimbic cortex; (B) Prelimbic cortex; (C) Dorsal cingulate cortex; (D) Ventral cingulate cortex. Asterisks in bars indicate statistically significant differences between groups (see graph legend) after univariate repeated measures ANOVA followed by multiple pair-wise comparisons with Bonferroni's correction; $p<0.05$ (*), $p<0.01$ (**), $p<0.001$ (***).Abbreviations: Endo-N, Endo-N-acetylneuraminidase; G.L., grey levels; IR, immunoreactivity; O.D., optic density; PPHT, 2-(N-Phenethyl-N-propyl)-amino-5-hydroxytetralin hydrochloride. Roman numbers indicate cortical layers.

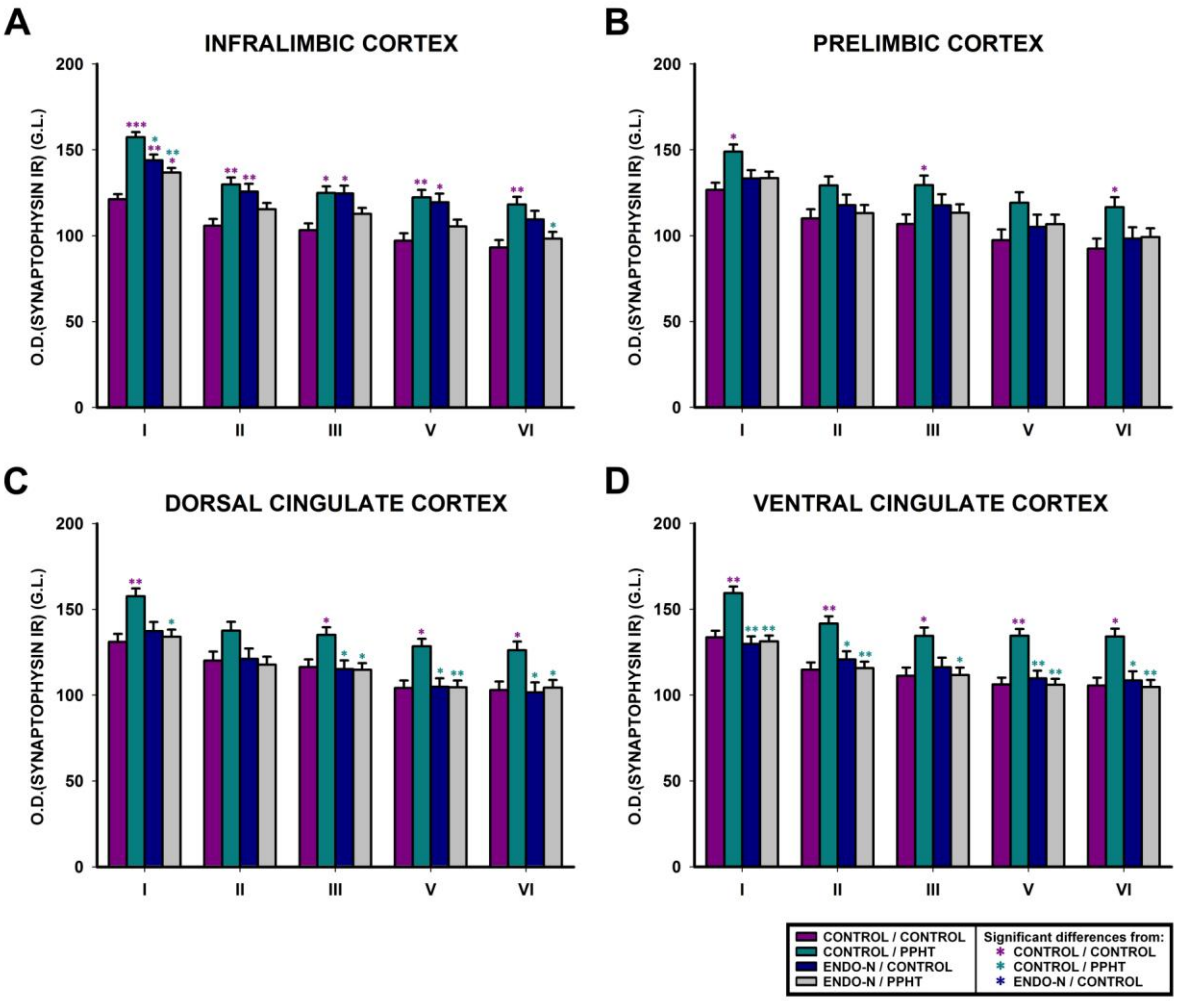

Figure 51. Graphs showing the changes in SYN neuropil expression after Endo-N and/or PPHT treatments. (A) Infralimbic cortex; (B) Prelimbic cortex; (C) Dorsal cingulate cortex; (D) Ventral cingulate cortex. Asterisks in bars indicate statistically significant differences between groups (see graph legend) after univariate repeated measures ANOVA followed by multiple pair-wise comparisons with Bonferroni's correction; $p<0.05$ (*), $p<0.01$ (**), $p<0.001$ (***). Abbreviations: Endo-N, Endo-N-acetylneuraminidase; G.L., grey levels; IR, immunoreactivity; O.D., optic density; PPHT, 2-(N-Phenethyl-N-propyl)-amino-5-hydroxytetralin hydrochloride. Roman numbers indicate cortical layers.

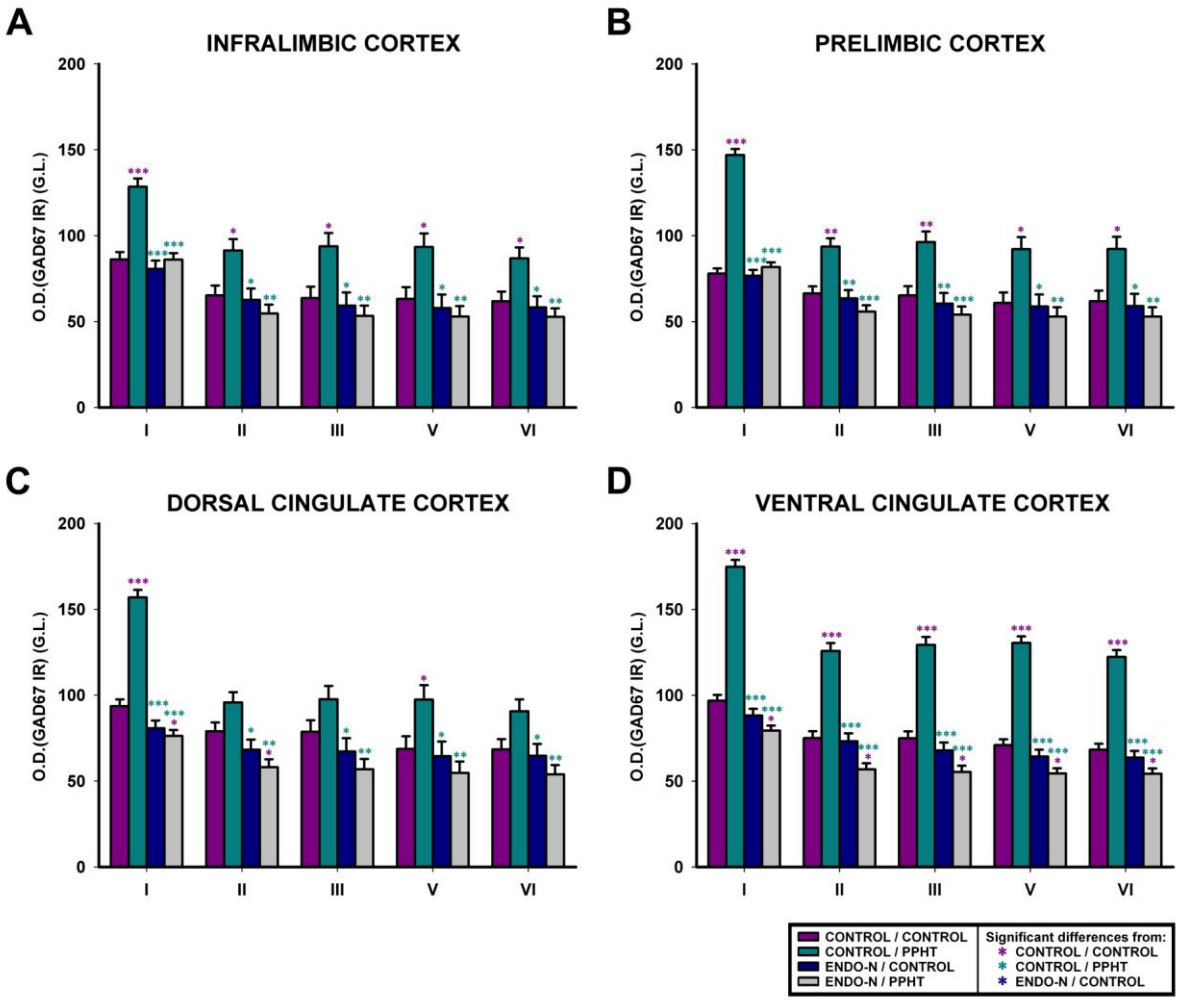

Figure 52. Graphs showing the changes in GAD67 neuropil expression after Endo-N and/or PPHT treatments. (A) Infralimbic cortex; (B) Prelimbic cortex; (C) Dorsal cingulate cortex; (D) Ventral cingulate cortex. Asterisks in bars indicate statistically significant differences between groups (see graph legend) after univariate repeated measures ANOVA followed by multiple pair-wise comparisons with Bonferroni's correction; $p<0.05$ (*), $p<0.01$ (**), $p<0.001$ (***). Abbreviations: Endo-N, Endo-N-acetylneuraminidase; G.L., grey levels; IR, immunoreactivity; O.D., optic density; PPHT, 2-(N-Phenethyl-N-propyl)-amino-5-hydroxytetralin hydrochloride. Roman numbers indicate cortical layers.

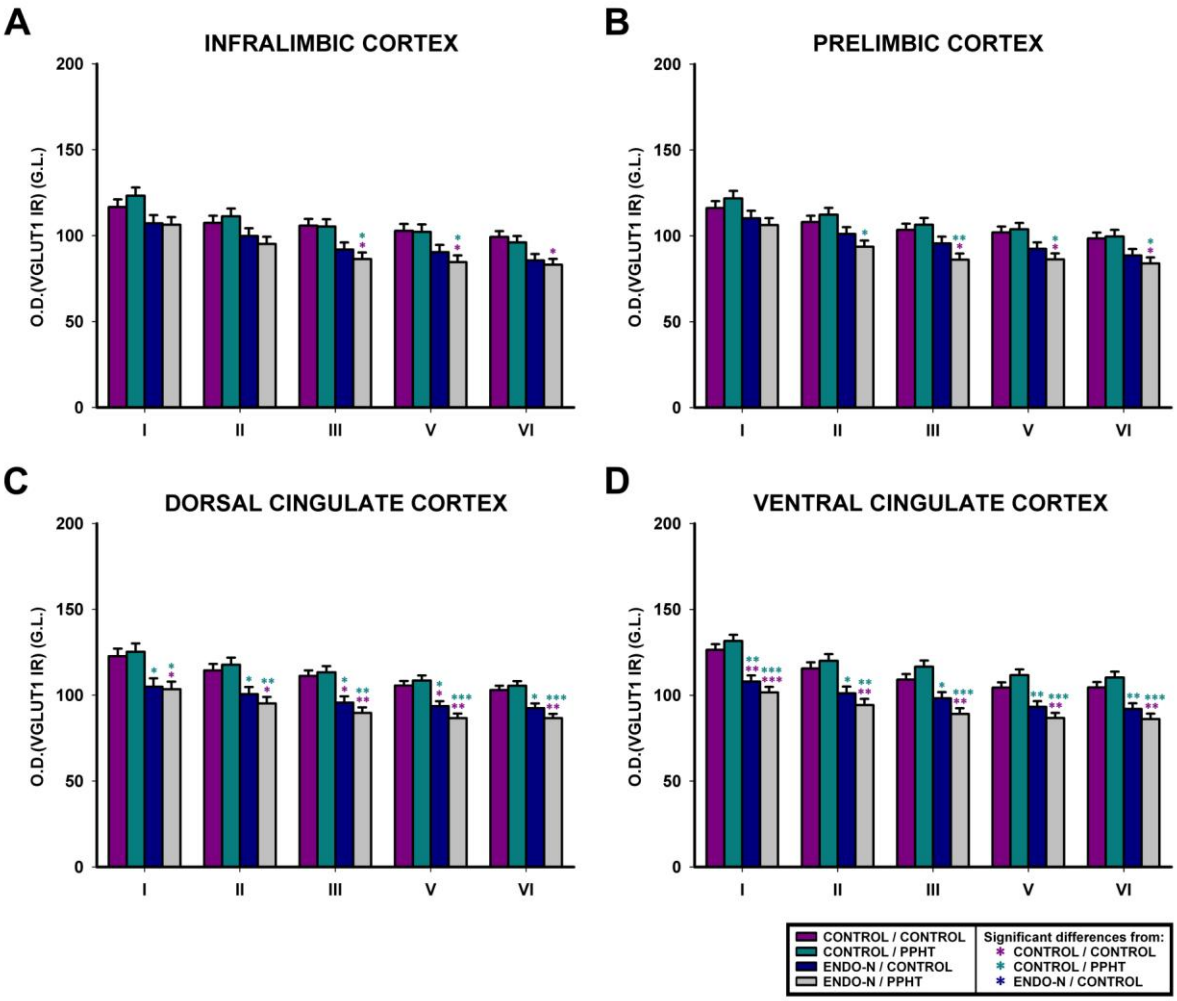

Figure 53. Graphs representing the changes in VGLUT1 neuropil expression after Endo-N and/or PPHT treatments. (A) Infralimbic cortex; (B) Prelimbic cortex; (C) Dorsal cingulate cortex; (D) Ventral cingulate cortex. Asterisks in bars indicate statistically significant differences between groups (see graph legend) after univariate repeated measures ANOVA followed by multiple pair-wise comparisons with Bonferroni's correction; $p<0.05$ (*), $p<0.01$ (**), $p<0.001$ (***). Abbreviations: Endo-N, Endo-N-acetylneuraminidase; G.L., grey levels; IR, immunoreactivity; O.D., optic density; PPHT, 2-(N-Phenethyl-N-propyl)-amino-5-hydroxytetralin hydrochloride. Roman numbers indicate cortical layers.

1.3. PPHT treatment increases the number of PSA-NCAM expressing interneurons in the mPFC, without affecting their phenotype.

In consonance with the observed increase in PSA-NCAM expression in the neuropil after PPHT treatment, the number of PSA-NCAM expressing interneurons in the mPFC was also higher in PPHT-treated animals than in non-treated ones ($p=0.0004$) (**figure 54 A & C**). In particular, statistically significant differences were observed in layers III, V and VI of infralimbic, prelimbic, dorsal cingulate and ventral cingulate cortices (**figure 55**).

Nevertheless, the percentages of PSA-NCAM expressing interneuron somata belonging to different interneuron subpopulations (defined by calcium-binding protein expression) did not change after PPHT treatment ($p>0.05$ in all comparisons; **figure** 54 **B**). Most PSA-NCAM interneurons co-expressed CB (74.0 ± 2.6% in control group, 75.3 ± 4.7% in PPHT treated group; **figure** 54 **B & D**), but much lower percentages co-expressed CR (3.7 ± 0.8% in control group, 4.5 ± 1.7% in PPHT treated group; **figure 54 B & E**) or PV (1.7 ± 0.8% in control group, 1.0 ± 0.6 % in PPHT treated group; **figure 54 B & F**).

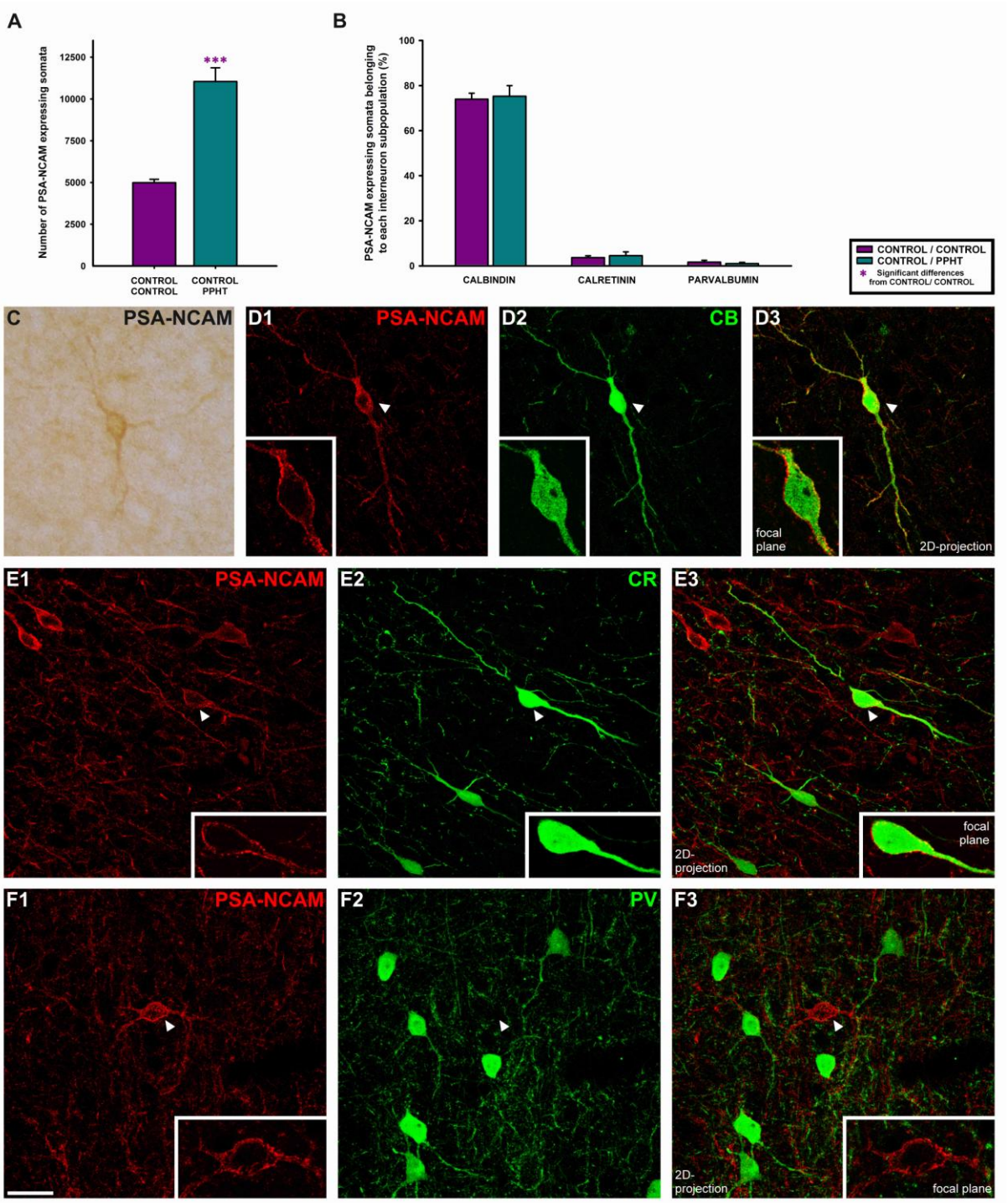

Figure 54. Quantification and confocal microscopic analysis of the neurochemical phenotype of PSA-NCAM expressing interneurons in mPFC after PPHT treatment. (A) Graph showing statistically significant differences in the number of PSA-NCAM expressing somata from control group after unpaired Student's t-test followed by Bonferroni's correction; $p<0.001$ (***). (B) Graph representing the percentages of PSA-NCAM expressing interneuron somata belonging to different interneuron subpopulations (defined by calcium-binding protein expression). No statistically significant differences from control group were observed after unpaired Student's t-tests followed by Bonferroni's correction ($p>0.05$ in all comparisons). (C) Multipolar neuron expressing PSA-NCAM in dorsal Cingulate Cortex (Cg1) layer V observed by conventional light microscopy. (D) PSA-NCAM interneuron in Cg1 layer V co-expressing CB. (E) PSA-NCAM / CR double labeled interneuron in ventral Cingulate Cortex (Cg2) layer V. (F) Lack of co-localization between PSA-NCAM (F1) and PV (F2) expressing neurons in Cg1 layer III. D-F images are 2D projections of focal planes located 1 µm apart. Scale bar: 10 µm. Insets in the images are 2X enlarged views taken from single confocal planes of the areas marked with arrowheads.

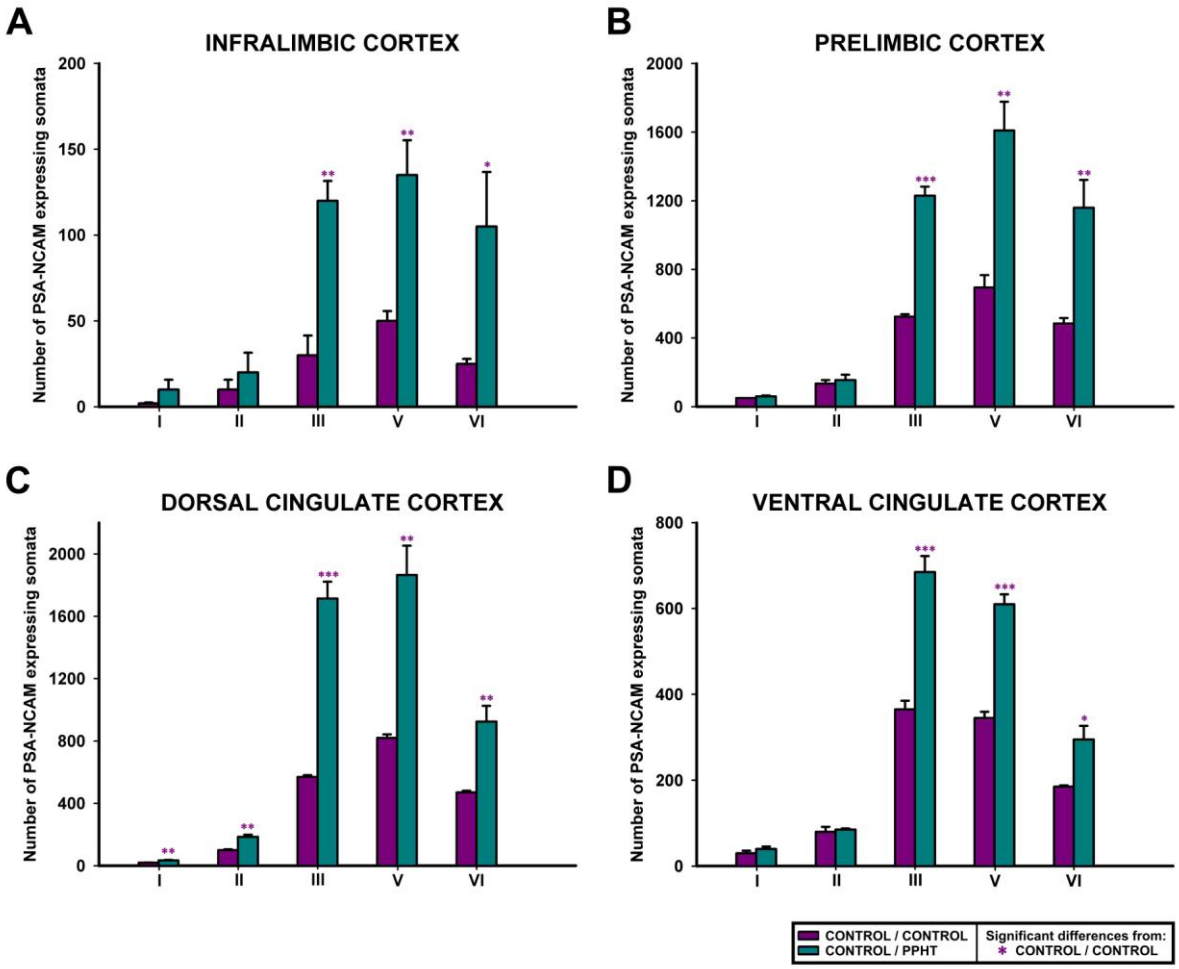

Figure 55. Graphs showing the changes in the number of PSA-NCAM immunoreactive neurons after PPHT treatment. (A) Infralimbic cortex; (B) Prelimbic cortex; (C) Dorsal cingulate cortex; (D) Ventral cingulate cortex. Asterisks in bars indicate statistically significant differences from control group after repeated measures ANOVA followed by multiple pair-wise comparisons with Bonferroni's correction; $p<0.05$ (*), $p<0.01$ (**), $p<0.001$ (***).Abbreviations: PPHT, 2-(N-Phenethyl-N-propyl)-amino-5-hydroxytetralin hydrochloride. Roman numbers indicate cortical layers.

1.4. Effects of PPHT and Endo-N treatments on perisomatic puncta on mPFC pyramidal neurons

1.4.1. PPHT treatment increases the density of PSA-NCAM expressing perisomatic puncta

PPHT treatment induces a statistically significant 123.8% increase in the density of PSA-NCAM expressing puncta surrounding pyramidal neuron somata (p=0.0023; **figure 56 A**), which is in line with the effects described above in PSA-NCAM expressing neuropil and interneurons (section **1.2** and **1.3**).

1.4.2. PPHT and/or Endo-N treatments increase the density of inhibitory perisomatic puncta

Both PPHT and Endo-N treatments when administered by themselves induced statistically significant increases (p<0.0001 in all cases) in the density of GAD65/67 (33.2% and 82.54%, respectively; **figure 56 B**) and PV (19.2% and 38.59%, respectively **figure 56 C**) expressing puncta in the perisomatic region of pyramidal neurons. However, the combination of both treatments induced statistically significant but lower increases than those observed after Endo-N treatment alone (45.8% increase, p<0.0001 for GAD65/67; 23.8% increase, p<0.0001 for PV; **figure 56 B & C**).

1.4.3. Endo-N, by itself or administered before PPHT treatment, increases the density of SYN perisomatic puncta

Endo-N administration by itself, induced a statistically significant 30.5% increase in the density of SYN expressing puncta surrounding pyramidal neuron somata (p<0.0001). Increases were even higher when PPHT was administered after Endo-N injection (44.7% increase; p<0.0001 compared with Control/Control; p=0.0008 compared with Endo-N/Control). By contrast, PPHT treatment alone did not change the density of SYN perisomatic puncta (p=0.6660) (**figure 56 D**).

1.4.4. PPHT decreases and Endo-N increases the percentage of PV perisomatic puncta co-expressing SYN

After PPHT treatment, 21.20 ± 0.53 % of PV expressing puncta surrounding pyramidal neuron somata were found to co-express SYN, which implied a small but

significant decrease of this percentage (p<0.0001) when compared with that of the control group (32.82 ± 0.56 %). Conversely, Endo-N administration induced a statistically significant increase of this percentage, reaching 48.16 ± 0.99 % (p<0.0001). When Endo-N was administered before PPHT treatment, 44.72 ± 0.65 % of PV puncta co-expressed SYN, a percentage significantly lower than that of Endo-N/Control group (p=0.0006) but still higher than that of the Control/Control group (p<0.0001) (**figure 56 E**).

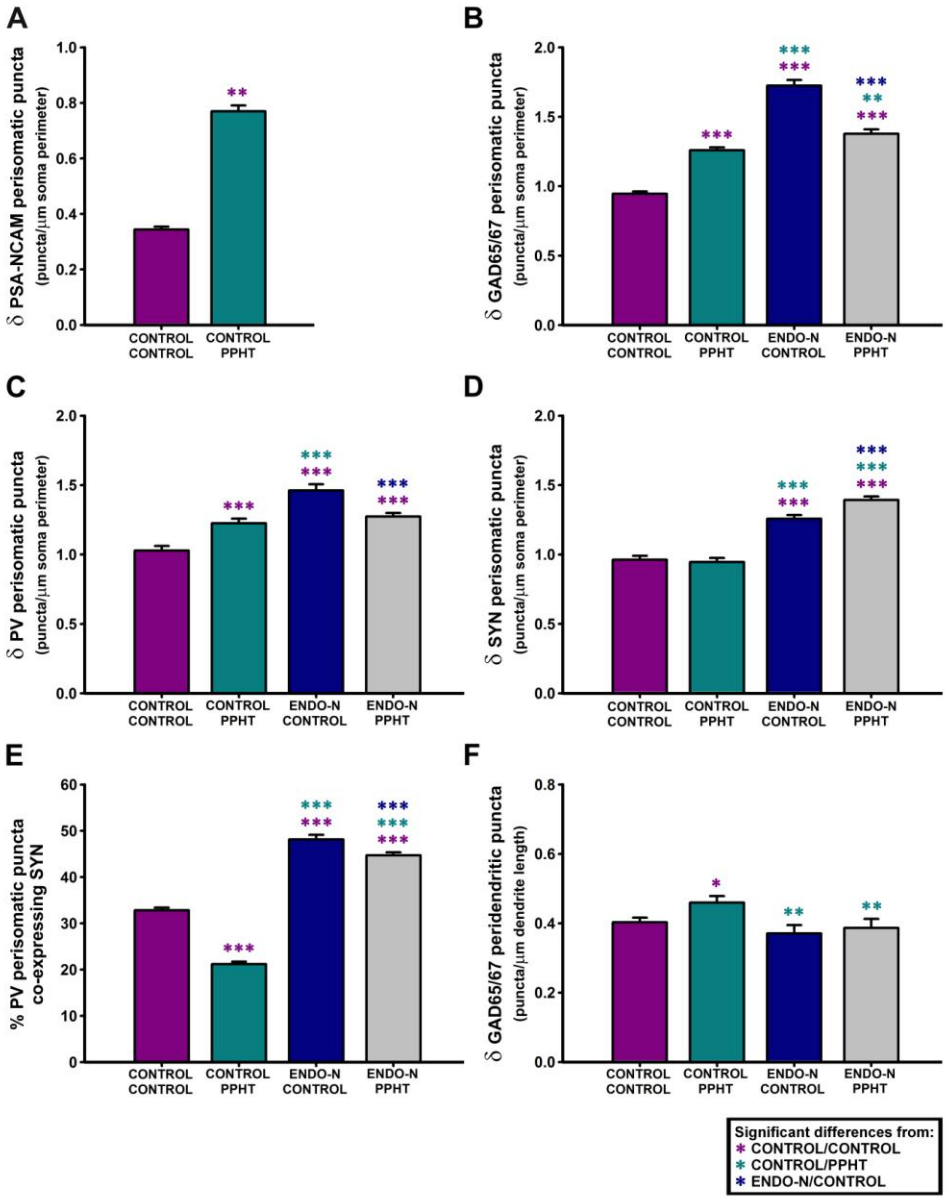

Figure 56. Graphs representing the changes in the density of PSA-NCAM, GAD67, PV and SYN expressing puncta in mPFC pyramidal neurons after Endo-N or PPHT treatments and their combination. (A-D) Perisomatic density of PSA-NCAM (A), GAD67 (B), PV (C) and SYN (D) expressing puncta, measured as the number of puncta/ μm of the pyramidal cell soma perimeter. **(E)** Percentage of PV expressing puncta co-expressing SYN. **(F)** Peridendritic density of GAD67 expressing puncta measured as number of puncta/ μm of the apical dendrite length. Asterisks in bars indicate statistically significant differences between groups (see graph legend) after one-way ANOVA followed by Bonferroni's correction; p<0.05 (*), p<0.01 (**), p<0.001 (***).

1.5. Endo-N blocks PPHT-induced increases in GAD65/67 puncta density on the apical dendrites of mPFC pyramidal neurons

Similar to that described above for GAD67 expression in mPFC neuropil (section **1.2**), PPHT treatment induced a significant increase (15.6%) in the density of peridendritic puncta expressing GAD65/67 (Control/Control vs. Control/PPHT: p=0.0215), which was blocked when animals were previously treated with Endo-N (Endo-N/Control vs. Endo-N/PPHT: p=0.5877). Endo-N administration by itself, did not change GAD65/67 peridendritic puncta density (p=0.2712) (**figure 56 F**).

1.6. PPHT and EndoN by themselves or in combination decrease dendritic spine density in mPFC pyramidal neurons

PPHT treatment induced a statistically significant overall decrease in dendritic spine density (Control/Control vs. Control/PPHT: p<0.0001; 20.7% decrease) (**figure 57 A**). Considering the distance from the soma, decreases in the spine density were only statistically significant from the second 50 µm-length segment onwards (first segment: p=0.4176; the rest of segments: p<0.0001) (**figure 57 B**).

When PSA was removed before PPHT treatment, the decrease in dendritic spine density was higher (37.9%) (Endo-N/PPHT vs. Control/Control: p<0.0001) (**figure 57 A**). Decreases were statistically significant from the second to the fourth 50 µm-length segment (p<0.0001 in all cases) (**figure 57 B**).

PSA depletion by itself also produced an overall 44.5 % decrease in spine density throughout the apical dendrites (200 µm-length) of mPFC pyramidal neurons (Control/Control vs. Endo-N/Control: p<0.0001) (**figure 57 A**). Statistically significant decreases in spine density were also found in all the four 50 µm-length segments in which the apical dendrites were divided (p<0.0001 in all cases) (**figure 57 B**).

When EndoN/PPHT group was compared with Endo-N/Control group, a statistically significant 10.5 % increase in the spine density throughout apical dendrites was detected (p=0.0058) (**figure 57 B**).

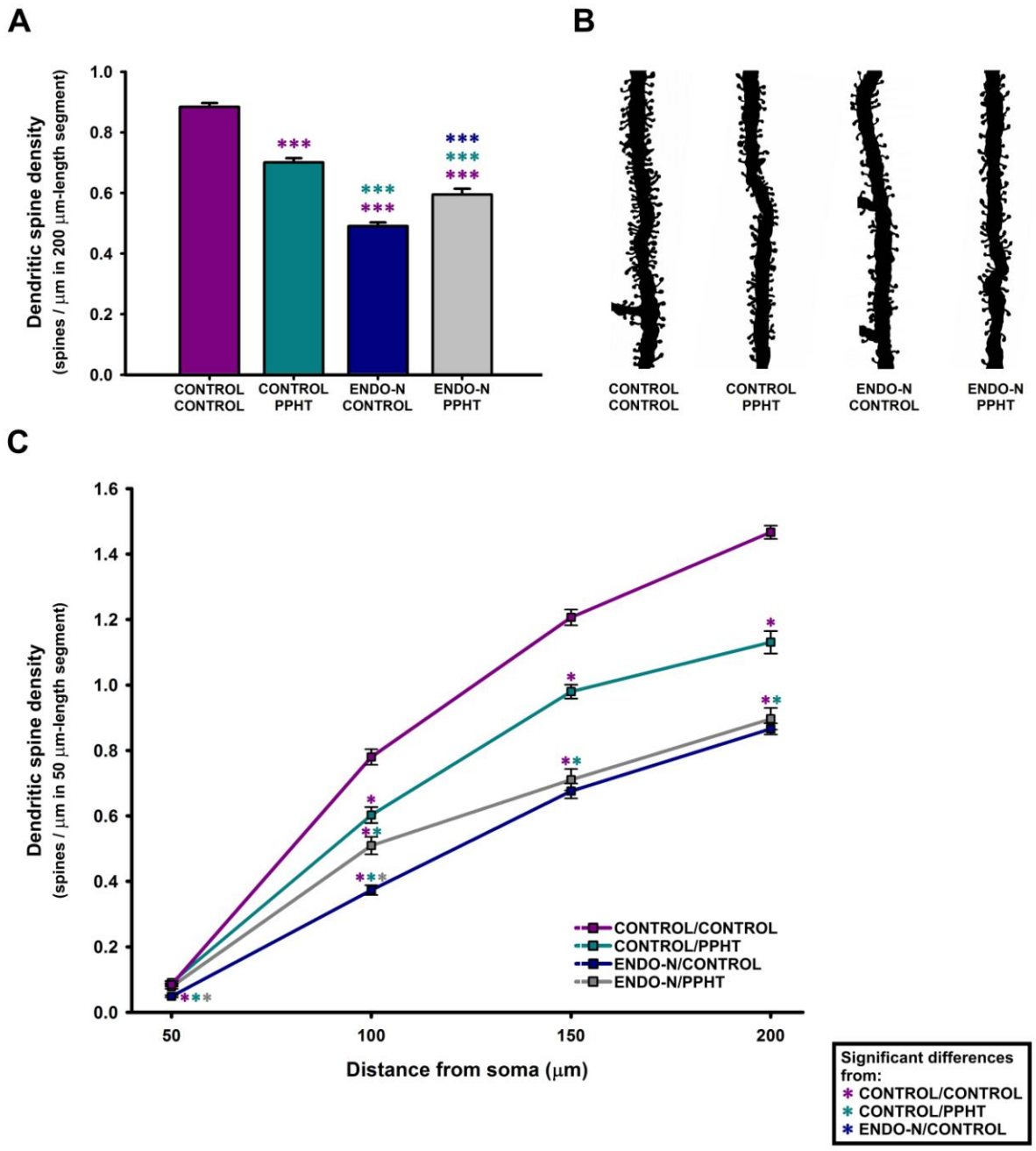

Figure 57. Dendritic spine density in mPFC pyramidal neurons is decreased after PPHT or Endo-N treatment and their combination. (A) Graph showing statistically significant differences between groups (see figure legend) when consider the total length (200 µm) of the measured dendrites. (B) Camera lucida drawings of 50 µm-length dendritic segments located 150-200 µm distal from the soma in dorsal cingulate cortex (Cg1), layer III. Note the decreased number of dendritic spines in all treated groups when compare with control/control group. (C) Graph representing dendritic spine density as function of distance from the soma in 50 µm-length segments. Asterisks in bars indicate statistically significant differences between groups (see graph legend) after one-way ANOVA followed by Bonferroni's correction. For graph (A): $p<0.05$ (*), $p<0.01$ (**), $p<0.001$ (***). For graph (B), please see p-values in the results section. For graph (C), please see p-values in the results section. Abbreviations: Endo-N, Endo-N-acetylneuraminidase; PPHT, 2-(N-Phenethyl-N-propyl) amino-5-hydroxytetralin hydrochloride.

Table 5. Summary of results: differences from Control/Control group

	CONTROL PPHT	ENDO-N CONTROL	ENDO-N PPHT
Neuropil protein expression			
PSA-NCAM	↑ ***		
SYN	↑ **	=	=
GAD67	↑ ***	=	=
VGLUT1	=	↓ *	↓ **
PSA-NCAM expressing neurons			
Number of neurons	↑ ***		
% of co-localization with CB	=		
% of co-localization with CR	=		
% of co-localization with PV	=		
Perisomatic puncta on pyramidal neurons			
δ PSA-NCAM	↑ **		
δ GAD65/67	↑ ***	↑ ***	↑ ***
δ PV	↑ ***	↑ ***	↑ ***
δ SYN	=	↑ ***	↑ ***
% of PV puncta co-expressing SYN	↓ ***	↑ ***	↑ ***
Apical dendrite of pyramidal neurons			
δ GAD65/67 peridendritic puncta	↑ *	=	=
δ spines	↓ ***	↓ ***	↓ ***

No statistically significant differences (=) or statistically significant increases (↑) or decreases (↓) on the parameters measured, when compared with control/control group following the appropriate statistical analysis (see materials and methods section); $p<0.05$ (*), $p<0.01$ (**), $p<0.001$ (***).

Abbreviations: δ, density (number of puncta or spines/μm of soma perimeter or dendrite length); PSA-NCAM, polysialylated form of de neural cell adhesion molecule; SYN, synaptophysin; GAD67, 67 kDa isoform of the glutamate decarboxilase enzime, GAD65/67, both 65 and 67 kDa isoforms of the glutamate decarboxilase enzyme; VGLUT1, vesicular glutamate transporter 1; CB, calbindin-D28k; CR , calretinin; PV, parvalbumin.

2. SHORT-TERM PSA DEPLETION IN VITRO INDUCES STRUCTURAL CHANGES IN INTERNEURONS AND AFFECTS THE CONECTIVITY OF PYRAMIDAL NEURONS

2.1. Microscopic architecture of mPFC and PSA-NCAM expression in organotypic cultures

After 14 days in vitro, mPFC conserved their appearance (**figure 58 A**) and microscopic architecture (**figure 58 A & B**) as it was *in vivo*. PSA-NCAM expression was observed in neurons and neuropil in the vehicle-treated slices (control; **figure 58 D1**) but it was completely absent in Endo-N treated slices (**figure 58 D2**).

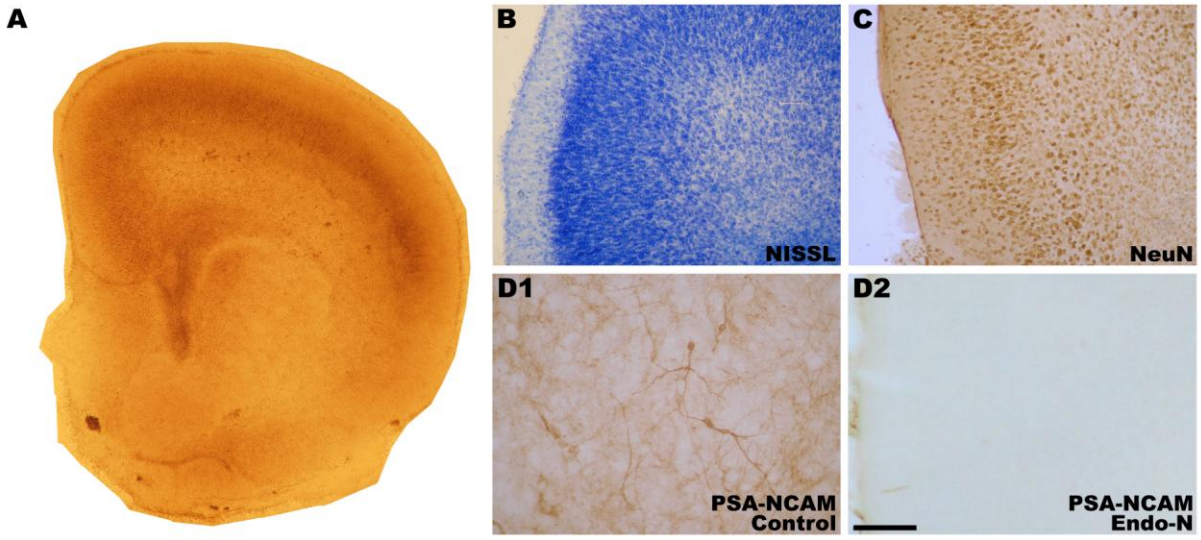

Figure 58. Photographs showing the microscopic architecture of mPFC and PSA-NCAM expression in organotypic cultures. (A) Panoramic view of mPFC slice after 14 days in vitro before being fixed. **(B-C)** Microphotographs showing that the layered organization of neurons in the mPFC is conserved after 14 days in vitro. **(B)** Nissl stained slice. **(C)** Slice processed for NeuN immunohistochemistry. **(C)** PSA-NCAM expression is observed in neurons and neuropil in the vehicle-treated slices (control; **D1**) but it is completely absent in Endo-N treated-slices (**D2**). Scale bar: 25 µm (B-C), 100 µm (D1-D2)

2.2. Endo-N decreases dendritic spine density in GAD-GFP expressing interneurons of mPFC organotypic cultures

Two days after the Endo-N delivery, GAD-GFP expressing interneurons showed a 28.1% decrease ($p=0.0485$) in dendritic spine density on the third 60 µm-length segment in which the dendrites were divided (120-180 µm distance from the soma). No statistically significant differences in spine density were found when we

analyzed the other segments or the overall dendrite length, but a trend towards a decrease could be observed in all these cases (**figure 59**).

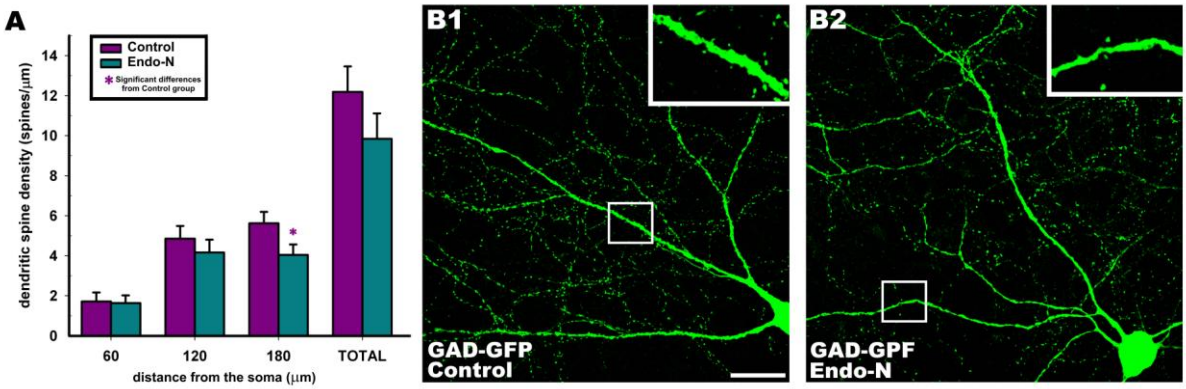

Figure 59. Confocal microscopic analysis of dendritic spine density in GAD-GFP expressing interneurons of mPFC organotypic cultures. (A) Graphs comparing dendritic spine density of GAD-GFP expressing interneurons from mPFC slices treated with Endo-N with those from slices treated with vehicle solution (control). 60, 120 and 180 indicate dendrite segments of 60 µm located from 0 to 60, 60 to 120 and 120 to 180 µm from the soma interneuron, respectively. Asterisk in bars indicate statistically significant differences in unpaired Student t-test: $p<0.05$ (*), $p<0.01$ (**), $p<0.001$. **(B1-B2)** Confocal microscopic images of GAD-GFP expressing interneurons in mPFC organotypic cultures treated with vehicle solution (control; **B1**) or Endo-N (**B2**). Note the decreased number of dendritic spines after Endo-N treatment. Insets in the images are 3X enlargements of squared areas. Scale bar: 250 µm

2.3. Effects of Endo-N treatment on the perisomatic puncta of mPFC pyramidal neurons

2.3.1. Endo-N increases the density of inhibitory perisomatic puncta

In consonance with the effects observed *in vivo* after long-term PSA depletion (section **1.4.1**), short-term Endo-N delivery *in vitro* also induced statistically significant increases in the density of inhibitory puncta surrounding the somata of pyramidal neurons ($\delta_{GAD\text{-}GFP}$: $p<0.0001$; δ_{VGAT}: $p=0.0007$; δ_{PV}: $p=0.0002$) (**figure 60 A**).

2.3.2. Endo-N increases the density of excitatory perisomatic puncta

The density of VGLUT1 expressing puncta in the perisomatic region of pyramidal neurons increased 2 days before the delivery of Endo-N in mPFC organotypic cultures ($p<0.0001$) (**figure 60 A**).

2.3.3. Endo-N increases the density of SYN perisomatic puncta

Short term PSA depletion induced a statistically significant increase in the density of SYN puncta surrounding the somata of pyramidal neurons ($p<0.0001$),

similar to what we observed *in vivo* after long-term PSA depletion (section **1.4.2**) (**figure 60 A**).

2.3.4. Changes in neuropil protein expression after Endo-N treatment

Endo-N induced a statistically significant decrease in VGAT neuropil expression ($p=0.0382$) and statistically significant increases in VGLUT1 and CB puncta ($p<0.0001$ in both cases). No statistically significant differences where found when analyzed GAD-GFP or SYN neuropil expression, in consonance with long-term PSA depletion results (**figure 60 B**).

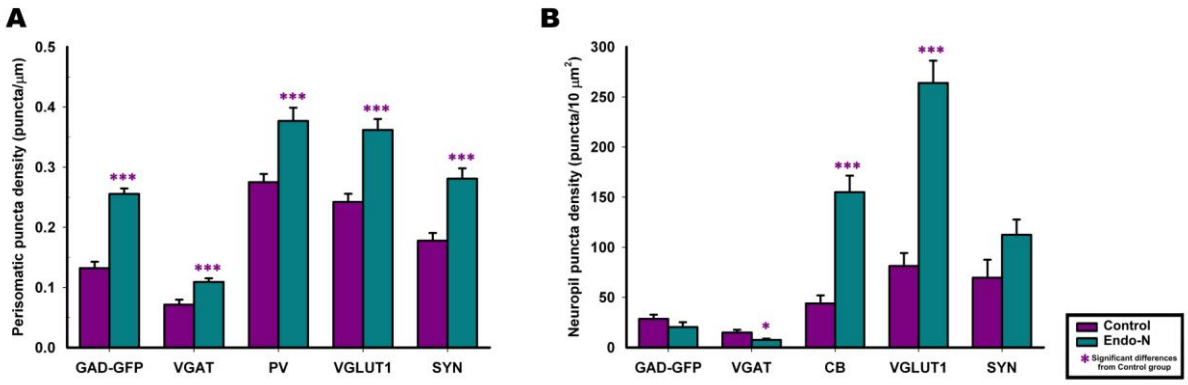

Figure 60. Graphs representing the changes in the density of GAD-GFP, VGAT, PV, CB, VGLUT1 or SYN expressing puncta in the perisomatic region of mPFC pyramidal neurons (A) and in neuropil (B) after Endo-N delivery in mPFC slices. (A) Perisomatic puncta density measured as the number of puncta/ µm of the pyramidal cell soma perimeter. **(B)** Neuropil density measured as the number of puncta/ μm^2 of tissue. Asterisks in bars indicate statistically significant differences between groups (see graph legend) after one-way ANOVA followed by Bonferroni's correction; $p<0.05$ (∗), $p<0.01$ (∗∗), $p<0.001$ (∗∗∗).

Chapter 7

DISCUSSION

1. PSA-NCAM EXPRESSION IN THE ADULT mPFC

In the mPFC of adult rats, PSA-NCAM expression is widely distributed through every region and layer and can be found in neuronal somata and neuropil elements.

As it has been commented in the introduction of this thesis, PSA-NCAM expressing neurons in the mPFC of adult rats correspond to different interneuronal subpopulations (attending to their expression of different calcium binding proteins and neuropeptides); the majority of them express CB, few of them express CR and almost none of them was found to co-express PV (Varea et al. 2005; Gómez-Climent et al. 2010). The number of PSA-NCAM expressing interneurons in this region is stable over lifetime (Varea et al. 2009), but pharmacological manipulations of monoaminergic neurotransmission (present work and Varea et al. 2007a) can decrease or increase it, indicating that inhibitory neurons in the mPFC can probably stop expressing, express “de novo” or re-express PSA-NCAM. Nevertheless, the percentages of PSA-NCAM expressing interneurons belonging to different interneuron subpopulations did not change, at least after D2R agonist treatment. Moreover, a very similar neurochemical phenotype has been found in PSA-NCAM expressing neurons in the mPFC of adult humans (Varea et al. 2007), mice (Nacher et al. 2010, Gómez-Climent et al. 2010) and cats (Varea et al. 2011), with only minor differences in the percentages across species. Together, all these data suggest that PSA-NCAM is always expressed by the same subgroups of mPFC interneurons, although additional studies exploring these interneurons in other species or after different pharmacological or behavioral conditions are necessary to confirm this hypothesis. It is also possible that all, or a subset of PSA-NCAM expressing interneurons retain this expression constitutively since their generation during embryonic development (Gómez-Climent el al. 2010; Varea et al. 2005) and could probably switch on and off this expression depending on synaptic activity.

The PSA-NCAM expressing puncta that surround pyramidal neurons in the mPFC of adult rats also seem to correspond to inhibitory and synaptic elements, as it has been described before for neocortical neuropil elements expressing this molecule (Gómez-Climent et al. 2010). Surprisingly, despite the fact that it is extremely rare to find this molecule in neuronal somata expressing PV (Varea et al., 2005; Gomez-Climent et al., 2010), we have found that co-expression of PV and PSA-NCAM is common in perisomatic puncta on pyramidal neurons. This suggests that in PV

expressing interneurons, PSA-NCAM may have a restricted expression pattern, similar to that of mature hippocampal granule neurons, which only express PSA-NCAM in their axons, but not in their somata or dendrites (Seki and Arai, 1999). Moreover, PSA-NCAM expression in this puncta may be regulated by the manipulation of dopamine neurotransmission in the mPFC, as demonstrated in the present work.

Although both polysialyltransferases, ST8SiaII and ST8SiaIV, are present in the adult mPFC (see Oltmann-Norden et al. 2008 for review), the absence of PSA-NCAM in the mPFC of *ST8SiaIV-/-* mice, but its normal expression in *ST8SiaII-/-* mice, indicate that *ST8SiaIV* is the solely responsible for PSA synthesis in prefrontocortical neurons during adulthood (Nacher et al. 2010). In fact, *ST8SiaIV* mRNA level in the mPFC increases after 4 days of D2R agonist treatment, while *ST8SiaII* gene expression does not change in any of the time points analyzed (present work). However, this does not necessarily imply that *ST8SiaII* could not be also responsible of PSA synthesis when it is induced by other pharmacological treatments or different behavioral challenges.

Given its anti-adhesive properties, PSA-NCAM expression in neurons has been traditionally linked to plastic events, such as dendritic or spine remodeling and synaptogenesis (Sandi, 2004; Bonfanti, 2006; Gascon et al., 2007; Rutishauser, 2008). However, a non-excluding insulating role for PSA-NCAM, preventing, totally or partially, the establishment of synapses should not be discarded. In fact, taking into account its steric effects (Johnson et al., 2005), the addition of PSA to NCAM in a synaptic contact should prevent or profoundly affect normal neurotransmission. Consequently, the expression of PSA-NCAM in certain neuropil elements and especially in perisomatic puncta on pyramidal cells may indicate that these structures are not establishing functional synaptic contacts. In connection with this idea, our laboratory has recently found that PSA-NCAM expressing interneurons have reduced synaptic input, reduced spine density and are less arborized than neighboring interneurons lacking PSA-NCAM, which suggests that they are partially disconnected from cortical circuitry (Gomez-Climent et al., 2010).

2. RELATIONSHIP BETWEEN PSA-NCAM EXPRESSING NEURONS AND DOPAMINERGIC INNERVATION IN THE mPFC

Interneurons in the mPFC express D2R (Santana et al. 2009), especially those expressing PV, but also, to a lesser extent, those expressing CB (Le Moine and Gaspar, 1998). We have found that most PSA-NCAM expressing neurons in the mPFC co-express D2R and CB. Since it has been demonstrated in several species that PSA-NCAM expressing cells are mainly a subpopulation of calbindin expressing interneurons (Gómez-Climent et al. 2010, Nacher et al. 2010, Varea et al. 2005, 2007c and unpublished results), it may be possible that they represent those displaying D2R expression.

Interneurons in the mPFC are common targets of dopaminergic innervation coming from the VTA and some of these dopaminergic contacts have the morphology characteristic of symmetric synapses (Sesack et al., 1995, 1998). Interneurons expressing PV appear to be the main target of dopaminergic terminals (Sesack et al., 1995, 1998) and although they do not express PSA-NCAM in their all extension, basket axon terminals in rats and PV cartridges in humans have been shown to express this molecule (present work and Arellano et al. 2002). Our study is the first to report dopaminergic fibers in close apposition to CB interneurons, suggesting that dopamine may also modulate their function. This hypothesis is also supported by our finding that D2R are present in this interneuronal subtype. Since we have found that some dopaminergic puncta appear to contact PSA-NCAM expressing interneurons and that some of them display synaptophysin expression, it is reasonable to think that, at least part of these structures, may be synaptic contacts.

3. THE LESION OF THE DOPAMINE MESOCORTICAL PATHWAY DECREASES THE EXPRESSION OF PLASTICITY-RELATED PROTEINS

6-OHDA-induced depletion of cortical dopaminergic terminals produces a significant reduction in PSA-NCAM expression in all prefrontocortical regions. This is consistent with other studies showing that modulation of dopaminergic neurotransmission by cocaine also affects PSA-NCAM expression in the hippocampus (Mackowiak et al., 2005) and that the expression of other cell adhesion molecules, such as L1 may also be regulated by 6-OHDA lesion (Poltorak et al., 1997). Given the implication of PSA-NCAM in neuronal structural plasticity (Bruses

and Rutishauser, 2001, Sandi, 2004) and the modulation of its expression by dopamine, it is reasonable to think that the ability of neurons in this region to undergo neuritic and/or synaptic remodeling may be affected after specific dopamine depletion. In fact, a study using neonatal rats has described dendritic atrophy in pyramidal neurons of the mPFC (Sherren and Pappas, 2005). We still do not know whether neuritic or spine remodeling occur in adult mPFC neurons after lesioning the VTA, but our finding of a concomitant reduction in synaptophysin probably reflects a decrease in synaptic density (Eastwood and Harrison, 2001, Masliah et al., 1990), which may occur in parallel to neuronal structural remodeling. This regressive event may be triggered via PSA-NCAM downregulation, since the removal of PSA from NCAM blocks the formation of synapses (Dityatev et al., 2004). Supporting this fact, we have recently found that the downregulation of PSA-NCAM expression in the amygdala after chronic fluoxetine treatment is accompanied by a concomitant decrease in synaptophysin expression (Varea et al., 2007b). Conversely, this treatment induces upregulation of both PSA-NCAM and synaptophysin expression in the mPFC (Varea et al., 2007a, 2007b).

PSA-NCAM expressing cells in the mPFC are mainly interneurons and puncta expressing this molecule in the neuropil, also appear to belong to these cells (Varea et al., 2005; Gómez-Climent el al. 2010, present work). Consequently, changes in PSA-NCAM expression should affect primarily inhibitory networks. This hypothesis is supported by our finding of a concomitant prefrontocortical downregulation of GAD67 expression after VTA lesion. This is consistent with similar studies reporting a decrease in GAD67 mRNA expression in the prelimbic cortex of adult rats (Retaux et al.,1994). Interestingly, this downregulation was due to a change in GAD67 expression in a subset of interneurons located in the prelimbic cortex deep layers, a region displaying a considerable density of PSA-NCAM expressing neurons (Varea et al., 2005).

4. EFFECTS OF D2R AGONIST AND ANTAGONIST TREATMENTS ON mPFC NEURONAL CIRCUITRY

Our results suggest that the effects of DA on PSA-NCAM, SYN and GAD67 expression in the mPFC are mediated by D2R, since agonists for this receptor upregulate the expression of these molecules and the opposite effect is found after treatment with D2R specific antagonists. However, although the data are consistent

with a D2R-mediated effect, due to the dose and pharmacology of the drugs used, alternative explanations may also exist.

In different telencephalic regions, including the mPFC, changes in PSA-NCAM expression correlate well with neuronal structural remodeling. While upregulation of PSA-NCAM expression is observed in parallel to dendritic outgrowth or increases in spine density, its downregulation accompanies dendritic atrophy or decreases in synaptic density (Cordero et al., 2005; Varea et al., 2007a). Our gene expression study during PPHT treatment indicates that the regulation of PSA-NCAM expression may be mediated by changes in the expression of the polysialyltransferases and NCAM, since *st8siaIV* mRNA levels in the mPFC increased after four days of treatment and *ncam* gene expression decreased at the end of the treatment.

Previous data have indicated the involvement of D2R in neuronal remodeling and are consistent with the dynamics of PSA-NCAM expression that we observe after our pharmacological manipulations. There is previous evidence that dopamine acting through D2R is capable of inducing changes in cortical synapses similar to those described in our study. A significant decrease in synaptic density in the rat PFC has been observed after administration of a selective D2R antagonist. Conversely, treatment with the selective D2R agonist PPHT (the same compound used in our study) increases synaptic density in this region (Sugahara and Shiraishi, 1999). The effects of chronic haloperidol treatment on synaptic plasticity appear to be more complex and probably depend on the duration of the treatment. Sixteen weeks of haloperidol treatment lead to a reduction of axon terminals with asymmetric synapses in the rat mPFC (Benes et al., 1985). However, chronic treatment for 3 weeks increases synapses on dendritic shafts and dendritic spines (Klintzova et al., 1989) and a 16 week treatment increases synaptophysin mRNA expression (Eastwood et al., 1997). Other study has failed to report changes in synaptophysin expression in the mPFC after chronic haloperidol treatment (Nakahara et al., 1998).

Our results indicate that the number of excitatory synapses is not affected in the mPFC neuropil after chronic PPHT treatment, because we do not detect changes in the expression of VGLUT1 in this cortical region. We have no data on the expression of markers of excitatory synapses in the mPFC after chronic D2R antagonist treatment. Previous ultrastructural analyses using chronic haloperidol treatment have rendered contradictory results. The study by Klintzova et al. (1989) indicated an increase in the number excitatory synapses because it found a higher

number of synapses on dendritic spines, which are mainly excitatory. By contrast, Benes et al. (1985), found a reduction in the number of asymmetric synapses in the mPFC.

By contrast, pharmacological manipulation of D2R appears to have a profound effect on inhibitory neurotransmission in the mPFC. Dopamine enhances the activity of interneurons in the PFC and induces the release of GABA from these cells (Retaux et al., 1994). The opposite effects have been observed after acute administration of haloperidol (Bourdelais and Deutch, 1994). Our results with haloperidol and PPHT treatments give support to these studies, indicating a role for D2R in the modulation of GABAergic neurotransmission in the mPFC. Moreover, our gene expression study showed that the two enzymes responsible for GABA synthesis are affected by D2R manipulation, since four days of PPHT treatment increased mRNA levels of both *gad65* and *gad67* genes in the mPFC. The upregulation of GAD65/67 protein expression in the neuropil also induced by PPHT probably reflects an increase in inhibitory synapses on pyramidal neurons, since the number of puncta expressing these GABA-synthesizing enzymes also increases in the peridendritic and perisomatic regions of these cells.

In the perisomatic region of pyramidal neurons we also detect a PPHT-induced increase in the density of puncta expressing PV, a calcium binding protein expressed by many fast spiking/basket interneurons. A direct effect of PPHT in these inhibitory structures is likely, because D2R are particularly abundant in basket interneurons (Le Moine and Gaspar, 1998) and D2R agonists activate these cells (Tseng and O'Donnell, 2007). Moreover, activation of D2R attenuates excitatory synaptic transmission in the adult PFC, involving GABA release by local interneurons (Retaux et al., 1994).

However, conflicting results regarding these effects of D2R activation on inhibitory neurotransmission have also been reported (Seamans et al., 2001; Gao et al., 2003; Trantham-Davidson et al., 2004). Moreover, although it is reasonable to think that most of the perisomatic immunoreactive puncta correspond to inhibitory axo-somatic synapses, the density of perisomatic SYN puncta is not affected by PPHT and there is a decrease in the percentage of PV expressing puncta expressing SYN, which may indicate that some of the new perisomatic puncta expressing GAD65/67 and PV induced by PPHT are not functional synapses. In fact, our gene

expression study during PPHT treatment also failed into find significant differences in the level of *syn* gene expression in any of the time points analyzed.

These effects of PPHT on inhibitory structures occur in parallel to a decrease in pyramidal neuron spine density. This is, to our knowledge, the first report describing effects of a selective D2R agonist on this structural parameter. However, there are previous evidences suggesting that manipulation of dopamine levels modulates spine density in this cortical region. Chronic treatments with drugs that promote dopaminergic neurotransmission (among other effects), such as cocaine, phencyclidine and amphetamine, have rendered conflicting results: Although there is evidence, at least in primates, that long term amphetamine treatment decreases spine density in the mPFC (Selemon et al., 2007), there are also reports describing increases in spine density (Robinson and Kolb, 1999; Robinson et al., 2001) and in the density of axospinous synapses (Morshedi et al., 2009). In consonance with our results, it is also important to note that either acute stress or exposure to estrogens, which decrease spine density in rat mPFC pyramidal neurons (Radley et al., 2005; Hao et al., 2006), also increase dopamine accumulation (Mangiavacchi et al., 2001; Arnsten et al., 2010). However, dopamine depletion from the mPFC, genetic deletions of D2R or decreases in dopamine levels frequently observed in schizophrenia or after chronic stress are also associated with reductions in spine density in this area (Wang and Deutch, 2008; Wang et al., 2009). Additionally, cultures of frontocortical neurons of fetal rats in the presence of a D2R selective agonist resulted in a dramatic increase in neurite length and branching, and these effects were blocked by D2R antagonists (Todd, 1992). Similar structural effects were found when a neuronal cell line transfected with D2R was treated with a specific D2R agonist (Swarzenski et al., 1994). Chronic treatment with the specific antagonist haloperidol reduce spine density in the striatum (Kelley et al., 1997) and this antagonist also induces a downregulation of spinophilin expression, a protein selectively located in dendritic spines and an increased phosphorylation of MAP2 in the mPFC, which may be indicative of dendritic atrophy (Lidow et al., 2001). These conflicting results may indicate that dopamine has an inverted-U shaped influence on mPFC pyramidal neuron structure, similar to its influence on the function of this cortical region (Arnsten, 2009).

The effects of PPHT on spine density may be directly mediated by D2R present in pyramidal neurons (these receptors can be localized in their spines) (Yao

et al., 2008); but also indirectly, through D2R present in interneurons (Santana et al., 2009). In fact, previous reports showed that D2R agonists decrease AMPA receptor expression in mPFC pyramidal neurons (Sun et al., 2005), which in turn decreases spine density in these cells (Nimchinsky et al., 2002).

5. EFFECTS OF PSA DEPLETION FROM THE mPFC

Although the effects of PSA depletion in the mPFC neuropil are only restricted to VGLUT1 expression, those on the perisomatic region of pyramidal neurons are more dramatic, increasing the density of perisomatic puncta expressing GAD65/67, PV and SYN, as well as the percentage of PV puncta that co-express SYN. Moreover, similar results were found in mPFC organotypic cultures after two days of PSA depletion. A possible explanation for these effects is that the removal of PSA from NCAM may activate some perisomatic synapses, which were previously blocked by the presence of PSA. Consequently, the expression of molecules related to active inhibitory neurotransmission, such as SYN, GAD65/67 and PV, is increased and more puncta become detectable. These results are in agreement with a previous study on the developing visual cortex, in which PSA depletion induced precocious maturation of perisomatic innervation by basket interneurons, resulting in enhanced inhibitory synaptic transmission (Di Cristo et al., 2007). Thus, the presence of PSA-NCAM in control adult mPFC may act as a regulator of perisomatic inhibitory innervation.

PSA removal from the mPFC also induces dramatic effects on dendritic spine density in pyramidal neurons. Since these excitatory cells do not express PSA-NCAM during adulthood (Gomez-Climent et al., 2010), this loss of spines, as well as the decrease in VGLUT1 expression in the neuropil, must be a secondary effect mediated by interneurons. However, in mPFC organotypic cultures VGLUT1 expression increases in the mPFC neuropil and also in the perisomatic region of pyramidal neurons after two days of PSA depletion. This may indicate that the decrease in excitatory neurotransmission detected in the mPFC after long-term PSA depletion is a rebound effect mediated by interneurons in response to an initial cortical hiperexcitability.

Removal of PSA from the mPFC completely blocks the effects of PPHT treatment on SYN and GAD65/67 expression in the neuropil and in the number of peridendritic GAD65/67 puncta on pyramidal neurons. Consequently, the appearance

of new structures belonging to interneurons and new synapses (presumably inhibitory ones, since VGLUT1 expression is not affected) may need the expression of PSA-NCAM. The anti-adhesive properties of this molecule may favor the extension/formation of neurites and synapses from certain interneurons in a similar way to what have been described in hippocampal granule neurons (Saegusa et al., 2004). The effects of Endo-N on PPHT-induced changes on perisomatic structures of pyramidal cells are more complex to interpret, since PSA depletion "*per se*" has important effects on these structures. Although it is known that PSA-NCAM is crucial for the maturation of these perisomatic inhibitory networks (Di Cristo et al., 2007), further research is needed to unravel the role of this molecule in the plasticity of these structures.

Our results also show that PSA depletion has an effect on the dendritic structure of mPFC interneurons. Two days of PSA depletion in organotypic cultures decreased spine density in the dendrites of mPFC interneurons. A recent study from our laboratory has shown that in the hippocampus of control adult mice interneurons expressing PSA-NCAM have less dendritic spines than those lacking PSA-NCAM expression (Gómez-Climent et al. 2010). Unfortunately, in our present experiment we have not monitored individual interneurons for PSA-NCAM expression before PSA depletion and, consequently, our data derive from the general population of interneurons, comprised by those expressing and those lacking PSA-NCAM. Future experiments following the structure of identified PSA-NCAM expressing interneurons should be performed to identify what subpopulation of interneurons is affected by PSA depletion and whether the removal of PSA affects initially the structure of those previously expressing this molecule.

The changes induced by PSA depletion or by alterations in the degree of NCAM polysialylation, may not only be caused by the regulation of NCAM adhesive properties, but also by the influence of PSA on NCAM-mediated signaling (see (Gascon et al., 2007) for review). Moreover, interference on NCAM may also impair dopaminergic neurotransmission, since NCAM regulates the trafficking, internalization and degradation of D2R (Xiao et al., 2009).

6. NEUROLOGICAL AND PSYCHIATRIC DISEASES

The results of our experiments using 6-OHDA lesion of the VTA and the consequent depletion of dopamine from the mPFC may have implications in our understanding of Parkinson's disease. This neurological disorder is mainly characterized by the disappearance of dopaminergic neurons in the substantia nigra, which are responsible of the motor problems associated with this disorder. However, it is known that neurons synthesizing dopamine in the VTA are also affected and, consequently, the dopaminergic mesocortical pathway. Different lines of evidence point to the lesion of this pathway as the responsible of certain cognitive deficits associated to Parkinson's disease. Moreover, this lesion may also be responsible of the prevalence in parkinsonian patients of psychiatric disorders in which the medial prefrontal cortex has a critical role. However, the exact contribution of dopaminergic deficiency to cognitive defects in Parkinson's disease is not well understood. Our results suggest that a reduction of dopaminergic innervation in the mPFC induces synaptic plasticity that may lead to altered wiring of intrinsic GABAergic circuits. In fact, humans with Parkinson's disease show reduced cortical synaptophysin expression, which is even more decreased in demented patients (Zhan et al.,1993), and decreased GAD expression in the prefrontal cortex (Lanoue et al., 2010). Our results suggest that PSA-NCAM is involved in these changes. This molecule is also expressed in the human PFC (Varea et al., 2007c), and, consequently, studies of PSA-NCAM expression in the prefrontal cortex of Parkinson's disease patients may be extremely interesting.

Dopamine and its receptors, especially D2R, are profoundly implicated in the etiology and the treatment of psychiatric disorders such as major depression or schizophrenia. Our results linking dopaminergic neurotransmission, structural plasticity and inhibitory neurons may have implications in the understanding of the molecular bases of these disorders, since decreased levels of dopamine (Di Forti et al., 2007; Arnsten, 2009) and D2R (Knable et al., 2001; Zhang et al., 2010), as well as deficits in GABAergic neurotransmission and PV expressing interneurons have been found in the PFC of patients and animal models of major depression and schizophrenia (Volk and Lewis, 2002; Schiavone et al., 2009).

The administration of dopamine receptor antagonists or drugs that reduce dopamine levels, induce symptoms resembling those of endogenous depression

(Willner, 1983). Conversely, dopamine receptor agonists, as well as drugs that increase dopamine function, have antidepressant-like profiles in animal models of depression (Muscat et al., 1992) and have been reported to have efficacy in the treatment of human depression (Willner et al., 2005). Dopamine can act by binding to different receptors, but the D2 subtype seems to play a key role in the response to antidepressant treatments (Gershon et al., 2007). The present results show that changes in neuronal remodeling and synaptic plasticity, as indicated by the modulation of the expression of PSA-NCAM, synaptophysin and molecules related to inhibitory neurotransmission, may participate in the antidepressant effects of dopamine mediated by D2R. We have recently shown that similar neuronal plasticity mediates the effects of antidepressants acting on serotoninergic neurotransmission (Varea et al., 2007a, 2007b), providing a substrate to the neuroplastic hypothesis of depression (Castren, 2005; Duman, 2002).

Our results may also have important implications in the understanding of the molecular bases of schizophrenia and antipsychotic treatment, since dopamine dysregulation underlies positive psychotic symptoms in schizophrenic patients (Di Forti et al., 2007) and D2R antagonists are the most widely used antipsychotics. Moreover, neuroimaging studies have revealed structural changes in the mPFC of patients suffering from schizophrenia (Harrison, 1999). PSA-NCAM expression may be involved in these modifications, since it is present in the PFC of adult humans (Varea et al., 2007c) and alterations in the number of PSA-NCAM expressing neurons have been described in the hippocampus of schizophrenic patients (Barbeau et al., 1995), a region which, like the mPFC, also shows structural modifications in these patients (McCarley et al., 1999). It would be thus interesting to perform PSA-NCAM expression analysis in the mPFC of postmortem tissue from depressed and schizophrenic patients, because, although traditionally the etiology of these psychiatric disorders has been attributed to neurochemical imbalances in the mPFC and other cerebral regions, recent hypotheses suggest that alterations in the structural plasticity of neuronal networks may also be involved in these mental diseases (Castren 2005; Duman et al., 1999; Frost et al., 2004). The fact that PSA-NCAM expression is restricted to interneurons in the mPFC is also very interesting (Varea et al., 2005, 2007c), because there are evidences indicating abnormalities in the density and distribution of these inhibitory cells in patients suffering schizophrenia

and major depression (Benes and Berretta, 2001; Daskalakis et al., 2007; Rajkowska et al., 2007).

Interestingly, there is evidence for a relationship between dysregulation of NCAM and its posttranslational modifications and the neural abnormalities found in different mood disorders (Vawter, 2000). Moreover, *ST8SiaII*, one of the enzymes responsible for NCAM polysialylation is a candidate susceptibility gene for schizophrenia and bipolar disorder (Arai et al., 2004; Tao et al., 2007) and PSA-NCAM expression is altered in the brain of schizophrenics (Barbeau et al., 1995). Our results showing the involvement of PSA-NCAM in the plasticity induced by D2R manipulation and its necessary presence for the maintenance of mPFC perisomatic inhibition also support the idea that altered PSA-NCAM expression may participate in the pathogenesis of these psychiatric disorders.

Chapter 8

CONCLUSIONS

1. PSA-NCAM expressing cells are widely distributed throughout every region and layer in the mPFC of adult rats and show a unipolar, bipolar or multipolar morphology.

2. There is a clear lamination pattern of PSA-NCAM expression in the mPFC neuropil, with low expression in superficial layers, moderate expression in layer III and intense expression in deep layers.

3. Pyramidal neurons in the mPFC do not express PSA-NCAM, but their somata are surrounded by PSA-NCAM expressing puncta, which co-express markers of inhibitory or synaptic structures. A high percentage of these PSA-NCAM expressing puncta co-express the calcium binding protein PV.

4. Most PSA-NCAM expressing somata in the mPFC co-express D2R and the majority of them pertain to the CB expressing interneuron subpopulation.

5. Dopaminergic fibers in the mPFC are closely apposed to PSA-NCAM expressing interneurons and some of them display SYN expression.

6. Both the lesion of the mesocortical dopamine pathway and the chronic treatment with a D2R antagonist, decrease the expression of PSA-NCAM, GAD67 and SYN in the mPFC neuropil. Chronic treatment with a D2R agonist has the opposite effects.

7. During chronic treatment with a D2R agonist, the mPFC show temporal differences in the expression of the majority of the plasticity related genes analyzed (*St8siaIV*, *ncam*, *gad65* and *gad67),* while others do not change their expression in any of the time points analyzed *(syn* and *St8siaII)*.

8. D2R agonist treatment increases the number of PSA-NCAM expressing interneurons and that of elements expressing this molecule in the neuropil and the perisomatic region of pyramidal neurons. This treatment also increases the expression of SYN in the neuropil and that of inhibitory markers in the neuropil and the perisomatic and peridendritic regions of pyramidal neurons. By contrast, spine density is reduced in these neurons.

9. PSA depletion from the mPFC using the enzyme Endo-N, prevents the effects of D2R agonist treatment on the neuropil and the peridendritic region of pyramidal neurons. However, changes in the perisomatic region or the spines of these principal neurons are not affected.

10. PSA depletion by itself increases the expression of SYN and inhibitory markers in the perisomatic region and reduces spine density in pyramidal neurons.

11. Short term PSA depletion *in vitro* decreases spine density in mPFC interneurons and increases the number of puncta expressing inhibitory, excitatory and synaptic markers surrounding the somata of pyramidal neurons.

Chapter 9

REFERENCES

A

Acheson A, Sunshine JL, Rutishauser U (1991) NCAM polysialic acid can regulate both cell-cell and cell-substrate interactions. J Cell Biol 114:143-153.

Angata K, Nakayama J, Fredette B, Chong K, Ranscht B, Fukuda M (1997) Human STX polysialyltransferase forms the embryonic form of the neural cell adhesion molecule. Tissue-specific expression, neurite outgrowth, and chromosomal localization in comparison with another polysialyltransferase, PST. J Biol Chem 272:7182-7190.

Angata K, Long JM, Bukalo O, Lee W, Dityatev A, Wynshaw-Boris A, Schachner M, Fukuda M, Marth JD (2004), Sialyltransferase ST8Sia-II assembles a subset of polysialic acid that directs hippocampal axonal targeting and promotes fear behavior. J Biol Chem 279: 32603-32613.

Arai M, Itokawa M, Yamada K, Toyota T, Haga S, Ujike H, Sora I, Ikeda K, Yoshikawa T (2004) Association of neural cell adhesion molecule 1 gene polymorphisms with bipolar affective disorder in Japanese individuals. BiolPsychiatry 55:804-810.

Arellano JI, DeFelipe J, Munoz A (2002) PSA-NCAM immunoreactivity in chandelier cell axon terminals of the human temporal cortex. Cereb Cortex 12:617-624.

Arellano JI, Espinosa A, Fairen A, Yuste R, DeFelipe J (2007) Non-synaptic dendritic spines in neocortex. Neuroscience 145:464-469.

Arnsten AF (1997) Catecholamine regulation of the prefrontal cortex. J Psychopharmacol 11:151-162.

Arnsten AF (2009) Stress signalling pathways that impair prefrontal cortex structure and function. Nat Rev Neurosci 10:410-422.

Arnsten AF, Paspalas CD, Gamo NJ, Yang Y, Wang M (2010) Dynamic Network Connectivity: A new form of neuroplasticity. Trends Cogn Sci 14:365-375.

Ascoli GA, Alonso-Nanclares L, Anderson SA, Barrionuevo G, Benavides-Piccione R, Burkhalter A, Buzsaki G, Cauli B, Defelipe J, Fairen A, Feldmeyer D, Fishell G, Fregnac Y, Freund TF, Gardner D, Gardner EP, Goldberg JH, Helmstaedter M, Hestrin S, Karube F, Kisvarday ZF, Lambolez B, Lewis DA, Marin O, Markram H, Munoz A, Packer A, Petersen CC, Rockland KS, Rossier J, Rudy B, Somogyi P, Staiger JF, Tamas G, Thomson AM, Toledo-Rodriguez M, Wang Y, West DC, Yuste R (2008) Petilla terminology: nomenclature of features of GABAergic interneurons of the cerebral cortex. Nat Rev Neurosci 9:557-568.

B

Ballesteros-Yáñez I, Muñoz A, Contreras J, Gonzalez J, Rodriguez-Veiga E, DeFelipe J (2005) Double bouquet cell in the in the human cerebral cortex and a comparison with other mammals. J Comp Neurol. 486: 344-60.

Barbeau D, Liang JJ, Robitalille Y, Quirion R, Srivastava LK (1995) Decreased expression of the embryonic form of the neural cell adhesion molecule in schizophrenic brains. Proc Natl Acad Sci U S A 92:2785-2789.

Barthels D, Vopper G, Wille W (1988) NCAM-180, the large isoform of the neural cell adhesion molecule of the mouse, is encoded by an alternatively spliced transcript. Nucleic Acids Res 16:4217-4225.

Becker CG, Artola A, Gerardy-Schahn R, Becker T, Welzl H, Schachner M (1996), The polysialic acid modification of the neural cell adhesion molecule is involved in spatial learning and hippocampal long-term potentiation. J Neurosci Res 45:143-152.

Beggs HE, Baragona SC, Hemperly JJ, Maness PF (1997), NCAM140 interacts with the focal adhesion kinase p125(fak) and the SRC-related tyrosine kinase p59(fyn). J Biol Chem 272: 8310-8319.

Benes FM, Berretta S (2001) GABAergic interneurons: implications for understanding schizophrenia and bipolar disorder. Neuropsychopharmacology 25:1-27.

Benes FM, Paskevich PA, Davidson J, Domesick VB (1985) Synaptic rearrangements in medial prefrontal cortex of haloperidol-treated rats. Brain Res 348:15-20.

Bhat S, Silberberg DH (1986) Oligodendrocyte cell adhesion molecules are related to neural cell adhesion molecule (N-CAM). J Neurosci 6:3348-3354.

Bonefeld BE, Elfving B, Wegener G (2008) Reference genes for normalization: a study of rat brain tissue. Synapse 62:302-9

Bonfanti L (2006) PSA-NCAM in mammalian structural plasticity and neurogenesis. Prog Neurobiol 80:129-164.

Bork K, Gagiannis D, Orthmann A, Weidemann W, Kontou M, Reutter W, Horstkorte R (2007) Experimental approaches to interfere with the polysialylation of the neural cell adhesion molecule in vitro and in vivo. J Neurochem 103 Suppl 1:65-71.

Bourdelais AJ, Deutch AY (1994) The effects of haloperidol and clozapine on extracellular GABA levels in the prefrontal cortex of the rat: an in vivo microdialysis study. CerebCortex 4:69-77.

Brodmann K (1909/2006) Brodmann's localization in the cerebral cortex (3rd ed). New York: Springer.

Brennaman LH, Maness PF (2008) NCAM in Neuropsychiatric and Neurodegenerative Disorders. NeurochemRes.

Bruel-Jungerman E, Davis S, Laroche S (2007) Brain plasticity mechanisms and memory: a party of four. Neuroscientist 13:492-505.

Bruses JL, Rutishauser U (2001) Roles, regulation, and mechanism of polysialic acid function during neural development. Biochimie 83:635-643.

Buttner B, Kannicht C, Reutter W, Horstkorte R (2003) The neural cell adhesion molecule is associated with major components of the cytoskeleton. Biochem Biophys Res Commun 310:967-971.

C

Cambon K, Hansen SM, Venero C, Herrero AI, Skibo G, Berezin V, Bock E, Sandi C (2004), A synthetic neural cell adhesion molecule mimetic peptide promotes synaptogenesis, enhances presynaptic function, and facilitates memory consolidation. J Neurosci 24:4197-4204.

Castren E (2004) Neurotrophic effects of antidepressant drugs. Curr Opin Pharmacol 4:58-64.

Castren E (2005) Is mood chemistry? Nat Rev Neurosci 6:241-246.

Chen F, Madsen TM, Wegener G, Nyengaard JR (2008) Changes in rat hippocampal CA1 synapses following imipramine treatment. Hippocampus 18:631-639.

Chothia C, Jones EY (1997) The molecular structure of cell adhesion molecules. Annu Rev Biochem 66:823-862.

Cline H, Haas K (2008) The regulation of dendritic arbor development and plasticity by glutamatergic synaptic input: a review of the synaptotrophic hypothesis. J Physiol 586:1509-1517.

Close BE, Colley KJ (1998) In vivo autopolysialylation and localization of the polysialyltransferases PST and STX. J Biol Chem 273:34586-34593.

Cohen S, Greenberg ME (2008) Communication between the synapse and the nucleus in neuronal development, plasticity, and disease. Annu Rev Cell Dev Biol 24:183-209.

Colonnier M (1964) The tangencial organization of the visual cortex. J. Anat., Lond 98: 327-344.

Cook SC, Wellman CL (2004) Chronic stress alters dendritic morphology in rat medial prefrontal cortex. Journal of Neurobiology 60:236-248.

Cordero MI, Rodriguez JJ, Davies HA, Peddie CJ, Sandi C, Stewart MG (2005) Chronic restraint stress down-regulates amygdaloid expression of polysialylated neural cell adhesion molecule. Neuroscience 133:903-910.

D

Dalva MB, McClelland AC, Kayser MS (2007), Cell adhesion molecules: signalling functions at the synapse. Nat Rev Neurosci 8: 206-220.

Daskalakis ZJ, Fitzgerald PB, Christensen BK (2007) The role of cortical inhibition in the pathophysiology and treatment of schizophrenia. Brain ResRev 56:427-442.

de Castilhos J, Forti CD, Achaval M, Rasia-Filho AA (2008) Dendritic spine density of posterodorsal medial amygdala neurons can be affected by gonadectomy and sex steroid manipulations in adult rats: a Golgi study. Brain Res 1240:73-81.

de Graaf-Peters VB, Hadders-Algra M (2006) Ontogeny of the human central nervous system: what is happening when? Early Hum Dev 82:257-66.

de Magalhaes JP, Sandberg A (2005) Cognitive aging as an extension of brain development: a model linking learning, brain plasticity, and neurodegeneration. Mech Ageing Dev 126:1026-1033.

DeFelipe J (1997) Types of neurons, synaptic connections and chemical characteristics of cells immunoreactive for calbindin-D28K, parvalbumin and calretinin in the neocortex. J Chem Neuroanat 14:1-19.

DeFelipe J, Farinas I (1992) The pyramidal neuron of the cerebral cortex: morphological and chemical characteristics of the synaptic inputs. Prog Neurobiol 39:563-607.

Degenetais E, Thierry AM, Glowinski J, Gioanni Y (2002) Electrophysiological properties of pyramidal neurons in the rat prefrontal cortex: an in vivo intracellular recording study. Cereb Cortex 12:1-16.

Diana G, Valentini G, Travaglione S, Falzano L, Pieri M, Zona C, Meschini S, Fabbri A, Fiorentini C (2007) Enhancement of learning and memory after activation of cerebral Rho GTPases. Proc Natl Acad Sci USA 104:636-41.

Di Cristo G, Chattopadhyaya B, Kuhlman SJ, Fu Y, Belanger MC, Wu CZ, Rutishauser U, Maffei L, Huang ZJ (2007) Activity-dependent PSA expression regulates inhibitory maturation and onset of critical period plasticity. Nat Neurosci 10:1569-1577.

Di Forti M, Lappin JM, Murray RM (2007) Risk factors for schizophrenia--all roads lead to dopamine. EurNeuropsychopharmacol 17 Suppl 2:S101-S107.

Dillon C, Goda Y (2005) The actin cytoskeleton: integrating form and function at the synapse. Annu Rev Neurosci 28:25-55.

Dityatev A, Dityateva G, Sytnyk V, Delling M, Toni N, Nikonenko I, Muller D, Schachner M (2004) Polysialylated neural cell adhesion molecule promotes remodeling and formation of hippocampal synapses. JNeurosci 24:9372-9382.

Dityatev A, Bukalo O, Schachner M (2008), Modulation of synaptic transmission and plasticity by cell adhesion and repulsion molecules. Neuron Glia Biol 4:197-209.

Doherty P, Rimon G, Mann DA, Walsh FS (1992) Alternative splicing of the cytoplasmic domain of neural cell adhesion molecule alters its ability to act as a substrate for neurite outgrowth. J Neurochem 58:2338-2341.

Drake PM, Nathan JK, Stock CM, Chang PV, Muench MO, Nakata D, Reader JR, Gip P, Golden KP, Weinhold B, Gerardy-Schahn R, Troy FA, 2nd, Bertozzi CR (2008) Polysialic acid, a glycan with highly restricted expression, is found on human and murine leukocytes and modulates immune responses. J Immunol 181:6850-6858.

Drake PM, Stock CM, Nathan JK, Gip P, Golden KP, Weinhold B, Gerardy-Schahn R, Bertozzi CR (2009) Polysialic acid governs T-cell development by regulating progenitor access to the thymus. Proc Natl Acad Sci U S A. 106:11995-2000.

Dubois B, Pillon B (1997) Cognitive deficits in Parkinson's disease. J Neurol 244:2-8.

Duffy AM, Zhou P, Milner TA, Pickel VM (2009) Spatial and intracellular relationships between the alpha7 nicotinic acetylcholine receptor and the vesicular acetylcholine transporter in the prefrontal cortex of rat and mouse. Neuroscience 161:1091-1103.

Duman RS (2002) Pathophysiology of depression: the concept of synaptic plasticity. European Psychiatry 17:306-310.

Duman RS, Malberg J, Thome J (1999) Neural plasticity to stress and antidepressant treatment. BiolPsychiatry 46:1181-1191.

Dunlop BW, Nemeroff CB (2007) The role of dopamine in the pathophysiology of depression. Arch Gen Psychiatry 64:327-337.

E

Eastwood SL, Harrison PJ (2001) Synaptic pathology in the anterior cingulate cortex in schizophrenia and mood disorders. A review and a Western blot study of synaptophysin, GAP-43 and the complexins. Brain Research Bulletin 55:569-578.

Eastwood SL, Heffernan J, Harrison PJ (1997) Chronic haloperidol treatment differentially affects the expression of synaptic and neuronal plasticity-associated genes. MolPsychiatry 2:322-329.

Eaton BA, Fetter RD, Davis GW (2002) Dynactin is necessary for synapse stabilization. Neuron 34:729-741.

Eckhardt M, Bukalo O, Chazal G, Wang L, Goridis C, Schachner M, Gerardy-Schahn R, Cremer H, Dityatev A (2000), Mice deficient in the polysialyltransferase ST8SiaIV/PST-1 allow discrimination of the roles of neural cell adhesion molecule protein and polysialic acid in neural development and synaptic plasticity. J Neurosci 20:5234-5244.

Everitt BJ, Robbins TW (1997) Central cholinergic systems and cognition. Annu Rev Psychol 48:649-684.

Eyre MD, Richter-Levin G, Avital A, Stewart MG (2003) Morphological changes in hippocampal dentate gyrus synapses following spatial learning in rats are transient. European Journal of Neuroscience 17:1973-1980.

F

Fox K (2008) Experience-dependent plasticity mechanisms for neural rehabilitation in somatosensory cortex. Philos Trans R Soc Lond B Biol Sci 369:381-364.

Friedlander DR, Grumet M, Edelman GM (1986) Nerve growth factor enhances expression of neuron-glia cell adhesion molecule in PC12 cells. J Cell Biol 102:413-419.

Frost DO, Tamminga CA, Medoff DR, Caviness V, Innocenti G, Carpenter WT (2004) Neuroplasticity and schizophrenia. Biological Psychiatry 56:540-543.

Fuster JM (2008) The Prefrontal Cortex (4th ed). London: Academic Press.

G

Gabbott PL, Dickie BG, Vaid RR, Headlam AJ, Bacon SJ (1997) Local-circuit neurones in the medial prefrontal cortex (areas 25, 32 and 24b) in the rat: morphology and quantitative distribution. JComp Neurol 377:465-499.

Galuska SP, Rollenhagen M, Kaup M, Eggers K, Oltmann-Norden I, Schiff M, Hartmann M, Weinhold B, Hildebrandt H, Geyer R, Muhlenhoff M, Geyer H (2010) Synaptic cell adhesion molecule SynCAM 1 is a target for polysialylation in postnatal mouse brain. Proc Natl Acad Sci U S A 107:10250-10255.

Gao WJ, Wang Y, Goldman-Rakic PS (2003) Dopamine modulation of perisomatic and peridendritic inhibition in prefrontal cortex. J Neurosci 23:1622-1630.

Gascon E, Vutskits L, Kiss JZ (2007) Polysialic acid-neural cell adhesion molecule in brain plasticity: from synapses to integration of new neurons. Brain Res Rev 56:101-118.

Gegelashvili G, Andersson AM, Schousboe A, Bock E (1993) Characterization of NCAM diversity in cultured neurons. FEBS Lett 324:337-340.

Gershon AA, Vishne T, Grunhaus L (2007) Dopamine D2-like receptors and the antidepressant response. BiolPsychiatry 61:145-153.

Gomez-Climent MA, Guirado R, Castillo-Gomez E, Varea E, Gutierrez-Mecinas M, Gilabert-Juan J, Garcia-Mompo C, Vidueira S, Sanchez-Mataredona D, Hernandez S, Blasco-Ibanez JM, Crespo C, Rutishauser U, Schachner M, Nacher J (2010) The polysialylated form of the neural cell adhesion molecule (PSA-NCAM) is expressed in a subpopulation of mature cortical interneurons characterized by reduced structural features and connectivity. Cereb. Cortex [in press].

Greer PL, Greenberg ME (2008) From synapse to nucleus: calcium-dependent gene transcription in the control of synapse development and function. Neuron 59:846-860.

Groenewegen HJ, Wright CI, Uylings HB (1997) The anatomical relationships of the prefrontal cortex with limbic structures and the basal ganglia. J Psychopharmacol 11:99-106.

Guirado R, Varea E, Castillo-Gomez E, Gomez-Climent MA, Rovira-Esteban L, Blasco-Ibanez JM, Crespo C, Martinez-Guijarro FJ, Nacher J (2009) Effects of chronic fluoxetine treatment on the rat somatosensory cortex: activation and induction of neuronal structural plasticity. Neurosci Lett 457:12-15.

H

Hajszan T, MacLusky NJ, Leranth C (2005), Short-term treatment with the antidepressant fluoxetine triggers pyramidal dendritic spine synapse formation in rat hippocampus. European Journal of Neuroscience 21:1299-1303.

Hallenbeck PC, Vimr ER, Yu F, Bassler B, Troy FA (1987), Purification and properties of a bacteriophage-induced endo-N-acetylneuraminidase specific for poly-alpha-2,8-sialosyl carbohydrate units. J Biol Chem 262:3553-3561.

Hao J, Rapp PR, Leffler AE, Leffler SR, Janssen WG, Lou W, McKay H, Roberts JA, Wearne SL, Hof PR, Morrison JH (2006), Estrogen alters spine number and morphology in prefrontal cortex of aged female rhesus monkeys. J Neurosci 26:2571-2578.

Harrison PJ (1999), The neuropathology of schizophrenia. A critical review of the data and their interpretation. Brain 122:593-624.

Hensch TK (2004), Critical period regulation. Annu Rev Neurosci 27:549-579.

Hildebrandt H, Becker C, Murau M, Gerardy-Schahn R, Rahmann H (1998), Heterogeneous expression of the polysialyltransferases ST8Sia II and ST8Sia IV during postnatal rat brain development. JNeurochem 71:2339-2348.

Hildebrandt H, Muhlenhoff M, Gerardy-Schahn R (2008), Polysialylation of NCAM. Neurochem Res.

Hildebrandt H, Muhlenhoff M, Weinhold B, Gerardy-Schahn R (2007), Dissecting polysialic acid and NCAM functions in brain development. J Neurochem 103 Suppl 1:56-64.

Hoffman S, Sorkin BC, White PC, Brackenbury R, Mailhammer R, Rutishauser U, Cunningham BA, Edelman GM (1982), Chemical characterization of a neural cell adhesion molecule purified from embryonic brain membranes. J Biol Chem 257:7720-7729.

Hoffman KB, Larson J, Bahr BA, Lynch G (1998), Activation of NMDA receptors stimulates extracellular proteolysis of cell adhesion molecules in hippocampus. Brain Res 811: 152-155.

Iversen SD, Iversen LL (2007), Dopamine: 50 years in perspective. Trends Neurosci 30:188-193.

J

Johnson CP, Fujimoto I, Rutishauser U, Leckband DE (2005), Direct evidence that neural cell adhesion molecule (NCAM) polysialylation increases intermembrane repulsion and abrogates adhesion. J Biol Chem 280:137-145.

K

Kaasinen V, Aalto S, K NA, Hietala J, Sonninen P, Rinne JO (2003) Extrastriatal dopamine D(2) receptors in Parkinson's disease: a longitudinal study. J Neural Transm 110:591-601.

Kandel E, Schwartz JH, Jessell TM (2000) Principles of neural sciences (4th ed). New York: McGraw-Hill.

Katidou M, Vidaki M, Strigini M, Karagogeos D (2008), The immunoglobulin superfamily of neuronal cell adhesion molecules: lessons from animal models and correlation with human disease. Biotechnol J 3:1564-1580.

Kawaguchi Y (1997), Selective cholinergic modulation of cortical GABAergic cell subtypes. J Neurophysiol 78:1743-1747.

Kelley JJ, Gao XM, Tamminga CA, Roberts RC (1997), The effect of chronic haloperidol treatment on dendritic spines in the rat striatum. ExpNeurol 146:471-478.

Kiss JZ, Wang C, Olive S, Rougon G, Lang J, Baetens D, Harry D, Pralong WF (1994), Activity-dependent mobilization of the adhesion molecule polysialic NCAM to the cell surface of neurons and endocrine cells. EMBO J 13:5284-5292

Kiss JZ, Rougon G (1997), Cell biology of polysialic acid. CurrOpinNeurobiol 7:640-646.

Klintzova AJ, Haselhorst U, Uranova NA, Schenk H, Istomin VV (1989), The effects of haloperidol on synaptic plasticity in rat's medial prefrontal cortex. JHirnforsch 30:51-57.

Knable MB, Torrey EF, Webster MJ, Bartko JJ (2001), Multivariate analysis of prefrontal cortical data from the Stanley Foundation Neuropathology Consortium. Brain Res Bull 55:651-659.

Kojima N, Tachida Y, Yoshida Y, Tsuji S (1996), Characterization of mouse ST8Sia II (STX) as a neural cell adhesion molecule-specific polysialic acid synthase. Requirement of core alpha1,6-linked fucose and a polypeptide chain for polysialylation. J Biol Chem 271:19457-19463.

Kolkova K, Novitskaya V, Pedersen N, Berezin V, Bock E (2000), Neural cell adhesion molecule-stimulated neurite outgrowth depends on activation of protein kinase C and the Ras-mitogen-activated protein kinase pathway. J Neurosci 20:2238-2246.

Krageloh-Mann I (2004), Imaging of early brain injury and cortical plasticity. Exp Neurol 190 Suppl 1:S84-90.

Kramer I, Hall H, Bleistein U, Schachner M (1997), Developmentally regulated masking of an intracellular epitope of the 180 kDa isoform of the neural cell adhesion molecule NCAM. J Neurosci Res 49:161-175.

Kubota Y, Hattori R, Yui Y (1994), Three distinct subpopulations of GABAergic neurons in rat frontal agranular cortex. Brain Res 649:159-173.

Kubota Y, Putkey JA, Waxham MN (2007), Neurogranin controls the spatiotemporal pattern of postsynaptic Ca2+/CaM signaling. Biophys J 93:3848-3859.

Kubota Y, Shigematsu N, Karube F, Sekigawa A, Kato S, Yamaguchi N, Hirai Y, Morishima M, Kawaguchi Y (2011), Selective coexpression of multiple chemical markers defines discrete populations of neocortical GABAergic neurons. Cereb Cortex [in press].

Kurosawa N, Yoshida Y, Kojima N, Tsuji S (1997), Polysialic acid synthase (ST8Sia II/STX) mRNA expression in the developing mouse central nervous system. J Neurochem 69:494-503.

L

Lambe EK, Krimer LS, Goldman-Rakic PS (2000), Differential postnatal development of catecholamine and serotonin inputs to identified neurons in prefrontal cortex of rhesus monkey. J Neurosci 20:8780-8787.

Lanoue AC, Dumitriu A, Myers RH, Soghomonian JJ (2010), Decreased glutamic acid decarboxylase mRNA expression in prefrontal cortex in Parkinson's disease. Exp Neurol 226:207-217.

Le Moine C, Gaspar P (1998), Subpopulations of cortical GABAergic interneurons differ by their expression of D1 and D2 dopamine receptor subtypes. Brain ResMolBrain Res 58:231-236.

Leuner B, Falduto J, Shors TJ (2003), Associative memory formation increases the observation of dendritic spines in the hippocampus. JNeurosci 23:659-665.

Lewis DA, Gonzalez-Burgos G (2008), Neuroplasticity of neocortical circuits in schizophrenia. Neuropsychopharmacology 33:141-165.

Lidow MS, Song ZM, Castner SA, Allen PB, Greengard P, Goldman-Rakic PS (2001), Antipsychotic treatment induces alterations in dendrite- and spine-associated proteins in dopamine-rich areas of the primate cerebral cortex. BiolPsychiatry 49:1-12.

Livak KJ, Schmittgen TD (2001) Analysis of relative gene expression data using real-time quantitative PCR and the 2(-Delta Delta C(T)) Method. 25:402-8.

Livingston BD, Jacobs JL, Glick MC, Troy FA (1988), Extended polysialic acid chains (n greater than 55) in glycoproteins from human neuroblastoma cells. J Biol Chem 263:9443-9448.

M

MacDonald ML, Eaton ME, Dudman JT, Konradi C (2005), Antipsychotic drugs elevate mRNA levels of presynaptic proteins in the frontal cortex of the rat. BiolPsychiatry 57:1041-1051.

Mackowiak M, Markowicz-Kula K, Fijal K, Wedzony K (2005), Acute and repeated administration of cocaine differentially regulates expression of PSA-NCAM-positive neurons in the rat hippocampus. Brain Res 1055:149-155.

Magarinos AM, McEwen BS, Flugge G, Fuchs E (1996), Chronic psychosocial stress causes apical dendritic atrophy of hippocampal CA3 pyramidal neurons in subordinate tree shrews. JNeurosci 16:3534-3540.

Maness PF, Beggs HE, Klinz SG, Morse WR (1996), Selective neural cell adhesion molecule signaling by Src family tyrosine kinases and tyrosine phosphatases. Perspect Dev Neurobiol 4:169-181.

Maness PF, Schachner M (2007), Neural recognition molecules of the immunoglobulin superfamily: signaling transducers of axon guidance and neuronal migration. Nat Neurosci 10:19-26.

Mangiavacchi S, Masi F, Scheggi S, Leggio B, De Montis MG, Gambarana C (2001), Long-term behavioral and neurochemical effects of chronic stress exposure in rats. J Neurochem 79:1113-1121.

Markham JA, Greenough WT (2004), Experience-driven brain plasticity: beyond the synapse. Neuron Glia Biol 1:351-363.

Markham JA, McKian KP, Stroup TS, Juraska JM (2005), Sexually dimorphic aging of dendritic morphology in CA1 of hippocampus. Hippocampus 15:97-103.

Markham JA, Juraska JM. 2002. Aging and sex influence the anatomy of the rat anterior cingulate cortex. Neurobiol Aging. 23:579-88.

Markham JA, Pych JC, Juraska JM (2002), Ovarian hormone replacement to aged ovariectomized female rats benefits acquisition of the morris water maze. Hormones and Behavior 42:284-293.

Masliah E, Iimoto DS, Saitoh T, Hansen LA, Terry RD (1990), Increased immunoreactivity of brain spectrin in Alzheimer disease: a marker for synapse loss? Brain Res 531:36-44.

McCarley RW, Wible CG, Frumin M, Hirayasu Y, Levitt JJ, Fischer IA, Shenton ME (1999), MRI anatomy of schizophrenia. BiolPsychiatry 45:1099-1119.

McEwen BS (1999), Stress and hippocampal plasticity. AnnuRevNeurosci 22:105-22:105-122.

McEwen BS (2000), The neurobiology of stress: from serendipity to clinical relevance. Brain Res 886:172-189.

McEwen BS (2005), Glucocorticoids, depression, and mood disorders: structural remodeling in the brain. Metabolism 54:20-23.

McEwen BS (2008), Central effects of stress hormones in health and disease: Understanding the protective and damaging effects of stress and stress mediators. Eur J Pharmacol 583:174-185.

McEwen BS, Chattarji S (2004), Molecular mechanisms of neuroplasticity and pharmacological implications: the example of tianeptine. EurNeuropsychopharmacol 14 Suppl 5:S497-502.:S497-S502.

Meyer G, Feldman EL (2002), Signaling mechanisms that regulate actin-based motility processes in the nervous system. J Neurochem 83:490-503.

Miner LA, Backstrom JR, Sanders-Bush E, Sesack SR (2003), Ultrastructural localization of serotonin2A receptors in the middle layers of the rat prelimbic prefrontal cortex. Neuroscience 116:107-117.

Mitra R, Jadhav S, McEwen BS, Vyas A, Chattarji S (2005), Stress duration modulates the spatiotemporal patterns of spine formation in the basolateral amygdala. ProcNatlAcadSciUSA 102:9371-9376.

Mitra R, Sapolsky RM (2008) Acute corticosterone treatment is sufficient to induce anxiety and amygdaloid dendritic hypertrophy. Proc Natl Acad Sci U S A 105:5573-8.

Miyahara R, Tanaka F, Nakagawa T, Matsuoka K, Isii K, Wada H (2001), Expression of neural cell adhesion molecules (polysialylated form of neural cell adhesion molecule and L1-cell adhesion molecule) on resected small cell lung cancer specimens: in relation to proliferation state. J Surg Oncol 77:49-54.

Morales-Medina JC, Sanchez F, Flores G, Dumont Y, Quirion R (2009), Morphological reorganization after repeated corticosterone administration in the hippocampus, nucleus accumbens and amygdala in the rat. J Chem Neuroanat 38:266-272.

Morshedi MM, Rademacher DJ, Meredith GE (2009), Increased synapses in the medial prefrontal cortex are associated with repeated amphetamine administration. Synapse 63:126-135.

Moult PR, Harvey J (2008), Hormonal regulation of hippocampal dendritic morphology and synaptic plasticity. Cell Adh Migr 2:269-275.

Muller D, Wang C, Skibo G, Toni N, Cremer H, Calaora V, Rougon G, Kiss JZ (1996), PSA-NCAM is required for activity-induced synaptic plasticity. Neuron 17:413-422.

Muller D, Toni N, Buchs PA (2000), Spine changes associated with long-term potentiation. Hippocampus 10:596-604.

Murase S, Schuman EM (1999), The role of cell adhesion molecules in synaptic plasticity and memory. Curr Opin Cell Biol 11:549-553.

Muscat R, Papp M, Willner P (1992), Antidepressant-like effects of dopamine agonists in an animal model of depression. BiolPsychiatry 31:937-946.

N

Nacher J, Alonso-Llosa G, Rosell DR, McEwen BS (2002), PSA-NCAM expression in the piriform cortex of the adult rat. Modulation by NMDA receptor antagonist administration. Brain Res 927:111-121.

Nacher J, Guirado R, Varea E, Alonso-Llosa G, Rockle I, Hildebrandt H (2010), Divergent impact of the polysialyltransferases ST8SiaII and ST8SiaIV on polysialic acid expression in immature neurons and interneurons of the adult cerebral cortex. Neuroscience 167:825-837.

Nakahara T, Nakamura K, Tsutsumi T, Hashimoto K, Hondo H, Hisatomi S, Motomura K, Uchimura H (1998), Effect of chronic haloperidol treatment on synaptic protein mRNAs in the rat brain. Brain ResMolBrain Res 61:238-242.

Nakayama J, Fukuda M (1996), A human polysialyltransferase directs in vitro synthesis of polysialic acid. J Biol Chem 271:1829-1832.

Neve KA (2009) The dopamine receptors (2nd ed). New York: Humana Press.

Nimchinsky EA, Sabatini BL, Svoboda K (2002) Structure and function of dendritic spines. Annu Rev Physiol 64:313-353.

O

O'Connell AW, Fox GB, Barry T, Murphy KJ, Fichera G, Foley AG, Kelly J, Regan CM (1997) Spatial learning activates neural cell adhesion molecule polysialylation in a corticohippocampal pathway within the medial temporal lobe. J Neurochem 68:2538-46.

O'Malley A, O'Connell C, Regan CM (1998) Ultrastructural analysis reveals avoidance conditioning to induce a transient increase in hippocampal dentate spine density in the 6 hour post-training period of consolidation. Neuroscience 87:607-613.

Olsen M, Krog L, Edvardsen K, Skovgaard LT, Bock E (1993), Intact transmembrane isoforms of the neural cell adhesion molecule are released from the plasma membrane. Biochem J 295 (Pt 3):833-840.

Oltmann-Norden I, Galuska SP, Hildebrandt H, Geyer R, Gerardy-Schahn R, Geyer H, Muhlenhoff M (2008), Impact of the polysialyltransferases ST8SiaII and ST8SiaIV on polysialic acid synthesis during postnatal mouse brain development. JBiolChem 283:1463-1471.

Ong E, Nakayama J, Angata K, Reyes L, Katsuyama T, Arai Y, Fukuda M (1998), Developmental regulation of polysialic acid synthesis in mouse directed by two polysialyltransferases, PST and STX. Glycobiology 8:415-424.

P

Paxinos G, Watson C (2007) The rat brain in stereotaxic coordinates (6th ed). London: Academic Press.

Paxinos G (2004) The rat nervous system (3rd ed). San Diego: Elsevier Academic Press.

Perez-Cruz C, Simon M, Czeh B, Flugge G, Fuchs E (2009a), Hemispheric differences in basilar dendrites and spines of pyramidal neurons in the rat prelimbic cortex: activity- and stress-induced changes. Eur J Neurosci 29:738-747.

Perez-Cruz C, Simon M, Flugge G, Fuchs E, Czeh B (2009b), Diurnal rhythm and stress regulate dendritic architecture and spine density of pyramidal neurons in the rat infralimbic cortex. Behav Brain Res 205:406-413.

Persohn E, Pollerberg GE, Schachner M (1989), Immunoelectron-microscopic localization of the 180 kD component of the neural cell adhesion molecule N-CAM in postsynaptic membranes. J Comp Neurol 288:92-100.

Peters A, Sethares C, Luebke JI (2008), Synapses are lost during aging in the primate prefrontal cortex. Neuroscience 152:970-981.

Petridis AK, El Maarouf A, Rutishauser U (2004), Polysialic acid regulates cell contact-dependent neuronal differentiation of progenitor cells from the subventricular zone. Developmental dynamics 230:675-684.

Pezze MA, Bast T, Feldon J (2003), Significance of dopamine transmission in the rat medial prefrontal cortex for conditioned fear. Cereb Cortex 13:371-380.

Poltorak M, Williams JR, Moore KD, Freed WJ (1997), Changes in L1 antigen expression in the rat striatum after substantia nigra lesions. JNeural TransplantPlast 6:59-62.

Probstmeier R, Bilz A, Schneider-Schaulies J (1994), Expression of the neural cell adhesion molecule and polysialic acid during early mouse embryogenesis. J Neurosci Res 37:324-335.

R

Radley JJ, Johnson LR, Janssen WG, Martino J, Lamprecht R, Hof PR, LeDoux JE, Morrison JH (2006), Associative Pavlovian conditioning leads to an increase in spinophilin-immunoreactive dendritic spines in the lateral amygdala. Eur J Neurosci 24:876-884.

Radley JJ, Rocher AB, Miller M, Janssen WG, Liston C, Hof PR, McEwen BS, Morrison JH (2005), Repeated Stress Induces Dendritic Spine Loss in the Rat Medial Prefrontal Cortex. CerebCortex 16:313-320.

Radley JJ, Sisti HM, Hao J, Rocher AB, McCall T, Hof PR, McEwen BS, Morrison JH (2004), Chronic behavioral stress induces apical dendritic reorganization in pyramidal neurons of the medial prefrontal cortex. Neuroscience 125:1-6.

Ragozzino ME (2000) The contribution of cholinergic and dopaminergic afferents in the rat prefrontal cortex to learning, memory, and attention. Psychobiology 28:238-247.

Rajkowska G, O'Dwyer G, Teleki Z, Stockmeier CA, Miguel-Hidalgo JJ (2007), GABAergic neurons immunoreactive for calcium binding proteins are reduced in the prefrontal cortex in major depression. Neuropsychopharmacology 32:471-482.

Renner M, Specht CG, Triller A (2008), Molecular dynamics of postsynaptic receptors and scaffold proteins. Curr Opin Neurobiol 18:532-540.

Retaux S, Trovero F, Besson MJ (1994), Role of dopamine in the plasticity of glutamic acid decarboxylase messenger RNA in the rat frontal cortex and the nucleus accumbens. European Journal of Neuroscience 6:1782-1791.

Robinson TE, Gorny G, Mitton E, Kolb B (2001), Cocaine self-administration alters the morphology of dendrites and dendritic spines in the nucleus accumbens and neocortex. Synapse 39:257-266.

Robinson TE, Kolb B (1999), Alterations in the morphology of dendrites and dendritic spines in the nucleus accumbens and prefrontal cortex following repeated treatment with amphetamine or cocaine. Eur J Neurosci 11:1598-1604.

Roos J, Hummel T, Ng N, Klämbt C, Davis GW (2000) Drosophila Futsch regulates synaptic microtubule organization and is necessary for synaptic growth. Neuron 26:371-82.

Rose JE, Woolsey CN (1948), Structure and relations of limbic cortex and anterior thalamic nuclei in rabbit and cat. J Comp Neurol 89:279-347.

Rosenkranz JA, Grace AA (2001), Dopamine attenuates prefrontal cortical suppression of sensory inputs to the basolateral amygdala of rats. J Neurosci 21:4090-4103.

Rosenzweig ES, Barnes CA (2003), Impact of aging on hippocampal function: plasticity, network dynamics, and cognition. ProgNeurobiol 69:143-179.

Rougon G, Nedelec J, Malapert P, Goridis C, Chesselet MF (1990), Post-translation modifications of neural cell surface molecules. Acta Histochem Suppl 38:51-57.

Rousselot P, Lois C, Alvarez-Buylla A (1995), Embryonic (PSA) N-CAM reveals chains of migrating neuroblasts between the lateral ventricle and the olfactory bulb of adult mice. J Comp Neurol 351:51-61.

Rubinow MJ, Drogos LL, Juraska JM (2009), Age-related dendritic hypertrophy and sexual dimorphism in rat basolateral amygdala. Neurobiol Aging 30:137-146.

Rutishauser U (1996), Polysialic acid and the regulation of cell interactions. Current Opinion in Cell Biology 8:679-684.

Rutishauser U (2008), Polysialic acid in the plasticity of the developing and adult vertebrate nervous system. Nat Rev Neurosci 9:26-35.

Rutishauser U, Landmesser L (1996), Polysialic acid in the vertebrate nervous system: a promoter of plasticity in cell-cell interactions. Trends Neurosci 19:422-427.

S

Sabel BA (2008), Plasticity and restoration of vision after visual system damage: an update. Restor Neurol Neurosci 26:243-247.

Saegusa T, Mine S, Iwasa H, Murai H, Seki T, Yamaura A, Yuasa S (2004), Involvement of highly polysialylated neural cell adhesion molecule (PSA-NCAM)-positive granule cells in the amygdaloid-kindling-induced sprouting of a hippocampal mossy fiber trajectory. Neuroscience Research 48:185-194.

Sandi C (2004), Stress, cognitive impairment and cell adhesion molecules. NatRevNeurosci 5:917-930.

Santana N, Mengod G, Artigas F (2009), Quantitative analysis of the expression of dopamine D1 and D2 receptors in pyramidal and GABAergic neurons of the rat prefrontal cortex. Cereb Cortex 19:849-860.

Sairanen M, O'Leary OF, Knuuttila JE, Castrén E (2007) Chronic antidepressant treatment selectively increases expression of plasticity-related proteins in the hippocampus and medial prefrontal cortex of the rat. Neuroscience 144:368-74.

Sawaguchi T, Goldman-Rakic PS (1994), The role of D1-dopamine receptor in working memory: local injections of dopamine antagonists into the prefrontal cortex of rhesus monkeys performing an oculomotor delayed-response task. J Neurophysiol 71:515-528.

Schiavone S, Sorce S, Dubois-Dauphin M, Jaquet V, Colaianna M, Zotti M, Cuomo V, Trabace L, Krause KH (2009), Involvement of NOX2 in the development of behavioral and pathologic alterations in isolated rats. Biol Psychiatry 66:384-392.

Schuster T, Krug M, Hassan H, Schachner M (1998), Increase in proportion of hippocampal spine synapses expressing neural cell adhesion molecule NCAM180 following long-term potentiation. J Neurobiol 37: 359-372.

Seamans JK, Gorelova N, Durstewitz D, Yang CR (2001), Bidirectional dopamine modulation of GABAergic inhibition in prefrontal cortical pyramidal neurons. J Neurosci 21:3628-3638.

Seamans JK, Lapish CC, Durstewitz D (2008), Comparing the prefrontal cortex of rats and primates: insights from electrophysiology. Neurotox Res 14:249-262.

Seeman P (2010), All Roads to Schizophrenia Lead to Dopamine Supersensitivity and Elevated Dopamine D2 Receptors. CNS Neurosci Ther.

Seib LM, Wellman CL (2003), Daily injections alter spine density in rat medial prefrontal cortex. NeurosciLett 337:29-32.

Seki T, Arai Y (1991), Expression of highly polysialylated NCAM in the neocortex and piriform cortex of the developing and the adult rat. Anat Embryol (Berl) 184:395-401.

Seki T, Arai Y (1999), Different polysialic acid-neural cell adhesion molecule expression patterns in distinct types of mossy fiber boutons in the adult hippocampus. JCompNeurol 410:115-125.

Selemon LD, Begovic A, Goldman-Rakic PS, Castner SA (2007), Amphetamine sensitization alters dendritic morphology in prefrontal cortical pyramidal neurons in the non-human primate. Neuropsychopharmacology 32:919-931.

Sesack SR, Hawrylak VA, Melchitzky DS, Lewis DA (1998), Dopamine innervation of a subclass of local circuit neurons in monkey prefrontal cortex: ultrastructural analysis of tyrosine hydroxylase and parvalbumin immunoreactive structures. CerebCortex 8:614-622.

Sesack SR, Snyder CL, Lewis DA (1995), Axon terminals immunolabeled for dopamine or tyrosine hydroxylase synapse on GABA-immunoreactive dendrites in rat and monkey cortex. JComp Neurol 363:264-280.

Sherren N, Pappas BA (2005), Selective acetylcholine and dopamine lesions in neonatal rats produce distinct patterns of cortical dendritic atrophy in adulthood. Neuroscience 136:445-456.

Solis O, Limón DI, Flores-Hernández J, Flores G (2007) Alterations in dendritic morphology of the prefrontal cortical and striatum neurons in the unilateral 6-OHDA-rat model of Parkinson's disease. Synapse 61:450-8

Somogyi P, Tamas G, Lujan R, Buhl EH (1998), Salient features of synaptic organisation in the cerebral cortex. Brain Res Brain Res Rev 26:113-135.

Sousa N, Lukoyanov NV, Madeira MD, Almeida OF, Paula-Barbosa MM (2000), Reorganization of the morphology of hippocampal neurites and synapses after stress-induced damage correlates with behavioral improvement. Neuroscience 97:253-266.

Stewart M, Popov V, Medvedev N, Gabbott P, Corbett N, Kraev I, Davies H (2008), Dendritic Spine and Synapse Morphological Alterations Induced by a Neural Cell Adhesion Molecule (NCAM) Mimetic. Neurochem Res.

Stewart MG, Davies HA, Sandi C, Kraev IV, Rogachevsky VV, Peddie CJ, Rodriguez JJ, Cordero MI, Donohue HS, Gabbott PL, Popov VI (2005), Stress suppresses and learning induces plasticity in CA3 of rat hippocampus: a three-dimensional ultrastructural study of thorny excrescences and their postsynaptic densities. Neuroscience 131:43-54.

Sugahara M, Shiraishi H (1998), Synaptic density of the prefrontal cortex regulated by dopamine instead of serotonin in rats. Brain Res 814:143-156.

Sun X, Zhao Y, Wolf ME (2005), Dopamine receptor stimulation modulates AMPA receptor synaptic insertion in prefrontal cortex neurons. J Neurosci 25:7342-7351.

Sunanda, Rao MS, Raju TR (1995), Effect of chronic restraint stress on dendritic spines and excrescences of hippocampal CA3 pyramidal neurons--a quantitative study. Brain Res 694:312-317.

Sutton MA, Schuman EM (2006), Dendritic protein synthesis, synaptic plasticity, and memory. Cell 127:49-58.

Suzuki M, Nakayama J, Suzuki A, Angata K, Chen S, Sakai K, Hagihara K, Yamaguchi Y, Fukuda M (2005), Polysialic acid facilitates tumor invasion by glioma cells. Glycobiology 15:887-894.

Swarzenski BC, Tang L, Oh YJ, O'Malley KL, Todd RD (1994), Morphogenic potentials of D2, D3, and D4 dopamine receptors revealed in transfected neuronal cell lines. ProcNatlAcadSciUSA 91:649-653.

Sytnyk V, Leshchyns'ka I, Delling M, Dityateva G, Dityatev A, Schachner M (2002), Neural cell adhesion molecule promotes accumulation of TGN organelles at sites of neuron-to-neuron contacts. J Cell Biol 159: 649-661.

Sytnyk V, Leshchyns'ka I, Nikonenko AG, Schachner M (2006), NCAM promotes assembly and activity-dependent remodeling of the postsynaptic signaling complex. J Cell Biol 174:1071-1085.

T

Tao R, Li C, Zheng Y, Qin W, Zhang J, Li X, Xu Y, Shi YY, Feng G, He L (2007), Positive association between SIAT8B and schizophrenia in the Chinese Han population. SchizophrRes 90:108-114.

Todd RD (1992), Neural development is regulated by classical neurotransmitters: dopamine D2 receptor stimulation enhances neurite outgrowth. BiolPsychiatry 31:794-807.

Trachtenberg JT, Chen BE, Knott GW, Feng G, Sanes JR, Welker E, Svoboda K (2002), Long-term in vivo imaging of experience-dependent synaptic plasticity in adult cortex. Nature. 420:788--794.

Trantham-Davidson H, Neely LC, Lavin A, Seamans JK (2004), Mechanisms underlying differential D1 versus D2 dopamine receptor regulation of inhibition in prefrontal cortex. J Neurosci 24:10652-10659.

Tseng KY, O'Donnell P (2007), D2 dopamine receptors recruit a GABA component for their attenuation of excitatory synaptic transmission in the adult rat prefrontal cortex. Synapse 61:843-850.

U

Uylings HB, Groenewegen HJ, Kolb B (2003), Do rats have a prefrontal cortex? Behavioural Brain Research 146:3-17.

Uylings HB, van Eden CG (1990), Qualitative and quantitative comparison of the prefrontal cortex in rat and in primates, including humans. Prog Brain Res 85:31-62.

V

Varea E, Blasco-Ibanez JM, Gomez-Climent MA, Castillo-Gomez E, Crespo C, Martinez-Guijarro FJ, Nacher J (2007a) Chronic fluoxetine treatment increases the expression of PSA-NCAM in the medial prefrontal cortex. Neuropsychopharmacol 32:803-812.

Varea E, Castillo-Gomez E, Gomez-Climent MA, Blasco-Ibanez JM, Crespo C, Martinez-Guijarro FJ, Nacher J (2007b) Chronic antidepressant treatment induces contrasting patterns of synaptophysin and PSA-NCAM expression in different regions of the adult rat telencephalon. Eur Neuropsychopharmacol 17:546-557.

Varea E, Castillo-Gomez E, Gomez-Climent MA, Blasco-Ibanez JM, Crespo C, Martinez-Guijarro FJ, Nacher J (2007c), PSA-NCAM expression in the human prefrontal cortex. J Chem Neuroanat 33:202-209.

Varea E, Castillo-Gomez E, Gomez-Climent MA, Guirado R, Blasco-Ibañez JM, Crespo C, Martinez-Guijarro FJ, Nacher J (2009), Differential evolution of PSA-NCAM expression during aging of the rat telencephalon. Neurobiol Aging 30:11.

Varea E, Nacher J, Blasco-Ibanez JM, Gomez-Climent MA, Castillo-Gomez E, Crespo C, Martinez-Guijarro FJ (2005), PSA-NCAM expression in the rat medial prefrontal cortex. Neuroscience 136:435-443.

Varea E, Belles M, Vidueira S, Blasco-Ibáñez JM, Crespo C, Pastor A, Nacher J (2011), PSA-NCAM is expressed in immature, but not recently generated, neurons in the adult cat cerebral cortex layer II. Front. Neurosc. [in press]

Vaithianathan T, Matthias K, Bahr B, Schachner M, Suppiramaniam V, Dityatev A, Steinhaüser C (2004), Neural cell adhesion molecule-associated polysialic acid potentiates alpha-amino-3-hydroxy-5-methylisoxazole-4-propionic acid receptor currents. J Biol Chem 279: 47975-47984.

Vawter MP (2000), Dysregulation of the neural cell adhesion molecule and neuropsychiatric disorders. European Journal Of Pharmacology 405:385-395.

Venero C, Herrero AI, Touyarot K, Cambon K, López-Fernández MA, Berezin V, Bock E, Sandi C (2006), Hippocampal up-regulation of NCAM expression and polysialylation plays a key role on spatial memory. Eur J Neurosci 23: 1585-1595.

Vimr ER, McCoy RD, Vollger HF, Wilkison NC, Troy FA (1984) Use of prokaryotic-derived probes to identify poly(sialic acid) in neonatal neuronal membranes. Proc Natl Acad Sci U S A. 81:1971-5.

Vitureira N, Andres R, Perez-Martinez E, Martinez A, Bribian A, Blasi J, Chelliah S, Lopez-Domenech G, De Castro F, Burgaya F, McNagny K, Soriano E (2010), Podocalyxin is a novel polysialylated neural adhesion protein with multiple roles in neural development and synapse formation. PLoS One 5:e12003.

Volk DW, Lewis DA (2002), Impaired prefrontal inhibition in schizophrenia: relevance for cognitive dysfunction. Physiol Behav 77:501-505.

Vyas A, Mitra R, Shankaranarayana Rao BS, Chattarji S (2002), Chronic stress induces contrasting patterns of dendritic remodeling in hippocampal and amygdaloid neurons. JNeurosci 22:6810-6818.

W

Wallace M, Luine V, Arellanos A, Frankfurt M (2006), Ovariectomized rats show decreased recognition memory and spine density in the hippocampus and prefrontal cortex. Brain Res 1126:176-182.

Walmod PS, Kolkova K, Berezin V, Bock E (2004), Zippers make signals: NCAM-mediated molecular interactions and signal transduction. Neurochem Res 29:2015-2035.

Walsh FS, Doherty P (1997), Neural cell adhesion molecules of the immunoglobulin superfamily: role in axon growth and guidance. Annu Rev Cell Dev Biol 13:425-456.

Wang HD, Deutch AY (2008), Dopamine depletion of the prefrontal cortex induces dendritic spine loss: reversal by atypical antipsychotic drug treatment. Neuropsychopharmacology 33:1276-1286.

Wang HD, Stanwood GD, Grandy DK, Deutch AY (2009), Dystrophic dendrites in prefrontal cortical pyramidal cells of dopamine D1 and D2 but not D4 receptor knockout mice. Brain Res 1300:58-64.

Watanabe Y, Gould E, Daniels DC, Cameron H, McEwen BS (1992), Tianeptine attenuates stress-induced morphological changes in the hippocampus. EurJPharmacol 222:157-162.

Waxman SG (2005), From neuroscience to neurology: neuroscience, molecular medicine, and the therapeutic transformation of neurology. San Diego: Elsevier Academic Press.

Wechsler A, Teichberg VI (1998), Brain spectrin binding to the NMDA receptor is regulated by phosphorylation, calcium and calmodulin. EMBO J 17: 3931-3939.

Wellman CL (2001), Dendritic reorganization in pyramidal neurons in medial prefrontal cortex after chronic corticosterone administration. Journal of Neurobiology 49:245-253.

West MJ (1993), New stereological methods for counting neurons. NeurobiolAging 14:275-285.

Wierenga CJ, Becker N, Bonhoeffer T (2008), GABAergic synapses are formed without the involvement of dendritic protrusions. Nat. Neurosci. 11:1044--1052.

Williams RK, Goridis C, Akeson R (1985) Individual neural cell types express immunologically distinct N-CAM forms. J Cell Biol. 101:36-42.

Williams SR, Atkinson SE (2008), Dendritic synaptic integration in central neurons. Curr Biol 18:R1045-1047.

Willner P, Hale AS, Argyropoulos S (2005), Dopaminergic mechanism of antidepressant action in depressed patients. JAffectDisord 86:37-45.

Wong WT, Faulkner-Jones BE, Sanes JR, Wong RO (2000) Rapid dendritic remodeling in the developing retina: dependence on neurotransmission and reciprocal regulation by Rac and Rho. J Neurosci. 5024:5036-20.

Woolley CS, McEwen BS (1994), Estradiol regulates hippocampal dendritic spine density via an N-methyl- D-aspartate receptor-dependent mechanism. JNeurosci 14:7680-7687.

X

Xerri C (2008), Imprinting of idiosyncratic experience in cortical sensory maps: neural substrates of representational remodeling and correlative perceptual changes. Behav Brain Res 192:26-41.

Xiao MF, Xu JC, Tereshchenko Y, Novak D, Schachner M, Kleene R (2009), Neural cell adhesion molecule modulates dopaminergic signaling and behavior by regulating dopamine D2 receptor internalization. J Neurosci 29:14752-14763.

Y

Yamada S, Nelson WJ (2007), Synapses: sites of cell recognition, adhesion, and functional specification. Annu Rev Biochem 76:267-294.

Yang P, Yin X, Rutishauser U (1992), Intercellular space is affected by the polysialic acid content of NCAM. J Cell Biol 116:1487-1496.

Yao WD, Spealman RD, Zhang J (2008), Dopaminergic signaling in dendritic spines. Biochem Pharmacol 75:2055-2069.

Yoshida K, Rutishauser U, Crandall JE, Schwarting GA (1999), Polysialic acid facilitates migration of luteinizing hormone-releasing hormone neurons on vomeronasal axons. JNeurosci 19:794-801.

Yuste R, Bonhoeffer T (2001), Morphological changes in dendritic spines associated with long-term synaptic plasticity. Annu Rev Neurosci 24:1071-1089.

Z

Zaitsev AV, Gonzalez-Burgos G, Povysheva NV, Kroner S, Lewis DA, Krimer LS (2005), Localization of calcium-binding proteins in physiologically and morphologically characterized interneurons of monkey dorsolateral prefrontal cortex. Cereb Cortex 15:1178-1186.

Zesiewicz TA, Hauser RA (2002), Depression in Parkinson's disease. Curr Psychiatry Rep 4:69-73.

Zhang JP, Lencz T, Malhotra AK (2010a), D2 receptor genetic variation and clinical response to antipsychotic drug treatment: a meta-analysis. Am J Psychiatry 167:763-772.

Zhang X, Bearer EL, Boulat B, Hall FS, Uhl GR, Jacobs RE (2010b), Altered neurocircuitry in the dopamine transporter knockout mouse brain. PLoS One 5:e11506.

Zuber C, Lackie PM, Catterall WA, Roth J (1992), Polysialic acid is associated with sodium channels and the neural cell adhesion molecule N-CAM in adult rat brain. J Biol Chem 267:9965-9971.

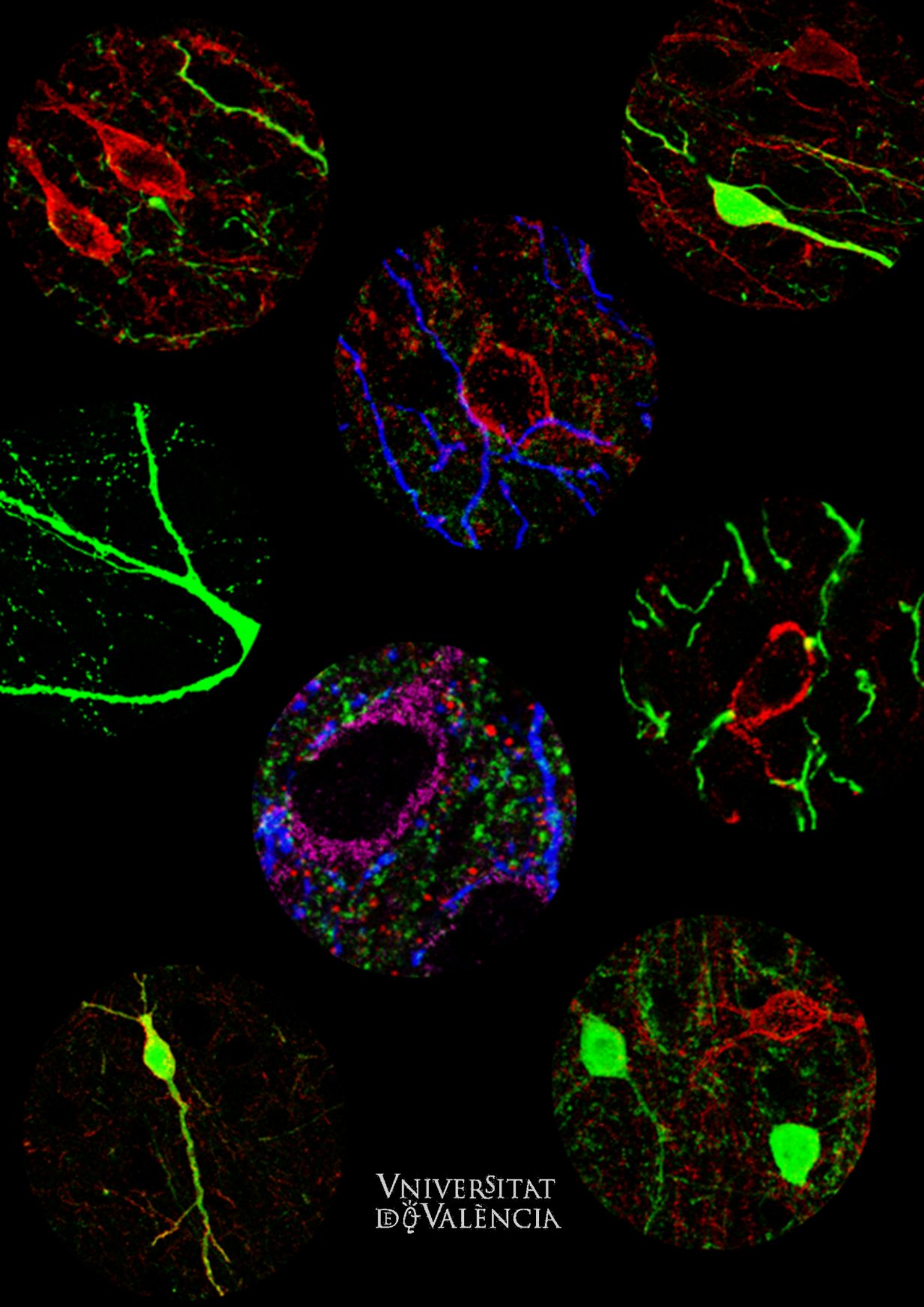
VNIVERSITAT
DE VALÈNCIA